# Dissertation

submitted to the

Combined Faculty of Mathematics, Engineering and Natural Sciences

of Heidelberg University, Germany

for the degree of

Doctor of Natural Sciences

Put forward by

**Hans Liew**

born in: Sendai, Japan

Oral examination: 18.01.2023

# The Creation of a Biophysical Modeling Universe:
# The UNIfied and VERSatile bio response Engine

Referees:                Prof. Dr. Dr. Jürgen Debus

                         Prof. Dr. Michael Hausmann

# Abstract

Radiotherapy is a crucial pillar of cancer therapy and ion beams promise superior dose conformity and potentially enhanced biological effectiveness in comparison to conventional radiation modalities. However, several factors are known to modify the biological effect of radiation. The capability to model their impact within a unified description of radiation action in conventional and ion beam fields would greatly enhance the ability to prescribe the optimal treatment and improve the knowledge of underlying mechanisms. To this end, the initial developments of the mechanistic *UNIfied and VERSatile bio response Engine* (UNIVERSE) are presented in this work. The effects of radiosensitizing drugs and mutations as well as DNA repair kinetics were modeled for each radiation quality. For sparsely ionizing radiation, the sparing effects at ultra-high dose-rates (uHDR) applied in FLASH radiotherapy were introduced based on oxygen depletion rates approaching measured values. Benchmarks against own or literature data are presented for each development. Challenges concerning the transition of oxygen and uHDR effects to ion beams as well as the vision of personalized biomarker-based patient plan adaptation based on UNIVERSE are discussed. UNIVERSE offers clinically relevant insights into radiobiological interdependencies and its versatility will allow it to follow future trends in radiotherapy.

# Zusammenfassung

Die Strahlentherapie ist ein wichtiger Pfeiler der Krebsbehandlung und Ionenstrahlen versprechen eine bessere Dosiskonformität sowie eine potenziell höhere biologische Wirksamkeit verglichen zu herkömmlichen Strahlungsmodalitäten. Es ist jedoch bekannt, dass verschiedene Faktoren die biologische Wirkung von Strahlung im beeinflussen. Die Möglichkeit, ihre Auswirkungen im Rahmen einer einheitlichen Beschreibung der Strahlenwirkung in konventionellen und Ionenstrahlfeldern zu modellieren, würde die Fähigkeit, die optimale Behandlung zu verschreiben und das Wissen über die zugrunde liegenden Mechanismen erheblich erweitern. Zu diesem Zweck werden in dieser Arbeit die ersten Schritte der Entwicklung des mechanistischen *UNIfied and VERSatile bio response Engine* (UNIVERSE) vorgestellt. Die Auswirkungen von radiosensibilisierenden Medikamenten und Mutationen sowie die DNA-Reparaturkinetik wurden für jede Strahlungsqualität modelliert. Für locker ionisierende Strahlung wurden Schonungseffekte bei ultrahohen Dosisraten (uHDR), wie sie in der FLASH-Strahlentherapie angewendet werden, auf der Grundlage von Sauerstoffzehrungssraten, die sich gemessenen Werten nähern, eingeführt. Für jede Entwicklung werden Benchmarks mit eigenen oder Literaturdaten vorgestellt. Herausforderungen bezüglich des Übergangs von Sauerstoff- und uHDR-Effekten zu Ionenstrahlen sowie der Vision einer personalisierten, auf Biomarkern basierenden Anpassung des Patientenplans auf der Grundlage von UNIVERSE werden diskutiert. UNIVERSE bietet klinisch relevante Einblicke in strahlenbiologische Zusammenhänge und wird aufgrund seiner Vielseitigkeit auch zukünftigen Trends in der Strahlentherapie folgen können.

# Contents

# List of Abbreviations

| | |
|---|---|
| **ATM** | Ataxia Telangiectasia Mutated |
| **ATP** | Adenosine Triphosphate |
| **BAX** | Bcl-2-Associated X |
| **BIANCA** | Biophysical Analysis of Cell Death and Chromosomal Aberration |
| **BRCA1/2** | Breastcancer 1/2 |
| **cdk2** | cyclin dependent kinase 2 |
| **cDSB** | complex/clustered Double Strand Break |
| **cGAS-STING** | cyclic GMP-AMP Synthase - Stimulator of Interferon Genes |
| **chk2** | checkpoint kinase 2 |
| **CL** | Clustered Lesions |
| **CPU** | Central Processing Unit |
| **CSDA** | Continuous Slowing Down Approach |
| **DDR** | DNA Damage Repair |
| **DDRi** | DNA Damage Repair interference / DNA Damage Repair inhibition |
| **DMSO** | Dimethyl Sulfoxide |
| **DNA** | Deoxyribonucleic Acid |
| **DNA-PKcs** | DNA dependent protein kinase catalytic subunit |
| **DSMKM** | Double-Stochastic Microsimetric Kinetic Model |
| **ER** | Endoplasmatic Reticulum |
| **FLUKA** | Fluktuierende Kaskade |
| **GLOBLE** | Giant Loop Binary Lesion |
| **GPU** | Graphics Processing Units |
| **GSI** | Gesellschaft für Schwerionenforschung |
| **HIT** | Heidelberg Ion Beam Therapy Center |
| **HPV** | Human Papillomavirus |
| **HR** | Homologous Recombination |
| **HRF** | Hypoxia Reduction Factor |

| | |
|---|---|
| **iDSB** | isolated Double Strand Break |
| **KC** | Kiefer-Chatterjee |
| **LBL** | Lawrence Berkeley Laboratories |
| **LEM** | Local Effect Model |
| **LET** | Linear Energy Transfer |
| **LL** | Lethal Lesion |
| **LQM** | Linear Quadratic Model |
| **MC/MCS** | Monte Carlo/ Monte Carlo Simulation |
| **MCDS** | Monte Carlo Damage Simulation |
| **Medras** | Mechanistic DNA Repair and Survival Model |
| **MKM** | Microdosimetric Kinetic Model |
| **mMKM** | modified Microdosimetric Kinetic Model |
| **MRI** | Magnetic Resonance Imaging |
| **MRN-complex** | Mre11-Rad50-Nbs1-complex |
| **NHEJ** | Non-Homologous End-Joining |
| **OER** | Oxygen Enhancement Ratio |
| **PARP** | Poly-(ADP-Ribose)-Polymerase |
| **PET** | Positron Emission Tomography |
| **PSI** | Paul-Scherrer-Institute |
| **PTCOG** | Particle Therapy Co-Operative Group |
| **Pub.** | Publication |
| **RBE** | Relative Biological Effectiveness |
| **RDD** | Radial Dose Distribution |
| **RER** | Rough Endoplasmatic Reticulum |
| **RMF** | Repair-Misrepair-Fixation |
| **RSF** | Radiosensitizazion Factor |
| **SDR** | Standard Dose Rate |
| **SER** | Sensitivity Enhancement Ratio |
| **SMKM** | Stochastic Microdosimetric Kinetic Model |
| **SOBP** | Spread-Out Bragg Peak |
| **SSB** | Single Strand Break |
| **TDRA** | Theory of Dual Radiation Action |
| **uHDR** | ultra-high dose-rate |
| **UNIVERSE** | UNIfied and VERSatile bio response Engine |

# Chapter 1

# Motivation

In his book *The Emperor of All Maladies - A Biography of Cancer* [1], Siddhartha Mukherjee shares the fascinating story of an ancient scroll that emerged in 1862 and was translated in 1930. It is thought to contain the collected teachings of Imhotep, an ancient Egyptian physician that lived around 2625 BC. In it, Imhotep reports 48 medical cases ranging from fractures to abscesses in a methodical and empirical language far ahead of his time. For each of the presented cases he describes his recommended therapy, even if it is only of palliative nature. Only in his 45th case, his remark concerning a possible therapy is as brief as it is sobering: "[There] is none." Case 45 is currently the oldest known written description of breast cancer. Fortunately, thanks to modern medicine and its advancements in cure and detection, the prospects for cancer patients have greatly improved: Breast cancer patients for example faced an average five-year survival rate of 89.7% between 2007 and 2013 in the United States [2]. Nevertheless, in 2018, an estimated 18 million new cases and about 10 million deaths were connected to cancer. Furthermore, it is predicted that the number of new cases per year will increase to a range of 29-37 million by 2040 [3]. In many high income countries, cancer is even about to surpass cardiovascular disease as the leading cause of death and is expected to develop into a leading cause of death and morbidity around the globe throughout the coming decades [4–7]. These developments are thought to be driven by growing and aging populations, as well as the reduction of mortality by other causes [4].

About every second cancer patient is estimated to receive some type of radiotherapy throughout his treatment, making it one of the most frequently applied tools of oncologists. Often, it is applied in combination with other treatment modalities

1

such as surgery or chemotherapy but is of special importance when surgery is not an option [8–10]. Roughly speaking, the rationale of radiotherapy is to apply ionizing radiation to the tumor cells to induce damages in their DNA, impeding their ability to replicate. Normal tissue cells surrounding the tumor commonly exhibit slightly higher repair capabilities, often allowing them to tolerate somewhat larger doses of radiation. This can lead to an exploitable *therapeutic window*, where the probability to control the tumor outweighs that of inducing normal tissue complications at certain doses [11].

Only about 60 days after Röntgens announcement of his discovery of the X-rays [12], on January 29th, 1896, E.H. Grubbe applied them for one hour to a patient with ulcerated breast cancer [13, 14]. In the more than 125 years that have passed since, technological advancement have greatly improved the accuracy of dose application to tumors and significantly reduced the amount of dose given to the surrounding healthy tissue by introducing - among other things - high-precision collimation of the beam and its application from multiple angles [11]. The latter approach especially addresses one key challenge of conventional photon radiotherapy: The applied dose within matter decreases exponentially with depth (after a short build-up region) for photon beams, inevitably leading to dose being deposited in front and behind of the tumor along the irradiation axis. In stark contrast, charged particles deposit most of their dose at the end of their finite range, leading to the so-called Bragg-peak (Figure 1.1) [15]. Furthermore, depending on their charge and kinetic energy, ion beams exhibit increased biological effectiveness compared to conventional photon beams [15, 16]. The idea to treat tumors with charged particle beams was first formulated by Wilson in 1946 [17] and first treatments with protons (and later helium ions) began in 1954 at the *Lawrence Berkeley Laboratories* (LBL) [15]. With only a few proton therapy centers being opened in that time period, the Bevatron at LBL was the only facility applying heavy ions (mostly Neon ions) between 1975 and 1992 when it closed [11, 15, 18]. Up to that point, treatment facilities utilized existing accelerators used primarily for physics experiments, but in the 90s the first dedicated medical accelerator facilities were opened in Loma Linda, USA (1990) and Chiba, Japan (1994) [11, 18]. The number of facilities has started to grow rapidly since [18] and technological breakthroughs, such as the development of active beam scanning techniques at the *Paul-Scherrer-Institut* (PSI), Switzerland [19] and the *Gesellschaft für Schwerionenforschung* (GSI), Germany [20], have further improved
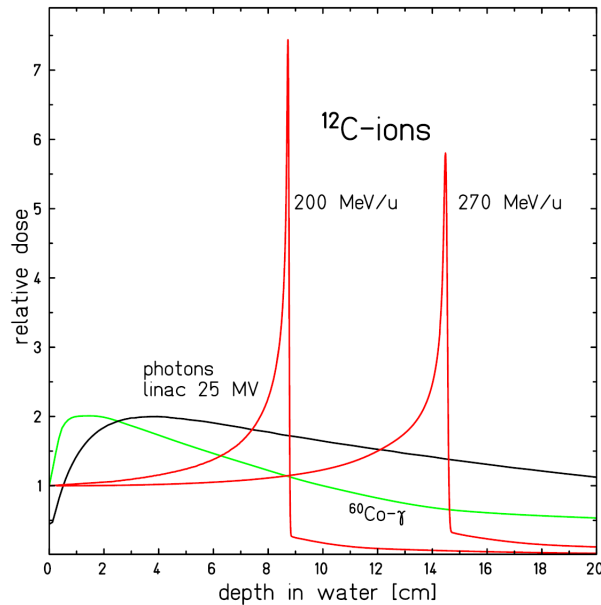
Figure 1.1: Depth-dose profiles of $^{60}$Co $\gamma$-radiation, megavolt photons, and $^{12}$C ions in water. Taken from [15].

dose conformity [15]. The *Heidelberg Ion Beam Therapy Center* (HIT) treated its first patient in 2009 [21]. Currently, there are about 100 ion beam therapy facilities in active clinical use, around 40 in construction and another approximately 30 in the planning phase worldwide [22–24]. While ion beam therapy has shown promising results in clinical practice [11, 15, 25], according to the Particle Therapy Co-Operative Group (PTCOG), only about 300.000 patients have been treated with it between 1954 and 2020, about 40.000 of them in the year 2019 [26, 27]. These numbers appear minuscule when considering that about half of the 18 million new cases in 2018 alone will - or have already - received some form of radiotherapy during their treatment, as mentioned earlier.

With its later and less widespread introduction into clinics, as well as limited number of accessible experimental setups, significantly less experience and data has been accumulated using ion beams compared to conventional photon radiation, leading to sparser measurements and understanding of its biological effects. This is especially the case for the number of different, more or less well established, modifiers of radiation action such as the oxygenation of the irradiated system, interference with the DNA damage repair process by drugs or mutations, presence of radical scavengers and the applied dose-rate: Low levels of oxygen in living cells and tissue (hypoxia) is well known to induce radioresistance and is thought to be responsible for a consider-

able amount of treatment failures in radiotherapy [8, 28, 29]. The inhibition of DNA damage repair (DDR) proteins generally increases the biological efficacy of radiation and tumors with known deficiencies in central DDR enzymes have been found to be treated with an improved success rate via radiotherapy [30–35]. Pharmaceutical DDR inhibition has thus been suggested as a possible approach to increase tumor control [36] or even to overcome hypoxia induced radioresistance [37], leading to numerous drugs being developed that target key DNA repair enzymes [38–42], with some having progressed in to pre-clinical [43–46] and clinical trials [45–47]. In contrast, radical scavengers have the ability to neutralize radiation induced radicals, a highly reactive chemical species that can mediate large parts of the radiation induced DNA damage [48–51], and have thus been considered for application as radioprotectors in normal tissue [52–54]. At sufficiently low dose-rates, the repair of DNA damages during the irradiation can lead to an increased radio-resistance of cells and tissues [55]. On the other hand, also ultra-high dose-rates have been found to have a sparing effect as early as in the late 1960s [56, 57]. The latter effect has re-gained significant interest since the first reports in the mid-2010s of an apparent absence of the sparing effect in tumors, while normal tissue sparing was still retained, promising a widening of the therapeutic window [58–60].

A theoretical framework versatile enough to describe and predict the effect of the different modifiers under a unified model of radiation action for conventional and ion beam radiation could greatly improve the capabilities to give patients the best possible care. It may be able to support the choice and planning of the appropriate treatment modality - possibly based on personalized readouts - and help to understand the underlying radiobiological mechanisms, which might be exploitable to progress this crucial pillar of cancer care as a whole. This thesis and the contained developments are meant to be a first step towards the development of such a framework. Its main concept and outline will be elaborated in Chapter 3, after covering some physical, technical, biological and biophysical modeling fundamentals underlying the presented work in the following chapter.

# Chapter 2

# Fundamentals

## 2.1 Physics of Radiation Therapy

### 2.1.1 Fundamental Physical Quantities

The most fundamental quantity in radiation therapy physics is the *absorbed dose D*. It is defined as the mean energy $d\bar{\epsilon}$ imparted per unit mass $dm$ delivered by ionizing radiation [48, 61]:

$$D = \frac{d\bar{\epsilon}}{dm} \qquad [D] = J \cdot kg^{-1} = Gy. \tag{2.1}$$

The special unit name is defined as *Gray* (Gy).

The *fluence* $\Phi$ of a particular radiation field is defined as the number of particles $dN$ passing a cross-sectional area $dA$ of a sphere [61]:

$$\Phi = \frac{dN}{dA} \qquad [\Phi] = m^{-2}. \tag{2.2}$$

The *mass stopping power* $\frac{S}{\rho}$ acting on a charged particle beam within a given material is characterized as,

$$\frac{S}{\rho} = \frac{1}{\rho}\frac{dE}{dl} \qquad \left[\frac{S}{\rho}\right] = J \cdot m^2 \cdot kg^{-1}, \tag{2.3}$$

with the mean energy lost by the charged particle $dE$ per unit distance $dl$, while traversing a material of density $\rho$ [61]. The mass stopping power can be broken

down into three independent contributions:

$$\frac{S}{\rho} = \frac{1}{\rho}\left(\frac{dE}{dl}\right)_{el} + \frac{1}{\rho}\left(\frac{dE}{dl}\right)_{rad} + \frac{1}{\rho}\left(\frac{dE}{dl}\right)_{nuc}. \qquad (2.4)$$

The first term is called the *mass electronic stopping power*. It represents the energy loss caused by interactions of the ions with electrons of the target atoms, leading to the ionization or excitation of the latter. The second term, the *mass radiative stopping power*, covers the emission of bremsstrahlung within the electric field of the target atoms or their electrons. The last term, the *mass nuclear stopping power*, introduces the elastic Coulomb interactions with atomic nuclei of the target. The name of this contribution can be misleading as it does not include any inelastic nuclear interactions, which can be highly relevant for many applications of ion beams [61]. Using the fluence of a particle beam and the mass stopping power within a target, the resulting deposited dose can be written as [15]:

$$D = \frac{S}{\rho} \cdot \Phi. \qquad (2.5)$$

Another central quantity in the field of radiation therapy physics is the so called *linear energy transfer* or LET. It is closely related to the *mass electronic stopping power* and is defined as:

$$L_\Delta = \frac{dE_\Delta}{dl}, \qquad (2.6)$$

where $dE_\Delta$ is specified to be *"the mean energy lost by the charged particles due to electronic interactions"* over the distance $dl$, *"minus the mean sum of the kinetic energies in excess of $\Delta$ of all the electrons released by the charged particles"* [61]. The energy cutoff $\Delta$ acts as a measure of the locality of the energy deposition by the ion, as it puts a limit on the range of freed electrons that are included into the measure. Therefore the LET is thought to be a measure for the ionization density caused by charged particles within a medium [48]. In practice, one mostly encounters the so called *unrestricted LET*, $L_\infty$ or often simply $L$, where $\Delta = \infty$. In this thesis *LET* will be used synonymously to the *unrestricted LET*. In this case the LET is by definition equal to the *electronic stopping power* $S_{el}$ [61]. In radiation therapy physics the LET is commonly given in the units $keV\,\mu m^{-1}$, while in other fields units of $MeV\,cm^2 g^{-1}$ are more widespread.

## 2.1.2 Interaction of Photons with Matter

At photon energies typical for medical applications three mechanisms dominate the interaction between the impinging photons and the target [49](energies are given for the case of a water target): Below an energy of 30 keV the *photoelectric effect*, where the entire energy of the photon is absorbed to free a bound electron, is the dominant process. The free electron carries the difference between the photon energy and the binding energy as its kinetic energy. Between photon energies of 100 keV to 2-3 MeV, *Compton scattering* dominates. In this process only a part of the photons energy is transferred to the electron and the remaining energy is carried by a scattered photon. At these energies, the binding energy of the electron can be neglected so that the electron is thought to carry the transferred energy away as its kinetic energy. At photons energies above double the rest energy of an electron ( = 1.022 MeV), the photons can interact with the electromagnetic field of the target atoms to form an electron-positron pair. This process is called *pair production*. Any photon energy exceeding this threshold is transferred as kinetic energy of both particles. Although the process is theoretically possible at energies above 1.022 MeV, the process only becomes dominant at energies above approximately 10 MeV [49]. The energy deposition of a photon beam along its depth in a medium can be described using the Lambert-Beer law, which describes an exponential absorption of the photon beam via the processes described above [48, 49]. However, the produced free electrons are the main mediator of the ionization process, while the direct ionization by photons is negligible. This is why photon radiation is also considered *indirectly ionizing radiation* [48]. As a result, the energy transferred to the medium by the photons is deposited slightly downstream along the beam direction carried by the electrons. This leads to the so called *build-up effect* at the proximal end of the depth-dose profile that transitions into the exponential decay described earlier. The resulting peak is shifted by about the mean free path length of the free electrons from the entry point to the medium [48, 49](Fig. 2.1).

## 2.1.3 Interaction of Ions with Matter

The deceleration of ions in matter is dominated by inelastic collisions with the electrons of the target within the energy range applied in radiotherapy (up to 430 MeV/u for carbon ions) [15]: In a statistical process, the ion ejects target electrons
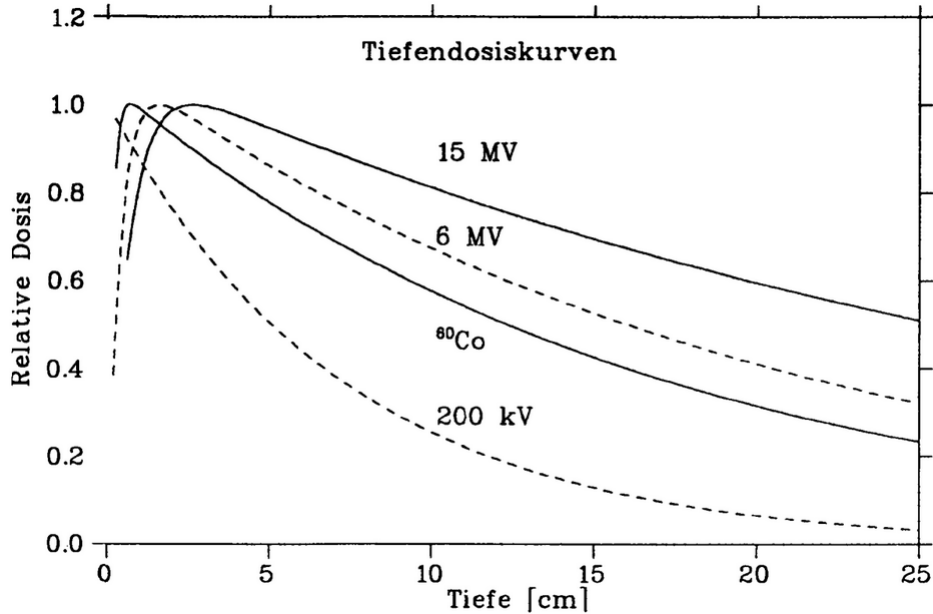
Figure 2.1: Depth-dose profiles of photon beams with different energies in water. The y-axis shows relative dose and the x-axis the depth in cm. Note that the peak shifts with photon energy. Taken from [49].

via Coulomb interactions. These so called secondary electrons subsequently travel through the medium and interact through elastic and inelastic collisions with surrounding atoms and molecules. The elastic collisions do only lead to a deflection of the electrons path, while the inelastic collisions lead to ionization and excitation events. These interactions result in a heterogeneous track structure surrounding the ion trajectory, comprising a spectrum of secondary electrons [15]. In Figure 2.2 a visualization of such an ion track structure is shown, which was produces using a Monte Carlo simulation.

The radial form of the dose deposition surrounding the ion track, the so called radial dose distribution (RDD) is important for a number of applications including the prediction of the response of detectors [62, 63] and the description of their biological effect [64]. Experimental studies using gas chambers, analytical models as well as Monte Carlo simulations agree, that the RDD decreases with the radial distance from the track $r$ following a $\frac{1}{r^2}$ dependency [15, 65, 66]. However, experimental data only exists down to a radial distance of about 0.8 nm [65]. Kiefer [67] applied *classical collision dynamics* (quantum mechanical effects were neglected) to derive the energy density in the RDD and an approximate expression of the maximum range of secondary electrons, which defines the maximal extent of
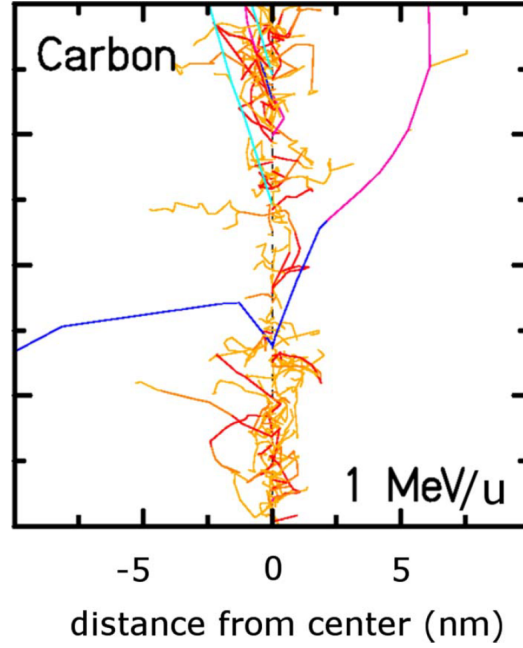
Figure 2.2: Visualizations of a microscopic track structure simulated by the *TRAX* Monte Carlo code for a 1 MeV/u carbon ion. The lines depict the tracks of individual secondary electrons. Taken from [15] (Image courtesy Michael Kraemer).

the RDD $r_{max}$ (in µm) as [66]:

$$r_{max} = \gamma E^{\delta}, \tag{2.7}$$

where $\gamma = 0.062$, $\delta = 1.7$ and $E$ is the particle energy in MeV/u.

Further, Chatterjee [68] supposed that half of the energy deposition by the ion is accounted for by *glancing* collisions that transfer the energy into a small *core* of the RDD with constant energy density, while the other half is deposited in the so called *penumbra* ($r^{-2}$- region) by secondary electrons produced by *close* collisions. Based on this equipartition, he derived the radius of a core region $r_{min}$:

$$r_{min} = \beta \cdot r_c, \tag{2.8}$$

where $\beta = \frac{v}{c}$, where $c$ is the velocity of light and $v$ is the velocity of the projectile and $r_c$ is the maximum core radius that was derived to be $r_c = 11.6 nm$.

The two most prominent parametrizations of the resulting RDD are the Geiß and Kiefer-Chatterjee parametrization [64, 66](Figure 2.3).

In the Geiß parametrization [62] the penumbra is directly attached to the core
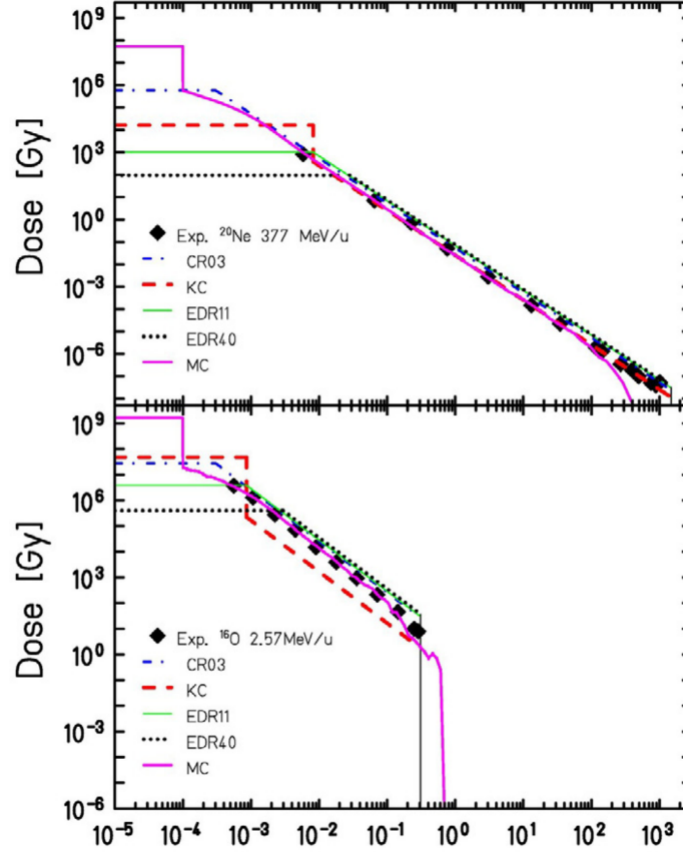
Figure 2.3: Radial dose distributions of 377 Mev/u neon ions (upper panel) and 2.57 MeV/u oxygen ions. The dash-dotted line (CR03) shows the Geiß parametrization using a constant core radius of 3nm, while the green solid line (EDR11) and the black dotted line (EDR40) show the Geiß parametrization with an energy dependent core radius based on an $r_c$ of 11.6nm and 40nm, respectively. The corresponding Kiefer-Chatterjee parametrization is shown as a red dashed line (KC). The Monte-Carlo simulation used to produce the RDD in magenta is described in [69]. Taken from [66], where the data was taken from [70, 71].

region and the dose in Gy at a distance $r$ from the track center can be written as:

$$D(r) = \begin{cases} D_c & r \leq r_{min} \\ D_c \left( \frac{r_{min}}{r} \right)^2 & r_{min} < r \leq r_{max}, \end{cases} \tag{2.9}$$

where $D_c$ is the dose in the core region.

The Kiefer-Chatterjee model is given by [66]:

$$D(r) = \begin{cases} D_c = \frac{1}{\pi r_{min}^2} \left( \frac{LET}{\rho} - 2\pi K_p \ln \left( \frac{r_{max}}{r_{min}} \right) \right) & r \leq r_{min} \\ 1.25 \cdot 10^{-4} \left( \frac{Z^*}{\beta} \right)^2 r^{-2} \equiv K_p \cdot r^{-2} & r_{min} < r \leq r_{max}, \end{cases} \tag{2.10}$$

where the expression for the penumbra region is based on the derivations of Kiefer [67]

mentioned earlier and $Z^*$ is the *effective charge*, which will be defined further below. For both parametrizations, the value of the finite core dose $D_c$ is determined normalizing the area integral of the RDD to the value of the electronic stopping power:

$$\frac{1}{\rho} \left( \frac{dE}{dl} \right)_{el} = 2\pi \int_0^{r_{max}} D(r)\, r\, dr. \tag{2.11}$$

The electronic stopping power for an ion is described by the Bethe-Bloch formula shown here in the relativistic version derived by Fano [15, 72–74]:

$$\left( \frac{dE}{dl} \right)_{el} = \frac{4\pi e^4 Z_t Z_p^2}{m_e v^2} \left[ \ln \left( \frac{2 m_e v^2}{\langle I \rangle} \right) - \ln \left( 1 - \beta^2 \right) - \beta^2 - \frac{C}{Z_t} - \frac{\delta}{2} \right]. \tag{2.12}$$

The parameters $m_e$ and $e$ describe the mass and charge of an electron, respectively, $Z_p$ and $Z_t$ describe the nuclear charges of the projectile and target atoms and $\langle I \rangle$ the mean excitation potential of the target material. $\langle I \rangle$ can be estimated by $\langle I \rangle \approx 12 eV \cdot Z + 7 eV$ for $Z < 13$ [75] or taken from experiments [15]. The term $C/Z_t$ and $\delta/2$ represent the shell correction and density effect correction, respectively.

At low energies ions can *pick up* charge from their environment as a product of ionization and recombination processes, so that their charge is reduced to an *effective charge* $Z^*$ for which Barkas [76] found the following empirical expression [15]

$$Z^* = Z_p \left[ 1 - \exp \left( -125 \beta Z_p^{-2/3} \right) \right]. \tag{2.13}$$

At very low energies ($\leq 10 keV/u$), elastic collisions with the target nuclei begin to contribute to the energy loss and thus to the stopping process of the projectile to a significant degree [15]. However, their contribution to the overall dose deposition is negligible in the context of radio therapy [77]. Figure 2.4 shows the energy dependent stopping power for protons and carbon ions as well as for the electronic and nuclear stopping processes. The described dependencies between the velocity and the energy loss of a particle result in the distinctive inverse depth-dose profile of charged particles referred to as a *Bragg-Peak* (Figure 2.5).

The contribution of the radiative stopping power can be neglected within the energy ranges applied in ion beam therapy as well. This is based on the fact, that the bremsstrahlung mechanism is only of significance when the kinetic energy of the charged particle begins to be in the order of its rest energy $E_0 = m_0 \cdot c^2$, where $m_0$ is its rest mass. With applied kinetic energies of up to $\approx 220\ MeV/u$ for protons
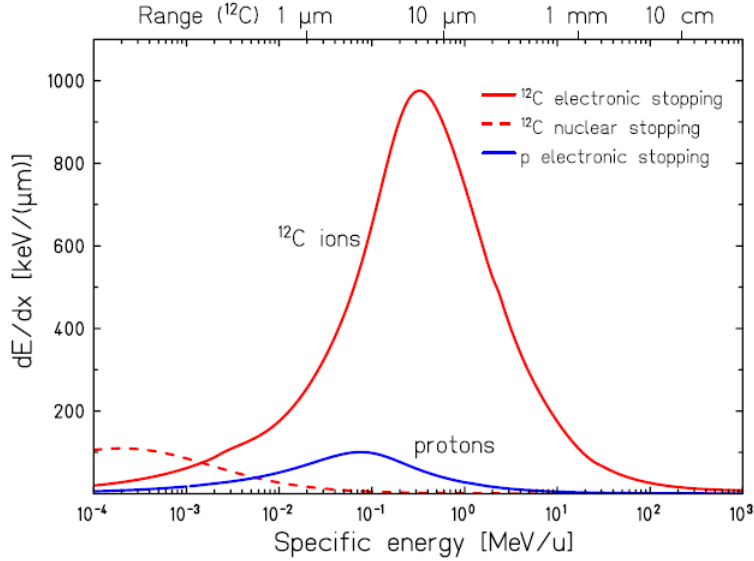
Figure 2.4: Stopping power of C-12 ions and protons in water. The residual range of the C-12 ions corresponding to their energy is shown as the top x-axis. Taken from [15].

and helium ions as well as $\approx 430~MeV/u$ for carbon ions [15]) and $1u \approx 932~MeV$ this is not to be expected for conventional ion beam therapy [48].

Inelastic nuclear interactions, i.e. fragmentation events, are another important aspect of ion beam interactions with the target medium. While, their probability (mean free paths of 85.2 cm and 20.8 cm for protons and carbon-ions with residual range of 25 cm, respectively [15]) is significantly lower than that of inelastic electronic interactions it results in a reduction of primary particles and an accumulation of lower-Z fragments, mostly hydrogen and helium nuclei. The amount of accumulated fragments increases steadily with the penetration depth. Fragments move with velocities comparable to that of the primary particles and they are ejected mainly in forward direction. As a result, the produced fragments are able to travel farther than the primary particles, leading to a so called dose tail behind the actual Bragg peak (Figure 2.6) [78, 79]. The inelastic collision events at high energies are frequently described in as two-step process called the *abrasion-ablation model* [81] (cp. Figure 2.7): In the first step the nucleons are abraded inside the overlap region between the two colliding nuclei and form a *fireball*. The nucleons outside of the overlap region are thought to be excited. In the second step, the excited remains of the nuclei deexcite, by releasing single or clustered nucleons.
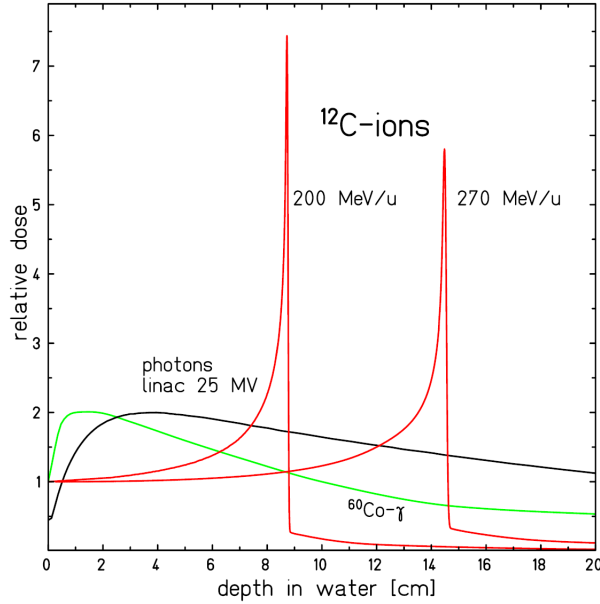
Figure 2.5: Depth-dose profiles of $^{60}$Co $\gamma$-radiation, megavolt photons, and $^{12}$C ions in water. Taken from [15].

## 2.1.4    Interlude: Interaction of Electron Beams

As data of cell survival after irradiation with electron beams will be included in this thesis, some brief remarks concerning distinct features of the interactions of electron beams shall be made here: While collision with large impact parameters between projectile and target electrons can be described in the same way as for ions, at small impact parameters Møller scattering needs to be considered. Furthermore, the maximum energy transfer is limited to half of the beam energy, due to the fact that both collision partners are indistinguishable. These considerations result in slightly modified version of the Bethe-Bloch equation that was given earlier (Equation 2.12). In addition, the density correction and energy loss via radiative stopping play a larger role for electron beams than for ions. Due to their smaller mass, scattering events can lead to larger scattering angles and depending on the target material even to significant back scattering of electron beams. These effects result in a less localized depth dose profile of electron beams in comparison to the bragg peaks of ions [11] (Figure 2.8). At energies commonly applied in medical physics, electron beams are considered low-LET/sparsely ionizing radiation [49].
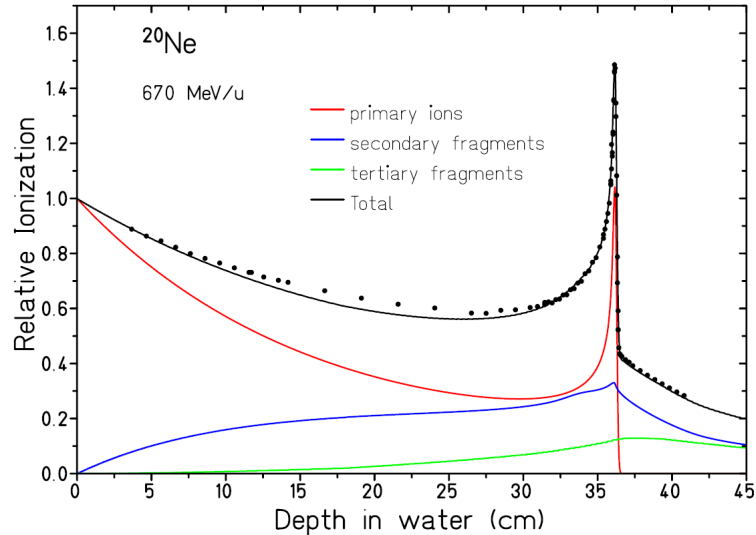
Figure 2.6: Bragg peak of 670 MeV/u $^{20}$Ne ions in water. Experimental data obtained at GSI are shown as black circles. Solid lines show contributions of primary ions, secondary and tertiary fragments. Taken from [15], where it was adapted from [80].
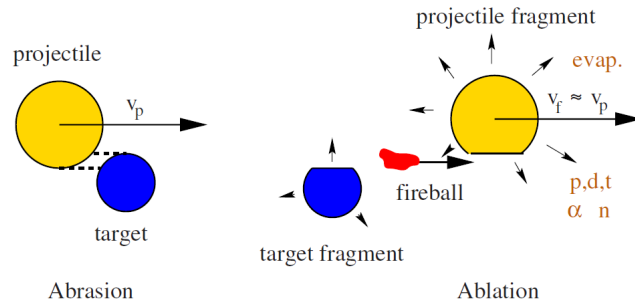


Figure 2.7: Visualization of the two-step abrasion-ablation model at high energies according to Serber [81]. Taken from [15], where it was adapted from [82].

### 2.1.5 Precision Dose Delivery with Ion Beams

The distinct shape of the Bragg peak allows for precise dose delivery inside a target volume using ion beams [21]: The position of the peak in depth can be varied by the set initial energy of the projectile ions. Following the *continuous slowing down approach* (CSDA) the range of a particle $R$ with the initial energy $E$ can be written as [49]:

$$R(E) = \frac{1}{\rho} \int_0^E dE' \frac{1}{S(E')}. \tag{2.14}$$

However, as the energy loss is a statistical process, the range of a group of particles with the same initial energy follows a distribution. The energy loss follows an asymetric Vavilov distribution [84], which converges to a Gaussian for a large amount

Figure 2.8: Depth dose profiles of electron beams with different initial energies in water. Taken from [83].

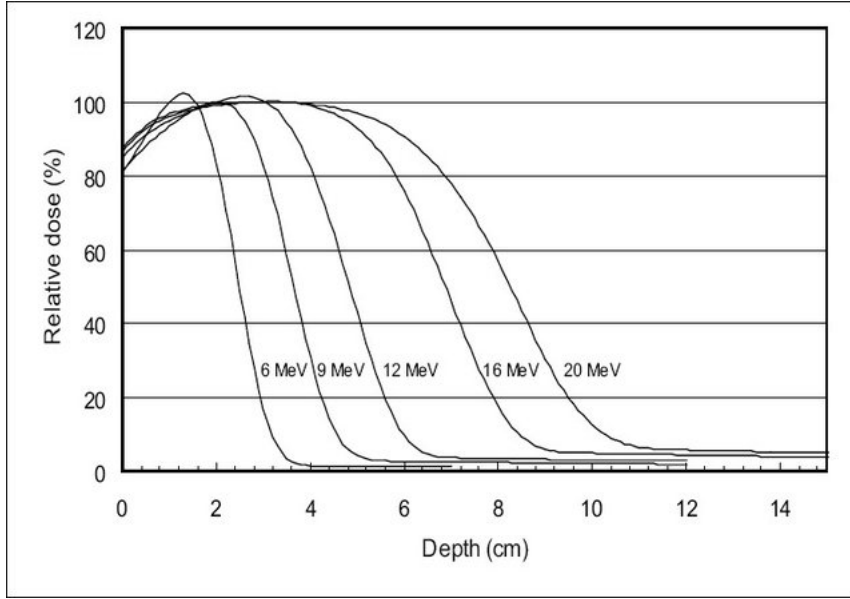of collision events [15]. Ultimately, the range of charged particles follows a Gaussian with the variance $\sigma_R$ that is characterized by [15]:

$$\sigma_R \propto R \frac{1}{\sqrt{M}}, \tag{2.15}$$

where $M$ is the projectiles mass. This shows, that the spreading effect increases with depth and is less pronounced for heavier ions. This spread of the bragg peak along the beam axis is also called *range-straggling* [15]. Besides the spread in beam direction, Coulomb scattering of the projectiles with the target nuclei also widens the beam laterally. While Bothe [85] worked out the statistical distribution of the scattering angles at a given depth, Molière [86] was able to provide an analytical solution of the equations. In Highlands [87, 88] approximation only small scattering angles are considered and the angular distribution becomes a Gaussian distribution with a standard deviation of [15]

$$\sigma_\theta \, [\text{rad}] = \frac{14.1 \text{ MeV}}{\beta pc} Z_p \sqrt{\frac{d}{L_{rad}}} \left[ 1 + \frac{1}{9} \log_{10} \left( \frac{d}{L_{rad}} \right) \right], \tag{2.16}$$

where $p$ is the projectiles momentum, $d$ the thickness of the absorber and $L_{rad}$ its radiation length, which introduces the material dependency of the spread. The $(\beta pc)^2$ term shows, that for particles with higher kinetic energies the spread is less pronounced.

Regarding the technical beam delivery to the patients one differentiates between *passive* and *active* beam delivery systems: While passive systems shape the beam using a number of devices, which absorb or scatter an otherwise rigid beam into the desired form, active systems guide the ion beam laterally using fast scanning dipole magnets. By applying a coordinated ensemble of Bragg peaks with different ranges a *spread out Bragg peak* (SOBP) with a constant dose throughout the volume can be realized [15] (Figure 2.9). These techniques allow for a higher precision of
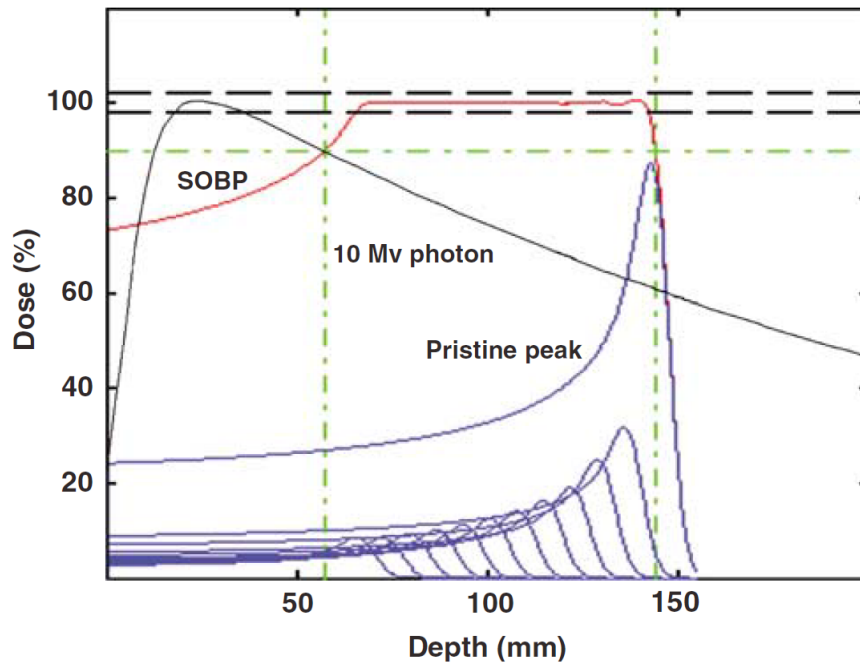


Figure 2.9: Visualization of the principle of a spread out Bragg peak (SOBP, red line), that is the sum of a composed group of single Bragg peaks (blue lines). The depth dose profile of a 10 MV photon beam (black line) is shown as a reference. Taken from [89].

dose application to the tumor in comparison to conventional treatment modalities, promising improved tumor control and reduced normal tissue complication probabilities. This makes ion beam cancer therapy especially favorable in cases where the tumors are located deep inside the patient with organs-at-risk nearby [90].

## 2.2 Technical Fundamentals

### 2.2.1 Monte Carlo Method

The vast range of applications and forms of simulations applying the Monte Carlo method (MCS) make it difficult to give a precise and concise definition or description of the concept. At the core, MCS are mathematical models driven by the generation of random objects or processes by means of computational devices [91]. They are often employed, when the investigated system is too complex to be formulated in manageable mathematical equations or their solution is not easily obtainable by analytical methods [92]. Most often, random values are assigned to variables at given steps of the modelled process, based on known or estimated probability distributions. The simulation or a simulation step is then repeated for many iterations to obtain estimates on metrics of interest and their possible range of variance [91, 93]. In physics, MCS can be used to describe processes that are intrinsically random (e.g., radioactive decay) or can be treated as random for "all intents and purposes" (e.g., brownian motion) [94]. The first known use of MCS in the context of particle physics involved the prediction of random neutron diffusion processes as part of the development of the nuclear bomb in the *Manhattan Project* [92, 93]. In this work, some analyses are based on the radiation transport Monte Carlo code FLUKA (Fluktuierende Kaskade) [95, 96], which is able to accurately simulate the passage of radiation through user-defined geometries and materials based on interaction cross-sections. Furthermore, the Monte Carlo method will be used frequently to simulate key processes within the presented modelling framework, such as the induction and repair of DNA damages or the position of charged particles passing the nucleus.

### 2.2.2 GPU Computation

While MCS have become versatile and valuable tools within and outside of science, depending on the investigated system, a large number of iterations is needed to achieve the desired accuracy of its results. This has made the appropriate computation speed a central point of concern for any application of the MC method. However, if the single iterations are independent of each other, as is the case in the simulations developed within this thesis, they can in principle be calculated in parallel. In order to do so, some of the most computationally intensive codes within

this work were realized with the CUDA C++ toolkit (NVIDIA, Santa Clara, CA, USA) to be run on Graphics Processing Units (GPUs) manufactured by NVIDIA (Santa Clara, CA ,USA). As the main code developed in this work is written in Python 3 [97] the *pycuda* tool [98] was used to integrate the GPU code into the framework. Conventional codes are run on the Central Processing Unit (CPU) of a computer, which is designed to perform computations sequentially at high speed. In contrast, GPUs can include several thousands of processing units, which can carry out calculations virtually in parallel. Although the single processing units on a GPU are less powerful than those found on a CPU of a comparable generation, the overall computations speed of parallelizable codes can be improved dramatically when implemented on GPU [99].

## 2.3 Biological Effect of Ionizing Radiation

Some of the subsections in this section (Section 2.3) are, to a varying degree, based on an unpublished report with the title *Radiobiology of the Cell* written by the author for the Seminar on Medical Physics in the winter semester 2017/2018 given by Prof. P. Bachert and Prof. J. Seco at the University of Heidelberg.

### 2.3.1 Fundamental Mechanisms and Effects of Ionizing Radiation in the Cell

**Cell Structure**

Human cells belong to the category of *eukaryotic* cells (Fig. 2.10) and are enclosed by a double lipid layer called the *plasma membrane*. Within the cells, functional subcompartments, so called organelles, are again surrounded by their own membranes. The most important cellular organelles are the *endoplasmic reticulum* (ER), the *Golgi-apparatus*, the *mitochondria*, the *lysosomes*, and the *cell nucleus*. Within the cell, the organelles are surrounded by *cytosol*, a solution of proteins, nucleid acids, sugars, lipids and other compounds comprising about 80% water. There are two types of ER, the *rough ER* (RER) and the *smooth ER* (SER), which can both be generally described as a network of membranes. While the membranes of the RER are lined with *ribosomes*, responsible for the synthesis of proteins, the SER is free of them. The exact roles of the SER are cell type dependent and can include

the production of specific hormones or the storage of calcium. The main tasks of the Golgi-apparatus lies in the modification of compounds produced in the ER, the management of the complex vesicle transport within the cell as well as the synthesis and processing of membranes. The appearance of the Golgi-apparatus is often described as a stack of "sack-formed cisterns". Mitochondria, often dubbed the *power house of the cell*, harbor the *Krebs-Cycle* and *respiratory chain*. These two biochemical processes are responsible for the production of *adenosine triphosphate* (ATP). The high energy contained in the chemical bonds of ATP is harnessed as a general source of energy throughout the cell. Carrying a concoction of specialized enzymes, the tasks of lysosomes encompass the digestion of nutrients and dissolution of cellular components if cells need to be restructured. In contrast to *prokaryotic* cells, the nucleus of an eukoryotic cell is surrounded by another membrane, called the *nuclear envelope*. The finishing steps of ribosome production take place in the so called nucleolus within the cell nucleus. Most importantly, the cell nucleus contains the chromatin structure, which is a combination of a plethora of auxiliary proteins and the DNA that encodes our genetic information [48, 100].
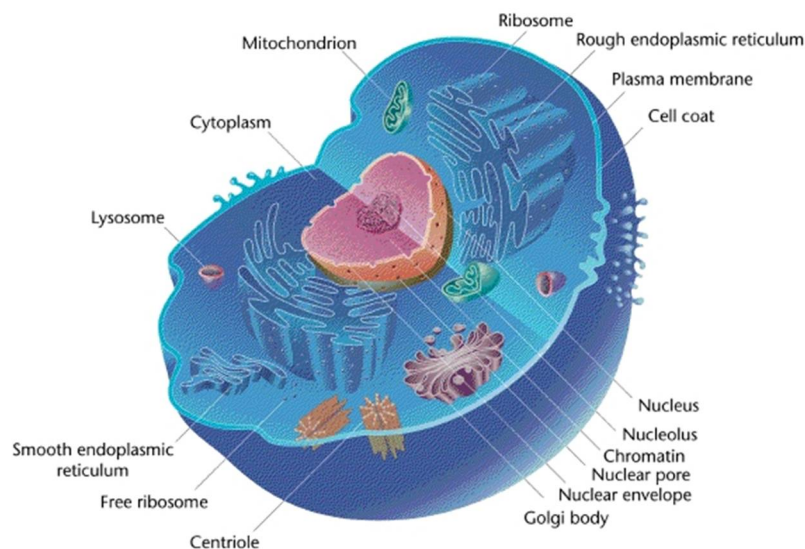


Figure 2.10: Schematic of an eukaryotic cell. Taken from [101].

### Direct and Indirect Damage

Damages inflicted on cellular components by ionizing radiation are generally divided into *direct* and *indirect* damage. When a macromolecule directly interacts with a component of the radiation field and is damaged in the process, one speaks

of direct damage. In contrast, indirect damage is mediated by highly reactive chemical species (e.g. radicals). These are produced via radiolysis in the cytosol and primarily include: $e_{aq}, H^\bullet, HO^\bullet, H^+, OH^-, H_2, H_2O_2$ [48], where the effect of the hydroxyl radicals $HO^\bullet$ is often seen as the main mediator of damage [102]. The timescale in which direct damages take place is about $10^{-16}$ s to $10^{-13}$ s, while the timescale of indirect damages being induced has been found to be about $10^{-12}$ s to $10^{-6}$ s [48, 49]. Furthermore, it was shown, that the contribution of the indirect damage to cell killing decreases with increasing LET of charged particle irradiation (Figure 2.11) [103].
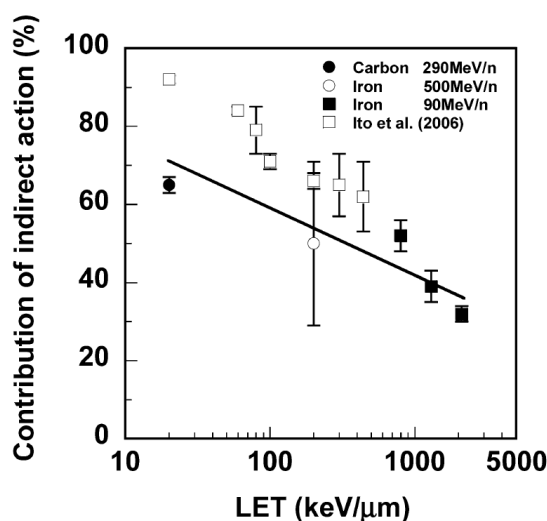


Figure 2.11: The contribution of the indirect damage to cell killing reduces with increasing LET for charged particles. Taken from [103] includes data from [104].

### Primary Effects of Ionizing Radiation

Outside of the cell nucleus, lipids and proteins are the two most important types of macromolecules damaged by ionizing radiation. Damage inflicted on lipids can cause numerous issues connected to the central role they play in membranes, including the disruption of ion gradients and transmembrane processes, the uncontrolled increase in permeability of membranes as well as the altered activity of membrane-associated proteins. This so called lipid stress can trigger cell *apoptosis* and in severe cases even *membrane lysis* and *necrosis*[1]. Proteins that are damaged by ionizing radiation can, to varying extent, lose their functionality [105], which can potentially disrupt biochemical processes such as synthesis, transport and signaling. Ultimately, the

---

[1]These types of cell death will be discussed further below.

cell is able to withstand large amounts of damages inflicted on lipids and proteins, primarily due to their large initial amount and the possibility of replacing them via resynthesization [106]. This is however not the case for the DNA, which makes the cell nucleus up to $10^6$ times more radiosensitive in comparison to the rest of the cell [49, 106].

## 2.3.2 DNA Damage: Types, Response and Consequences

**DNA Structure**

The general structure of the DNA molecule (Fig. 2.12) comprises a double-helical polymer of sugar-phosphate compounds that are connected by pairs of nitrogenous bases: the *purine* bases *adenine* and *guanine* as well as the *pyrimidine* bases *thymine* and *cytosine*. Each base has a fixed counterpart: Adenine and thymine are coupled by a double-hydrogen-bridge-bond, while guanine and cytosine are linked by a triple-hydrogen-bridge-bond (Fig. 2.12). The sequence of these base pairs within the DNA encode the genetic information of an organism [48]. The diameter of the DNA-molecule is about 2 nm and the double-helix takes a full turn every 10 base pairs (bp), corresponding to about 3.4 nm [100].
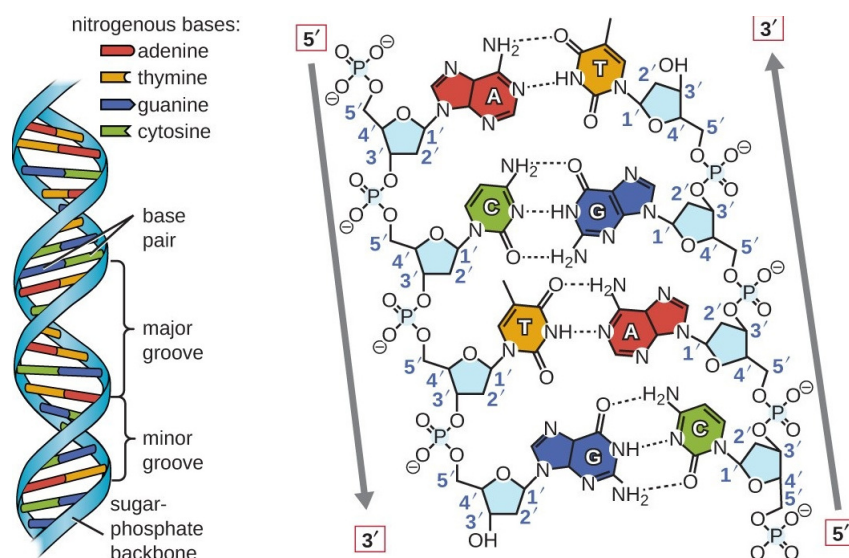


Figure 2.12: left: The double-helical structure of the DNA molecule. right: The chemical structure of the sugar-phosphate backbone and linking base pairs. Taken from [107].

Within the cell nucleus, the DNA is found in a modified and condensed state, which ultimately shortens its extension by a factor of about 10 000 (Fig. 2.13). In an

initial step, the DNA is partly wrapped around specialized proteins called histones, leading to the so called beads-on-a-string form. Subsequently, this structure is further coiled up in to a solenoid form with a diameter of about $25 - 30$ nm. When the cell initiates cell division (mitosis), the structure is further coiled up into a super-solenoid with a diameter of about $700$ nm. Outside of mitotic phases, actively used parts of the DNA are kept in a more relaxed and extended form (*euchromatin*), while less active portions are kept in the high condensation form (*heterochromatin*) [48, 100].
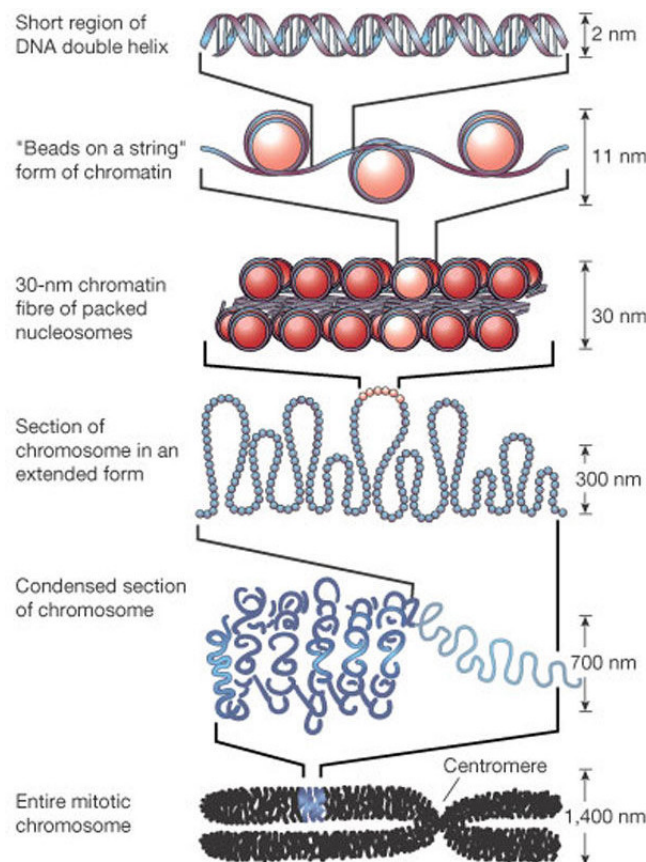


Figure 2.13: The different levels of compactification of the DNA. Taken from [108].

**DNA Damage Types and Response Mechanisms**

Depending on the location and the type of damage, the cell activates different repair pathways. Damages can either affect the linking bases or the sugar-phosphate backbone of the DNA. In the former target, ionizing radiation can lead to mismatch of the bases or their chemical alteration, the loss of an entire base, a *pyrimidine dimerisation* (bond between neighboring pyrmidine bases) or a base crosslink. Base mismatches are routinely double checked during DNA polymerization and chemical

alterations can be directly detected and repaired by specialized enzymes. For the other damage types a more complex repair machinery is activated. If only one base is damaged (e.g. a base loss), the corresponding location is detected by the *glykosy-lase* enzyme and the damaged base is replaced by the collected effort of numerous enzymes, including the *insertase* enzyme. The so called short-strand excision pathway is activated if several base pairs are damaged in close vicinity. In this case the *endonuclease* enzyme is responsible for removing the DNA strand containing the damaged base pairs. After the removal, the *DNA-polymerase* resynthesizes the correct base sequence based on the corresponding base pairs on the other DNA strand. Ultimately, the *DNA-ligase* connects the ends of the repaired sequence to the surrounding DNA. However, in the case that the cell was not able to repair such base damages before entering cell division, it can activate the so called postreplicative recombination repair if the DNA has already been replicated. In a process called partial recombination, the intact DNA sequence homologous to the damaged area is then transferred from the sister strand to the location of the damage. As a consequence, both double strands contain one intact and one damaged base combination, which can finally be resolved via short-strand excision repair [48].

Also for damages in the sugar-phosphate backbone of the DNA, several distinct types of damages and responses exist. Breakage of only one DNA strand is termed a single strand break (SSB) and are detected by the *poly-(ADP-ribose)-polymerase* (PARP) enzyme. Their detection triggers a repair machinery comparable to that of the short strand excision repair mentioned earlier, where the site surrounding the damage is cut out and resynthesized based on the undamaged opposing DNA strand [48, 109]. The damage that is thought to be the most lethal type of DNA damage, which triggers a highly complex response, including numerous detection, mediation and repair mechanisms [48, 109, 110] is the breakage of both DNA strands in close vicinity, a so called double strand break (DSB). While the cellular response to DSB goes far beyond it, a possible part of its effort to repair the induced damage could look as the following (Fig. 2.14): After the DSB has been detected by the *Mre11-Rad50-Nbs1-complex* protein (MRN-complex), it begins to recruit the protein kinase *ataxia telangiectasia mutated* (ATM) to the damage site. ATM is the starting point of two pathways: Firstly, it activates the *checkpoint kinase 2* (chk2), which in turn leads to the stabilization of the p53 protein. The stabilized p53 then fulfills its role as a transcription factor of p21, leading to its increased expression.

The p21 enzyme inactivates the *cyclin dependent kinase 2* (cdk2), which arrests the cell cycle. This grants the cell additional time to process the DSB. Secondly, ATM facilitates the phosphorylation of the histone protein *H2A.X* to $\gamma H2A$. Through a certain signaling cascade this leads to the recruitment of 53BP1 enzymes to the damage site. Depending on the activity of 53BP1 the cell chooses between the two main DSB repair pathways: *non-homologous end-joining* (NHEJ) and *homologous recombination* (HR) [100, 111, 112].
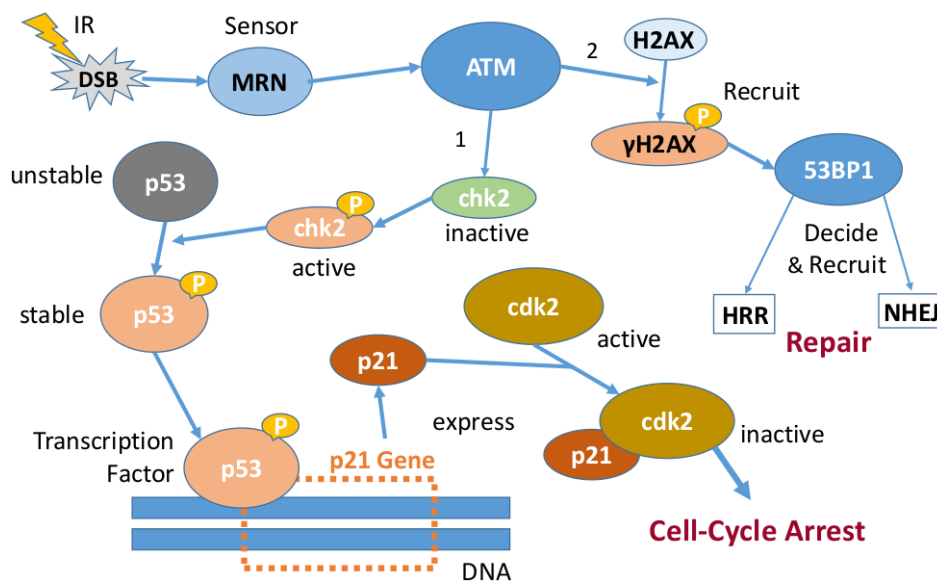


Figure 2.14: One possible pathway of DSB response, leading to cell-cycle arrest and initiation of damage repair. Created based on [100, 111, 112].

The HR repair pathway goes through four major phases (Fig. 2.15). In the first phase, the free ends of the broken double strands are resected and prepared. In the second phase, the double strands that have been damages by the irradiation *invade* the undamaged sister-chromatin at the location homologous to the damaged sequence. Thus, the cell can only resort to HR in phases where the DNA has already been replicated and the cell division has not yet been completed. In the third phase, based on the information on the sister-chromatin, the resected sequence on the damaged chromatin is resynthesized. In the final phase, the so called Holliday junctions that resulted from the strand invasion are resolved [16, 48]. Noteworthy enzymes involved in the HR repair pathway are the *breastcancer 1* (BRCA1), *breastcancer 2* (BRCA2) and Rad51 proteins [8, 46, 112].

In contrast to the HR pathway, the NHEJ repair process is possible even without
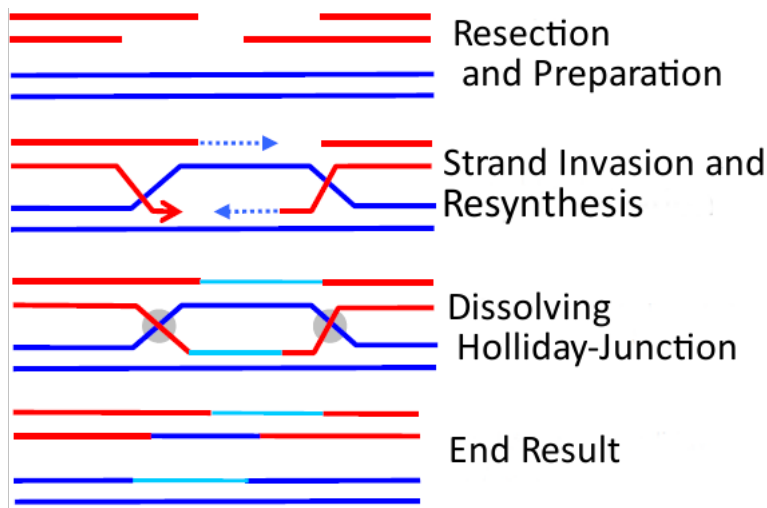
Figure 2.15: The key steps of homologous recombination repair. Modified from [48].

the presence of a sister-chromatin. Thus, it is available throughout each cell cycle phase and is responsible for the majority of the DSB repaired in a cell [16]. In the first phase after the initiation of NHEJ repair (Fig. 2.16), Ku70 and Ku80 proteins attach to the open ends of the double-strands. Their main role is to recruit copies of the *DNA dependent protein kinase catalytic subunit* (DNA-PKcs), which in turn triggers a response by other repair proteins such as the MRN-complex or *Artemis*. These enzymes then proceed to process the open ends of the double-strands. Following this preparation, the *Ligase IV* reconnects the severed ends of the DNA double-strands [16, 113]. While it allows the NHEJ to be active throughout the cell cycle, the absence of an intact blueprint makes it an error-prone repair in comparison to HR. The efficiency of NHEJ repair is thus reduced for complex DNA damages that might include several lesions in close vicinity [16].
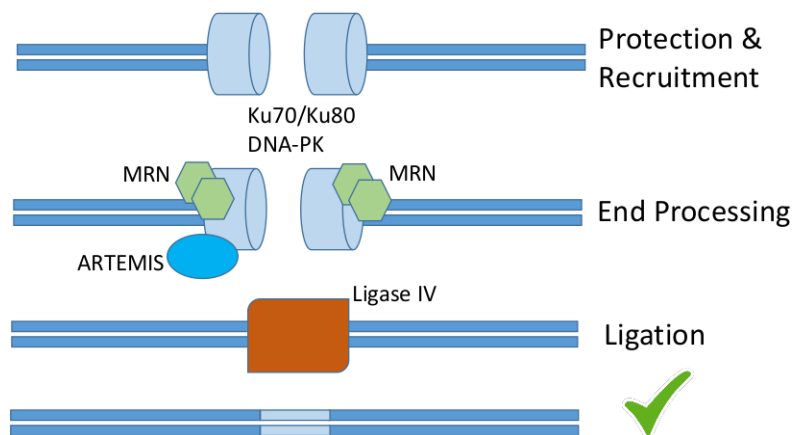


Figure 2.16: The key steps of non-homologous end-joining. Reconstructed from [16, 113].

**DNA Damage Consequences**

If the cell is unable to properly repair DNA damages by the processes mentioned earlier, it can have various consequences. One of the possible effects might be the alteration of the stored genetic information leading to mutations that might modify the structure and functionality of the encoded proteins. While mutations induced in germ cells can be passed on to the offspring, mutations in somatic cells can jeopardize the vitality of the cell or even lead to a malignant transformation [48]. Such a transformation can be induced by the inactivation of *tumor suppressor genes* or the mutation of *proto-oncogenes* to *oncogenes*. As their name implies, proteins derived from tumor suppressor genes (e.g., p53) are key enzymes involved with processes that suppress malignant behavior, such as DNA-damage repair. Should its activity be hampered by a mutation, the protein does no longer act as a *brake* to the possible development of tumors. On the other hand, the majority of proteins encoded by proto-oncogenes are involved in signaling pathways that promote cell proliferation. For example, the normal function of the *Ras* enzyme is to prompt a cell to initiate cell division after receiving a corresponding signal from another enzyme. If the proto-oncogene that encodes Ras mutates to its oncogene-version, the modified Ras protein continues to drive cell division even without any outside trigger. Therefore, oncogenes are often referred to as *accelerators* of malignant behavior [100]. Both the loss of function mutations in tumor-suppressor genes and the transformation of proto-oncogenes to oncogenes are believed to be key factors in the emergence of cancers [100, 109].

Among other things, to suppress the development of tumors, the cell initiates a controlled *suicide program* called apoptosis, when it senses a large amount of DNA damage. While this form of cell death can be triggered by a number of factors, one of the most prominent pathways in the context of DNA damage was found to be the following: As described earlier, p53 is stabilized in cells which have detected DSB. Besides its other effects, p53 also upregulates the expression of the pro-apoptotic protein *Bcl-2-associated X* (BAX). The accumulation of BAX leads to the release of *cytochrome c* from the mitochondria into the cytosol, triggering the so called caspase cascade, the activation of a plethora of proteases (caspases) designed to selectively disintegrate all cell structures. Ultimately, neighboring cells take up the dissolved remains of cells that underwent apoptosis [100, 109, 114].

If DSB are not repaired before the cell initiates mitosis they can cause chromosome aberrations when the DNA is condensed. Depending on whether aberrations occur within one chromosome or include two different chromosomes, one differentiates between so called *intrachromosomal* and *interchromosomal* aberrations, respectively. In the case of intrachromosomal aberrations the loss (*deletion*) of parts of one or both chromatides, the shift (*translocation*) of parts of the chromosome, and the emergence of rings formed out of parts of the chromosome can occur. On the other hand, the asymmetrical interchromosomal exchange of chromatide parts resulting in a dicentric chromosome and mixed fragments as well as reciprocal translocation of terminal parts of the chromosomes are examples of interchromosomal aberrations. While chromosomal aberrations can generally lead to mutations or the complete loss of genetic information, together with other forms of DNA damage which alter the geometrical conformation of the DNA molecule, they can also cause a failure of the cell division process, a so called mitotic catastrophe [48]. Similar to apoptosis, such an even ultimately leads to cell death [115].

In the previous paragraphs a simplified image was created in which the cell dies either by recognizing the severity of the damage and inducing apoptosis or by missing to recognize unrepaired damage prior to mitosis and falling victim to a mitotic catastrophe. In practice one is often less interested in the complete *destruction* of the cell, but rather in its loss of ability to further divide, its so called clonogenic potential. This can temporarily be the case, when the cell enters the reversible state of *senescence*, a *sleeping* state. Furthermore, cell death pathways such as *autophagy* or *necrosis*, that were believed to be largely *uncontrolled* in stark contrast to the *controlled* or *orchestrated* mode of apoptosis, were lately shown to be much more regulated processes that are partly related and could thus be triggered by the cell as reaction to DNA damage, too. However, the exact biochemical reactions and signaling pathways that govern these processes and decide between the mentioned pathways towards loss of the clonogenic potential are still unclear and subject to active research [8, 116, 117].

## 2.3.3 Factors Influencing the Biological Effects of Ionizing Radiation

There are numerous factors which can influence the biological effects of ionizing radiation, including the morphological differentiation grade of cells, their cell cycle status or even the temperature of the medium during irradiation [48]. In the following subsections the focus will be put on those factors relevant for the thesis on hand.

**Dose**

The dependency of the biological effect on the physical dose is probably the most fundamental dependency described in radiobiology. This dependency is most frequently presented in the form of *cell-survival curves*, which show the applied physical dose on the abscissa and the logarithm of the surviving fraction (often simply termed *survival*) $S$ on the ordinate. The survival fraction is often obtained using *clonogenic assays* in which the survival fraction is defined as:

$$S := \frac{\left(\frac{\text{Cells forming colonies}}{\text{Cells seeded}}\right)_{\text{Post-IR}}}{\left(\frac{\text{Cells forming colonies}}{\text{Cells seeded}}\right)_{\text{Control}}}. \tag{2.17}$$

It is noteworthy, that *survival* is defined here to be the ability of a cells to form a colonies and is thus a measure of the clonogenic potential of a cell population (mentioned in the section above) and that the survival fraction can also be interpreted as the probability of one cell in a given population to form a colony. It has become the norm to describe the resulting survival curves using the *linear-quadratic model* (LQM):

$$S(D) = exp(-\alpha D - \beta D^2), \tag{2.18}$$

where D is the applied dose and $\alpha$ and $\beta$ are empirically determined factors [118]. The ratio of both constants, $\alpha/\beta$, has been used to describe and compare the characteristics of cell survival over the different cell lines: The survival curves of cell lines with small $\alpha/\beta$ show a pronounced shoulder shape, indicating an increased capacity to repair damages. On the other side, survival curves of cell lines with comparably large $\alpha/\beta$ exhibit a more linear form, indicating reduced repair capacity [119](Fig. 2.17).

The exponent in Equation 2.18 can be interpreted as the expected (or mean)
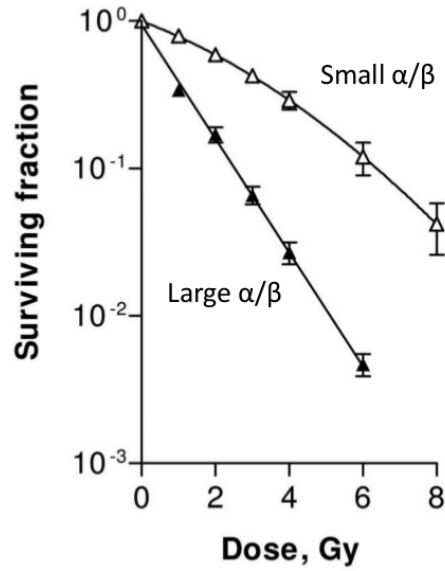


Figure 2.17: Typical cell survival curves of large and small $\alpha/\beta$ cell lines. Taken and modified from [120].

amount of lesions which lead to the loss of clonogenic potential for a cell. These lesions are commonly referred to as *lethal lesions* (LL). Assuming these to occur following a Poisson distribution $P(n)$, the probability of having no LL ($n = 0$) and thus *surviving* the irradiation is:

$$S(D) = \mathrm{P}(0) = exp(-\langle LL(D)\rangle), \qquad (2.19)$$

where $\langle LL(D)\rangle$ is the expected number of lethal lesions at the given dose. With the lack of a true biological meaning to its parameters, the LQM could be seen as a low-dose approximation or Taylor expansion of the function $\langle LL(D)\rangle$ [118, 121].

**Radiation Type/Quality**

In most cases, high-LET radiation exhibits a higher potential for cell inactivation per applied unit dose compared to low-LET irradiation, including per definition photon irradiation [15, 16]. This is reflected by the fact that cell survival curves after irradiation with high-LET beams show a steeper and more linear form [48]. The *relative biological effectiveness* (RBE) is used to quantify the enhanced biological effectiveness of a given irradiation in comparison to a conventional low-LET setup. The RBE is defined as the ratio of the applied dose by a low-LET reference field

$D_{ref}$ and the applied dose of the radiation type of interest $D_x$, leading to the same biological effect (Fig. 2.18):

$$\text{RBE} = \frac{D_{ref}}{D_x}\bigg|_{\text{iso-effect}}. \tag{2.20}$$

Often a $250\,\text{kV}$ x-ray source or a Co-60 $\gamma$ source is used as the low-LET reference field [48].
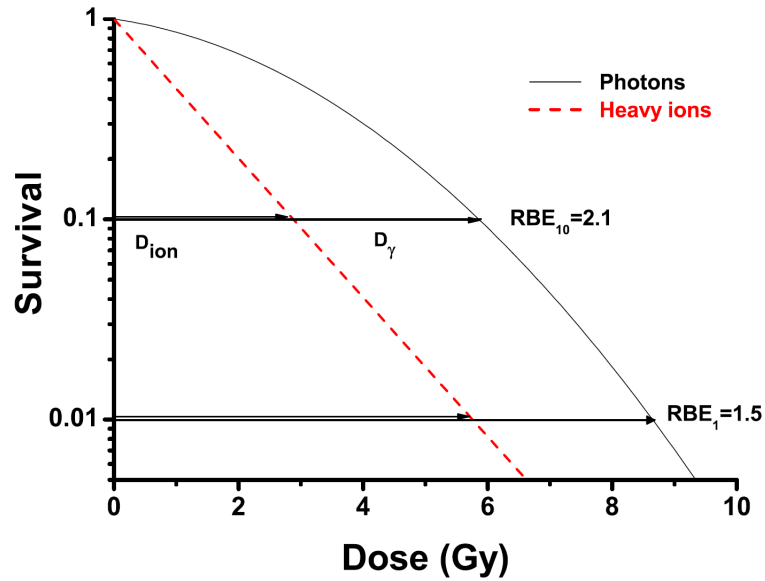


Figure 2.18: Heavy-ions usually show an enhanced cell killing potential with steeper and more linear cell survival curves in comparison to conventional photon irradiation. This effect can be quantified with the RBE, which depends on several factors, such as the applied dose or the biological endpoint. Taken from [15].

The exact value of the RBE is influenced by numerous factors: As the survival curves of the reference radiation and radiation of interest can have different curvature, the RBE can change depending on the applied dose (Fig. 2.18). When the effect of heavy-ions is compared to a low-LET reference radiation, the RBE usually decreases with increasing dose. Furthermore, the measured RBE can change when different tissues or cell lines are used as targets of the irradiation. In addition, the value of RBE is dependent on the *biological endpoint* on which it is based. The biological endpoint is the exact biological measure that is used to compare the irradiation types. For example, the RBE based on the 10% survival might differ from the RBE based on the 1% survival after irradiation (Fig. 2.18). Finally, the RBE strongly depends on the particle types and their LET contained in the radiation

field of interest [15].

The important dependency of RBE on the LET is often explained as follows: Radiation fields with a very low-LET, such as photon radiation used in conventional radiotherapy, induce a homogeneous ionization density throughout the target. Furthermore, within a cell, its effect is mainly based on indirect damage which is driven by reactive chemical species. Ultimately, the induced damages are randomly spread over the DNA and are separated by large distances after irradiation with a low-LET source [15, 16]. In contrast, the increasing stopping power and decreasing diameter of the RDD of an ion track towards higher LET leads to an increasing ionization density around the tracks trajectory [122]. When the DNA molecule, especially in its condensed form, is hit with such densely ionizing particle tracks, multiple spatially correlated DNA lesions can be induced. With increasing ionization density the complexity as well as probability of inducing such clustered damages rises (Figure 2.19).
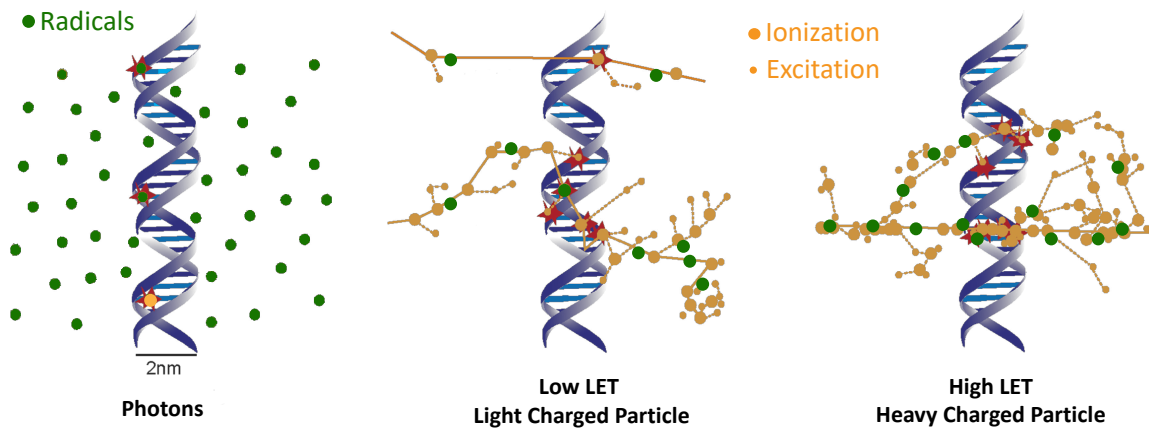


Figure 2.19: Schematic representation of the increasing induction of clustered damages towards higher-LET radiation. Modified from [110] and [123].

Compared to isolated lesions, clustered damages are repaired slower, less accurately and less completely, ultimately leading to the enhanced biological effectiveness of high-LET radiation [16, 110]. While experiments have shown an initial increase of RBE with the LET, they also observed a drop-off of the RBE beyond a certain LET value leading to a "bell-shaped" form of the RBE-LET dependency (Fig. 2.20) [16].

This trend can be explained by the *overkill effect*: At a given LET value, the passage of a single track is able to trigger the desired effect (e.g., taking the clonogenic potential from a cell). Any additional dose delivered by a further increase in LET would not add any effect and is wasted [15, 122]. The LET value at which the RBE reaches its maximum depends on the type of particle (Fig. 2.20). Considering the RBE maximum of a given ion species, an ion with a higher charge might have the same LET, yet if it has a higher mass, it carries a higher kinetic energy, resulting in a broader track structure with a lower ionization density. Thus, to achieve a comparable ionization density and biological effect, an ion with a higher charge (and higher mass) need to reach a higher LET, reducing its kinetic energy and the lateral extension of the RDD [15].
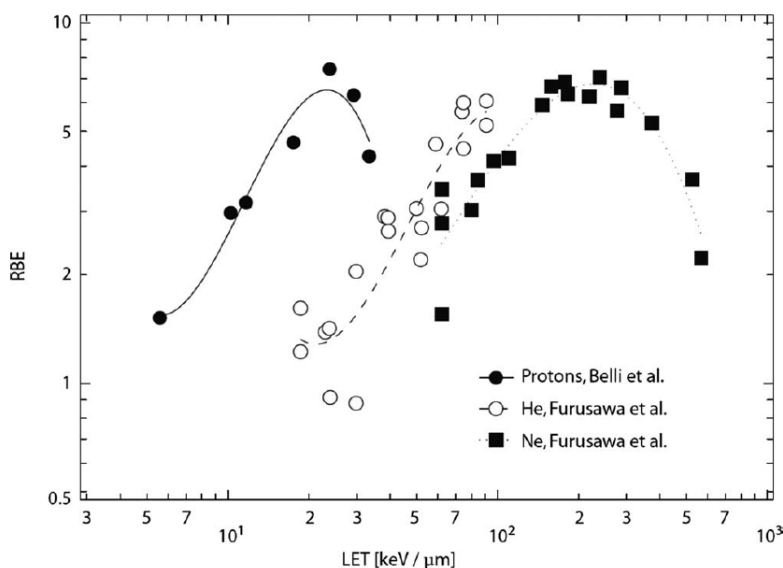


Figure 2.20: $RBE_\alpha = \alpha_{ion}/\alpha$ over LET for protons, helium ions and neon ions. $\alpha$ and $\alpha_{ion}$ are the factors taken from the survival curves of the reference radiation and ions, respectively [15]. Taken from [124] where the data has been taken from [125] and [126].

**Oxygen Effect**

Cells under low oxygen concentrations (hypoxia) exhibit larger radioresistence in comparison to cells under atmospheric oxygen concentrations (normoxia) (Fig. 2.21). The effect is most frequently explained by the *oxygen fixation hypothesis*: Radicals that are induced in the DNA can react with free $H^+$ to return to their former chemical form (*chemical repair*). However, the radicals can also react with free molecular oxygen, resulting in a configuration no longer able to be resolved chemically by $H^+$,
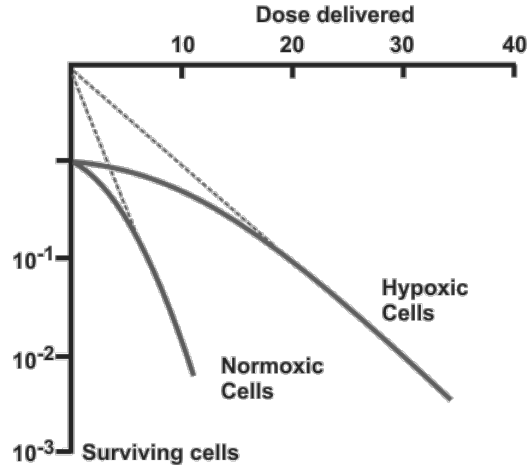
Figure 2.21: Hypoxic tissue exhibits larger radioresistence in comparison to normoxic tissue. Taken from [127].

which is thus *fixated* and needs to be repaired by the cells repair machinery [8]. Experiments in the late 1970s [128, 129] revealed, that the fixation process is not instantaneous but follows a decay kinetic with a half-life time of about 1ms. Further, it could be shown, that the oxygen effect is mainly mediated by the radical mediated indirect mode of damage and the direct damage action is only slightly affected [51]. The oxygen enhancement ratio (OER) is used to quantify the effect and is defined as:

$$\text{OER} = \left.\frac{D_{hypoxia}}{D_{normoxia}}\right|_{\text{iso-effect}}, \tag{2.21}$$

where $D_{hypoxia}$ is the applied dose needed for irradiation under hypoxia to reach the same effect as the dose applied under normoxia $D_{normoxia}$.

The dependency of the OER from the oxygen concentration can be parametrized by a function proposed by Carlson [130] (motivated by the original study of Alper and Howards-Flanders [131]):

$$OER\left([O_2]\right) = \frac{mK + [O_2]}{K + [O_2]}, \tag{2.22}$$

where $m$ is the maximum OER and $K$ the concentration at which the OER reaches $m/2$. The dependency is illustrated in Figure 2.22.

An increase in LET is generally accompanied by a decrease in OER(Figure 2.23). This is commonly explained by the fact, that high-LET radiation predominantly unfolds its effect by the induction of directly induced damage and thus being relatively independent of radical mediated indirect damage. Therefore, heavy-ion is regarded
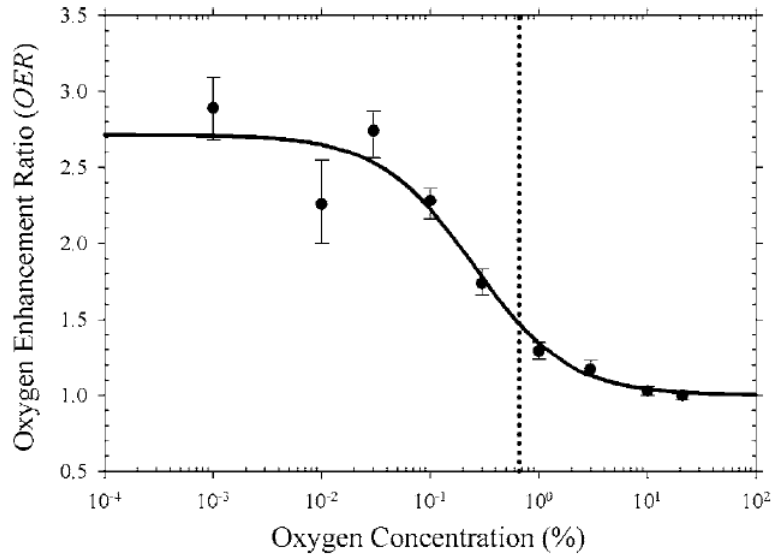
Figure 2.22: The dependency of the OER from the oxygen concentration. The data represents values derived from survival data using V79 cells. The line is given by Equation 2.22 with $m = 2.7$ and $K = 0.25$. Taken from [130], where the data was taken from [132]. The dotted line was included in the original publication to show the oxygen concentration below which tumor cells are characterized as being hypoxic in the clinical study of [133].

as a promising tool to treat hypoxic tumors. [15, 16]

**Dose-Rate**

When discussing the effect of the applied dose-rate on the biological effect of an irradiation, one needs to differentiate between the *classical* dose-rate effect and the *ultra-high* dose-rate (uHDR) effect.

The amount of DSB after irradiation was shown to be reduced by repair in a biphasic exponential fashion over time, with a shorter half-life time in the order of minutes and a longer half-life time in the order of hours [135–137]. The slower component is believed to be associated to clustered damages [138, 139]. This leads to a steadily increased survival of cells when the dose-rate of the applied radiation is decreased from a couple of Gy per minute (range of conventional medical applications) down to fractions of a Gy per hour [55], as more lesions can be removed and the creation of complex damage is suppressed.

Starting in the late 1960s and into the early 1980s a number of publications showed, that cells [56, 57, 129, 140–142] and tissue [143, 144] exhibit increased radio-resistance when irradiated with uHDR exceeding tens of Gy per second at sufficiently high
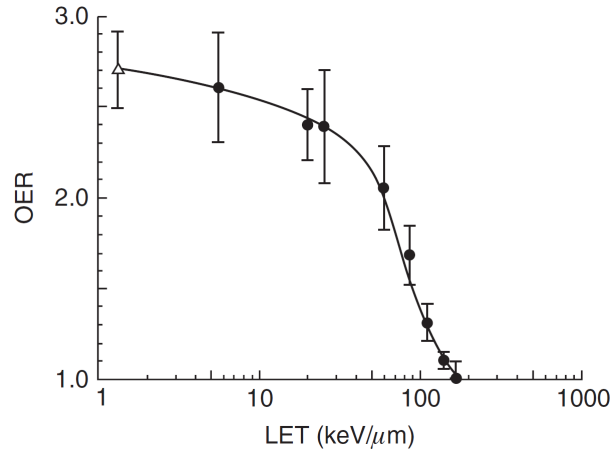
Figure 2.23: The OER generally decreases with increasing LET of a charged particle. The circles refer to monoenergetic $\alpha$ particles and deuterons, while the open triangle refers to a 250kV X-ray source. Taken from [8], where it was taken from [134].

doses ($\gtrsim 10$ Gy). The application of uHDR has been experiencing a renaissance since the mid-2010s, when first studies were published which showed sparing of normal tissue while the effect on the tumor remained at the level of standard dose-rates (SDR), dubbed the *FLASH* effect [58–60]. Since then, also the debate surrounding the underlying mechanisms of the sparing at uHDR in general was reignited: The emergence of sparing at hypoxia but not at normoxia or anoxia (absence of oxygen) [140–143, 145, 146] has been seen by many to be an indicator that oxygen must play a central role. While the theory of radiochemical depletion of oxygen and the resulting transient hypoxia was one of the first to be formulated [56, 142] and remains to be considered to atleast explain part of the sparing [59, 60, 147, 148], some have expressed their doubts about the consistency of this hypothesis [149], proposing alternative mechanisms such as a reduction of radicals by radical-radical interactions [150] or radical clustering [151]. Concerning the differential sparing of normal tissue and tumor (the FLASH effect), several hypothesis were put forward, including differential oxygenation status and its spatial distribution, processing of radicals, repair of DNA damage or even immune system response between normal tissue and the tumor [60, 147, 152, 153]. However, none has gained widespread acceptance yet.

Most uHDR studies were - and are - conducted using electron beams, while studies involving ion beams remain sparse due to technical challenges [60, 154, 155]. For protons, an in-vitro study applying 4.5 MeV particles under atmospheric oxygen concentration found no difference in cell survival or DNA damage induction

between standard dose-rate (SDR) and uHDR irradiations [156], while an in-vivo study applying a 230 MeV beam was able to show the FLASH effect in mice [157]. Our group published the first experimental study applying helium ions (4.5 keV/µm and 16 keV/µm) to cells at uHDR and could show increased survival and reduced DNA damage being induced in comparison to SDR irradiations under hypoxia but not under normoxia [154](Figure 2.24). In regards to carbon ions, the first in-vitro study was published in cooperation with our division, using a 280 MeV/u beam at the GSI [158]. The study showed an oxygen dependent increase of cell survival for the uHDR setting that reached its maximum at 0.5% oxygen. At normoxia and anoxia no sparing was observed. Shortly after, simultaneous sparing of normal tissue and improved tumor control was observed at the same facility applying a 240 MeV/u carbon beam at uHDR in comparison to SDR [159].
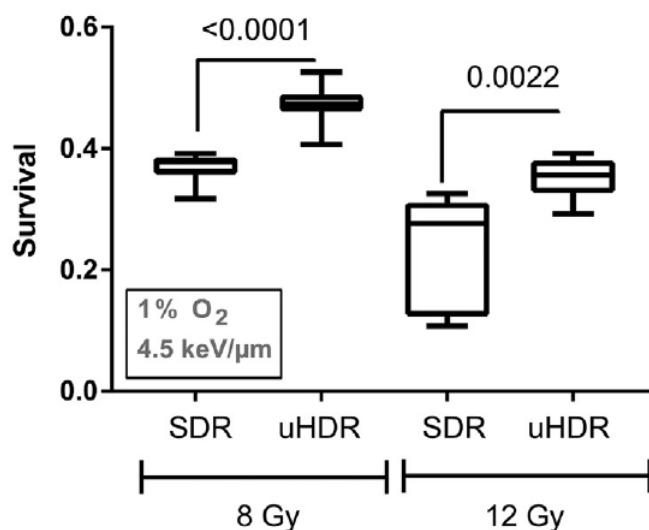


Figure 2.24: The survival of A549 cells after irradiation with 8Gy and 12 Gy of 4.5 keV/µm helium ions using a standard dose-rate of 0.12-0.21 Gy/s (SDR) and ultra-high dose-rate of 139-216 Gy/s (uHDR) under 1% oxygen. The p-value was computed using 2-tailed unpaired Student t-test. Taken from [154].

## DNA Damage Response Interference

As described earlier, the damage to the DNA is resolved by an intricate repair machinery consisting of a network of enzymes. Inhibition or lack of these would thus significantly hamper the cells ability to retain its clonogenic potential after exposure to ionizing radiation (or any other DNA damaging agent). Pharmacological inhibition of key DNA damage repair (DDR) enzymes has therefore been

seen as a potential mechanism to improve the efficacy of ionizing radiation against their cellular targets. Inhibitors have been developed against ATM as one of the key DSB detector proteins [38, 39, 42, 160] as well as against key enzymes of the NHEJ and HR pathways, such as DNA-PK [40, 42] and Rad51 [41]], respectively. Several inhibitors against the named proteins have even progressed into pre-clinical (animal model) [43–46] and clinical trials [45–47]. Key DDR proteins can also be under-expressed or even inactivated by mutations in tumors [46]. A loss-of-function mutation of the ATM enzyme was found to improve the tumor control after radiotherapy across different types of cancer [30]. Furthermore, low activity of the enzymes DNAPK and Ku70, key contributors in NHEJ, have been linked to increased tumor control in prostate cancer patients [31, 32] and the improved therapy outcome of radiotherapy for HPV positive head and neck cancer patients has been correlated to the suppression of an array of proteins involved in both main DSB repair pathways [33–35].

In radiobiology the effect of radiosensitizing agents or mutations is usually characterized using the concept of the *sensitivity enhancement ratio* (SER). The concept is very similar to the RBE as it describes the ratio between the applied dose to the non-treated or wild type (non-mutated) system $D_{ref}$ and the applied dose to the treated or mutated (modified) system $D_{mod}$, leading to the same biological effect (Fig. 2.18). In mathematical form:

$$\text{SER} = \left.\frac{D_{ref}}{D_{mod}}\right|_{\text{iso-effect}}. \tag{2.23}$$

Besides the dependency on the applied modification, usually, the value of the SER depends on the applied dose and the investigated endpoint.

The interplay of DDR interference and charged particle irradiation is subject of ongoing research: On the one hand, the RBE of carbon ions was found to be reduced in a NHEJ deficient cell-line in comparison to the wild type cell-line [161] as well as in HPV-positive cell-lines when compared to HPV-negative cell-lines [162, 163]. As mentioned earlier, HPV-positive cell-lines were shown to have numerous DDR defects [33–35]. In addition, the RBE of protons at 9.9 keV/µm was found to decrease with increasing DDR interference using a panel of DDR inhibitors, including DNA-PKcs, PARP, Rad 51 and ATM [164]. Furthermore, experimental data included in this thesis suggest a reduced RBE of helium ions when DNA-PKcs or ATM is

suppressed as well as a reduction of SER with increasing helium ion LET [165]. On the other hand, proton RBE was found to be increased in lung cancer cell lines with defective HR or the closely related *Fanconi Anemia* pathway [166]. Furthermore, HR interference based on the suppression of BRCA1 lead to an increased radiosensitivity at moderately high proton LET (4 and 7keV/µm) but not at low LET (1-2.2keV/µm) [167, 168].

**Radical Scavengers**

As mentioned earlier, a substantial amount of the damage produced by ionizing radiation is mediated by highly reactive chemical species including radicals. *Radical scavengers* are compounds able to neutralize the radicals and thus protect the DNA from indirect damage. Cells contain *built-in* radical scavengers such as vitamin E [169] or express radical scavenging enzymes such as *superoxide dismutase* and *catalase* [52, 53]. Furthermore, pharmacological research has went into several compounds that could act as radical scavengers, in order to reduce the damage burden on normal tissue [53, 54]. In radiobiological studies *dimethyl sulfoxide* (DMSO) has been used for decades as effective hydroxyl radical scavenger [51, 103, 170–173]. It has been used extensively to investigate the fraction of indirect damage induced by different radiation qualities, proving the reduction of indirect damage fraction with increasing LET [51, 103, 170] (Fig. 2.11).

## 2.4 Models of Radiation Action

In this section, the most relevant existing models of radiation action shall be described. All of the described approaches are atleast guided by a mechanistic understanding of radiation action. As the developments within this thesis fall into the same category, purely phenomenological approaches are not considered.

### 2.4.1 Theory of Dual Radiation Action and Mixed Field Model

The *theory of dual radiation action* (TDRA) was first formulated by Kellerer and Rossi in 1972 in order to provide a theoretical basis for the linear-quadratic form of cell survival curves [174]. The description of the combined effect of two or more

simultaneous exposures to ionizing radiation derived on the basis of TDRA has been widely adopted and is still frequently applied in order to describe the effect of mixed fields [175, 176]. Here, the derivation of this mixed field model shall be presented based on [177]:

In the TDRA the yield of so called sublesions is given by $cz$, the product of a constant $c$ and the specific energy $z$. The specific energy is defined by the energy imparted by a microscopic volume divided by its mass and thus represents the stochastical dose on the micro scale [49]. The sublesions are thought to interact pairwise to create the lethal lesions. With the interaction probability $A$ and $k = Ac^2$, the yield of lethal lesions can be written as:

$$LL(z) = Ac^2 z^2 = kz^2. \tag{2.24}$$

As the specific energy follows a stochastic distribution, for a given macroscopic dose $D$ one can determine the average number of lethal lesions to be:

$$\langle LL(D) \rangle = \int LL(z) f(z; D) dz. \tag{2.25}$$

The distribution $f(z; D)$ describes probability of the specific energy to be within $z$ and $z + dz$ as a function of the macroscopic dose and satisfies following conditions:

$$\int f(z; D) dz = 1 \tag{2.26}$$

and

$$\int z \cdot f(z; D) dz = D. \tag{2.27}$$

Furthermore, Kellerer and Rossi could show, that under given assumptions the average number of lethal lesions could also be written as [178]

$$\langle LL(D) \rangle = k(z_{1D} D + D^2), \tag{2.28}$$

where $z_{1D}$ is the dose averaged specific energy imparted through single events.

When two different radiation qualities are applied simultaneously, the yield of sublesions is assumed to be additive ($= c_1 z_1 + c_2 z_2$), so that the yield of lethal lesions can be written as:

$$LL(z_1, z_2) = A \left( c_1 z_1 + c_2 z_2 \right)^2 = \left( \sqrt{k_1} z_1 + \sqrt{k_2} z_2 \right)^2. \tag{2.29}$$

The dose dependent formulation can be written as:

$$\langle LL(D_1, D_2) \rangle = \int \int LL(z_1, z_2) f(z_1, z_2; D_1, D_2) dz_1 dz_2. \qquad (2.30)$$

However, if one assumes the specific energies of both irradiations to appear independently, one can write:

$$f(z_1, z_2; D_1, D_2) dz_1 dz_2 = f_1(z_1; D_1) \cdot f_2(z_2; D_2). \qquad (2.31)$$

Inserting Equation 2.29 into Equation 2.30 and using Equation 2.31, one yields:

$$\langle LL(D_1, D_2) \rangle = \int \int \left( \sqrt{k_1} z_1 + \sqrt{k_2} z_2 \right)^2 f_1(z_1; D_1) \cdot f_2(z_2; D_2) dz_1 dz_2, \qquad (2.32)$$

which extends to

$$\langle LL(D_1, D_2) \rangle = \int \int \left( k_1 z_1^2 + 2\sqrt{k_1}\sqrt{k_2} z_1 z_2 + k_2 z_2^2 \right) f_1(z_1; D_1) \cdot f_2(z_2; D_2) dz_1 dz_2, \qquad (2.33)$$

redistribution allows the application of Equations 2.24, 2.26 and 2.27:

$$\langle LL(D_1, D_2) \rangle = \int \underbrace{k_1 z_1^2}_{LL(z_1)} f_1(z_1; D_1) dz_1 \underbrace{\int f_2(z_2; D_2) dz_2}_{=1} \qquad (2.34)$$

$$+ 2\sqrt{k_1}\sqrt{k_2} \underbrace{\int z_1 f_1(z_1; D_1) dz_1}_{=D_1} \underbrace{\int z_2 f_2(z_2; D_2) dz_2}_{=D_2} \qquad (2.35)$$

$$+ \int \underbrace{k_2 z_2^2}_{LL(z_2)} f_2(z_2; D_2) dz_2 \underbrace{\int f_1(z_1; D_1) dz_1}_{=1}. \qquad (2.36)$$

Equating the expressions 2.25 and 2.28 one arrives at:

$$\langle LL(D_1, D_2) \rangle = k_1 z_{1D,1} D_1 + k_1 D_1^2 + 2\sqrt{k_1}\sqrt{k_2} D_1 D_2 + k_2 z_{1D,2} D_2 + k_2 D_2^2. \qquad (2.37)$$

Using $\alpha = k \cdot z_{1D}$ and $\beta = k$ and using Equation 2.19, the survival after the mixed irradiation can be written as:

$$S = exp(-\langle LL(D_1, D_2) \rangle) = exp(-(\alpha_1 D_1 + \beta_1 D_1^2 + \alpha_2 D_2 + \beta_2 D_2^2 + 2\sqrt{\beta_1}\sqrt{\beta_2} D_1 D_2)). \qquad (2.38)$$

For a mixed field with $N$ components it can be shown that the survival is given by:

$$S = exp(-\langle LL(D_1, D_2, ..., D_N)\rangle) = exp\left(-\left(\sum_{i=1}^{N}\alpha_i D_i + \left(\sum_{i=1}^{N}\sqrt{\beta_i}D_i\right)^2\right)\right).$$
(2.39)

## 2.4.2 Microdosimetric Kinetic Model

Inspired by the TDRA, Hawkins published *"A Statistical Theory of Cell Killing by Radiation of Varying Linear Energy Transfer"* in 1994 [64, 179], which will later be known as the *Microdosimetric Kinetic Model* (MKM). The MKM is used as the basis for treatment planning in Japanese ion beam therapy facilities [180]. Numerous extensions and modifications of the original model have been proposed (even during the time of writing of this thesis [181]). The description of all these developments would by far exceed the scope of this section and the reader is kindly referred to the publication of Bellinzona et al. for a more extensive review [182]. This section will focus on the original model of Hawkins, key steps that enabled its implementation into treatment planning and some select recent developments.

The following summary of the core model is mainly based on the description by Hawkins published in 2003 [183]. In the MKM the cells nucleus is believed to be subdivided into domains of diameter $d$. Within these, two types of lesions are induced, with both their yields proportional to the specific energy $z$. So called Type I lesions are lethal lesions that are induced with the proportionality constant $\lambda_d$. The so called Type II lesions, induced with the proportionality constant $k_d$, are thought to be able to undergo four kinds of transformations: First, they can convert to lethal lesions by a first order rate constant $a$. Second, they can combine pairwise to lethal lesions with a second order rate constant $b$. Third, they can get repaired by the cell with the first order rate constant c. Fourth, if this type of lesions persists for a time $t_r$ it transforms into a lethal lesion. Hawkins derived the expected amount of lethal lesions in a domain to be given by [183, 184]:

$$\langle LL\rangle_d(z) = Az + Bz^2,$$
(2.40)

with

$$A = \frac{ak_d}{(a+c)} + \lambda_d + k_d e^{-(a+c)t_r},$$
(2.41)

and

$$B = \frac{bk_d^2}{2(a+c)} \left[ 1 - e^{-2(a+c)t_r} \right]. \tag{2.42}$$

In the following description, the passage of a particle that deposits energy in a given domain will be called an *event*. The number of events is thought to be a random variable $j$ that follows a Poisson distribution with the mean and the variance $\mu$. Further, the dose deposited by one event is a random variable $z_1$ with the mean $\langle z_1 \rangle$ and the variance $V_{z1}$.

Now if one considers a domain with exactly $j$ events, the absorbed dose can be written as the sum of the dose deposited by the single events $z_{1i}$:

$$z_j = j\frac{1}{j}\sum_{i=1}^{j} z_{1i} = j\overline{z_{1j}}, \tag{2.43}$$

where $\overline{z_{1j}}$ is the mean of a $j$-membered sample of $z_1$. $\overline{z_{1j}}$ itself is a random variable with the same mean as $z_1$ ($\langle z_1 \rangle$) and variance $V_{z1}/j$. Using Equation 2.40 and Equation 2.43 one can write:

$$\langle LL \rangle_d (z_j) = Aj\overline{z_{1j}} + Bj^2\overline{z_{1j}}^2, \tag{2.44}$$

to describe the expected amount of lethal lesions in a domain after $j$ events and absorption of $j\overline{z_{1j}}$ Gy. In order to yield the average number of lethal lesions per domain over all domains that have had $j$ events, the average over the distribution of $\overline{z_{1j}}$ is taken from both sides:

$$\langle\langle LL \rangle_d (z_j)\rangle = Aj \langle\overline{z_{1j}}\rangle + Bj^2 \langle\overline{z_{1j}}^2\rangle. \tag{2.45}$$

As $\langle\overline{z_{1j}}\rangle = \langle z_1 \rangle$ and $\langle\overline{z_{1j}}^2\rangle = V_{z1}/j + \langle z_1 \rangle^2$ one can rewrite to:

$$\langle\langle LL \rangle_d (z_j)\rangle = Aj \langle z_1 \rangle + Bj^2 \left( V_{z1}/j + \langle z_1 \rangle^2 \right) \tag{2.46}$$

$$= (A \langle z_1 \rangle + BV_{z1}) j + B \langle z_1 \rangle^2 j^2. \tag{2.47}$$

Now taking the average over the Poisson distributed variable $j$ yields:

$$\langle\langle\langle LL\rangle_d (z_j)\rangle\rangle = (A\langle z_1\rangle + BV_{z1})\mu + B\langle z_1\rangle^2(\mu+\mu^2) \tag{2.48}$$

$$= \left(A\langle z_1\rangle + BV_{z1} + B\langle z_1\rangle^2\right)\mu + B\langle z_1\rangle^2\mu^2 \tag{2.49}$$

$$= \left(A\langle z_1\rangle + B\langle z_1^2\rangle\right)\mu + B\langle z_1\rangle^2\mu^2 \tag{2.50}$$

$$= \left(A + B\frac{\langle z_1^2\rangle}{\langle z_1\rangle}\right)\langle z_1\rangle\mu + B(\langle z_1\rangle\mu)^2. \tag{2.51}$$

This expression describes the average number of lethal lesions per domain over all domains $\langle LL\rangle_d$. With $\mu$ being the average number of events per domain after exposure to the microscopic dose D and $\langle z_1\rangle$ being the average dose deposited in a domain by a single event, one can write $\langle z_1\rangle\mu = \langle z\rangle$ which is equal to the macroscopic dose $D$. The expression $\langle z_1^2\rangle/\langle z_1\rangle$ is the dose weighted average of the dose depositions by single events $z_{1D}$. Using these expressions one can write:

$$\langle LL\rangle_d = (A + Bz_{1D})D + BD^2. \tag{2.52}$$

With the total number of domains $N_{dom}$, the total expected amount of lethal lesions in the nucleus is given by:

$$\langle LL\rangle = N_{dom}\cdot\langle LL\rangle_d = (\alpha_0 + \beta z_{1D})D + \beta D^2, \tag{2.53}$$

where $\alpha_0 = N_{dom}\cdot A$ and $\beta = N_{dom}\cdot B$ [185]. The values of $\alpha_0$ and $\beta$ can be determined from low LET data where $z_{1D}\to 0$ and are then equivalent to the respective LQM parameters.

In situations where the expected amount of events is very low (e.g. at low doses or high LET), the probability of no event occurring at all increases and needs to be taken into account by a *saturation correction*, which was first introduced by Hawkins in 2003 [183]. Kase et al. extended the correction to be applicable to any given energy spectrum [185] and found that $z_{1D}$ in Equation 2.53 needed to be replaced by a saturation corrected dose-averaged specific energy deposited by single events $z_{1D}^\star$, which is given by:

$$z_{1D}^\star = \frac{\int_0^\infty z_{sat}zf_1(z)dz}{\int_0^\infty zf_1(z)dz}, \tag{2.54}$$

where $f_1(z)$ is the probability density distribution of $z$ being deposited in a single event in a domain and $z_{sat}$ is the saturation corrected specific energy given by:

$$z_{sat} = \frac{z_0^2}{z}\left(1 - exp\left(-\frac{z^2}{z_0^2}\right)\right),\qquad(2.55)$$

with the empirical saturation coefficient $z_0$ determined as:

$$z_0 = \frac{(R_n/r_d)^2}{\sqrt{\beta\left(1 + (R_n/r_d)^2\right)}},\qquad(2.56)$$

where $R_n$ and $r_d$ describe the radius of the nucleus and the domain respectively [186]. These radii are seen as cell-line specific variables [64]. The version of the MKM that includes the saturation correction as described above is known as the *modified MKM* (mMKM) [186]. Inaniwa et al. showed that $z_{1D}^\star$ for a mixed radiation field could be computed by the dose-weighted average of the respective values of each contributing mono-energetic field [186]. The distribution $f_1(z)$ can in principle be measured experimentally using so called tissue-equivalent proportional counter (TEPC) but in practice is computed based on the Kiefer-Chatterjee parametrization (Equation 2.10) of the radial dose distribution surrounding the particle tracks [64, 176, 185, 186].

The MKM was shown to be successful over a large range of clinically relevant LET but cell survival predictions were found to deviate for high LET and high doses [187, 188]. While measured values for $\beta$ decrease towards higher LET, MKM assumes it to be constant [188, 189]. Sato and Furusawa identified the issue to be the fact that MKM disregards the stochastic nature of the specific energy received by the nucleus $z_n$ and assumes all nuclei to receive $z_n = D$. While for low LET this can be seen as a good approximation, the variability increases towards high LET [188, 190]. As a result, Sato and Furusawa developed a model that considers the statistical nature of the specific energies imparted by both the domain ($z_d$) and the nucleus ($z_n$) called the *Double-Stochastic Microdosimectric Kinetic Model* (DSMKM). They derived that the survival $S(D)$ after irradiation with the microscopic dose $D$ is given by:

$$\ln(S(D)) = \ln\left(\int_0^\infty S_n(z_n)f_n(z_n, D)dz_n\right),\qquad(2.57)$$

where $f_n(z_n, D)$ is the probability density function of the specific energy in the nucleus $z_n$ given the macroscopic dose $D$ and $S_n(z_n)$ is the survival fraction of cells after exposure to $z_n$, that is given by:

$$\ln(S_n(z_n)) = -\alpha_0 \int_0^\infty z_d' f_d(z_d, z_n) dz_d \tag{2.58}$$

$$-\beta \int_0^\infty z_d'^2 f_d(z_d, z_n) dz_d, \tag{2.59}$$

where $f_d(z_d, z_n)$ is the probability density function of the specific energy $z_d$ being applied to a domain given the nucleus being exposed to $z_n$. The updated saturation-corrected specific energy $(z_d')$ and its saturation parameter $(z_0)$ are now given by:

$$z_d' = z_0 \sqrt{1 - \exp\left[-(z_d/z_0)^2\right]}, \tag{2.60}$$

and

$$z_0 = \frac{l_d}{m_d} \frac{\rho_d \pi r_d R_n^2}{\sqrt{\beta(r_d^2 + R_n^2)}}, \tag{2.61}$$

where $l_d$, $m_d$ and $\rho_d$ are the mean chord length, mass and density of the domain, respectively [188, 190].

Equations 2.57 and 2.58 are solved numerically using a Monte-Carlo approach. However, as the associated computational burden is quite significant, Sato and Furusawa also proposed the *Stochastic Microdosimetric Kinetic Model* (SMKM), where the stochastic nature of the specific energy applied to the domains $z_d$ is represented by its mean value and variance [190]. To further reduce the computation time, Inaniwa and Kanematsu developed a further modification, in which the dose-averaged nucleus specific energy per event $\overline{z}_{n,D}$ is introduced instead of the full distribution of $z_n$. This *modified SMK* could also be implemented into a treatment planning platform [188].

### 2.4.3 Local Effect Model

The development of the *local effect model* (LEM) began in the mid 1990s at the GSI in Darmstadt, Germany [191, 192] and its original version is still in routine clinical use as basis for ion beam treatment planning [176, 193]. In order to determine the effect of a given microscopic dose distribution $d(x, y, z)$ within a cell nucleus of volume $V$, which can be highly heterogeneous for charged particle fields, the LEM

considers sub-volumes $dV$ small enough so that a homogeneous dose distribution can be assumed within. The LEM now assumes that the yield of lethal lesions within this sub-volume equals the yield for a cell exposed to the same dose by homogeneous (photon/low-LET) radiation solely scaled down by its volume. Using Equation 2.19, the expected number of lethal lesions within the sub-volume can thus be written as:

$$d \langle LL \rangle (x,y,z) = -\ln S(d(x,y,z))dV/V, \qquad (2.62)$$

and the total expected number of lethal lesions can then be determined by integrating this expression over the nucleus volume:

$$\langle LL \rangle = \int \frac{-\ln S(d(x,y,z))}{V} dV. \qquad (2.63)$$

The survival probability after this given dose distribution can then be determined using Equation 2.19 [176]. While in principle any survival information could be fed into the LEM, a modified linear-quadratic parametrization was chosen, where the survival curve transitions into a linear form above a dose threshold $D_t$:

$$S(D) = \begin{cases} e^{-\alpha D - \beta D^2} & D \leq D_t \\ S(D_t) \cdot e^{-s(D-D_t)} & D > D_t, \end{cases} \qquad (2.64)$$

with the slope $s = \alpha + 2\beta D_t$ of the linear form [65].

As the microscopic dose distribution it self is of stochastic nature, the survival probability after irradiation with a given macroscopic setting (dose, particle energy etc.) is determined by averaging the survival for a large number of random microscopic dose distributions created using Monte Carlo methods [176, 192]. In its original version (LEM I), the Geiß parametrization of the RDD (Equation 2.9) was choses with a constant core radius of $r_{min} = 10$nm to implicitly consider the diffusion of radicals away from the track.

In 2007 a second version (LEM II) with two major changes was introduced [65]: First, a damage enhancing factor $\eta$ was introduced. It is based on the observation, that at doses exceeding several hundreds of Gy the linear dependency between dose and induced DSB turns super-linear, which is attributed to the increasing amount of DNA single strand breaks (SSB) that are induced on the opposite strands of the DNA in close proximity and transform into DSB [194–202]. While the authors of the

extension explicitly claimed, that they do not equate DSB with lethal lesions, they believed a correlation to exist, so that the relative enhancement of the DSB yield could be assumed to be equal to the relative enhancement of lethal lesions. When LEM II was first published, $\eta$ was determined using a Monte Carlo approach, which was later followed by an analytical expression derived by Friedrich et al. [203]:

$$\eta = 1 + \frac{1 - e^{-\frac{\alpha_{SSB} \cdot D}{L_{gen}} \cdot t_{SSB}}}{3 - e^{-\frac{\alpha_{SSB} \cdot D}{L_{gen}} \cdot t_{SSB}}} \cdot e^{-\frac{\alpha_{DSB}}{L_{gen}} \cdot t_{SSB}} \cdot \frac{\alpha_{SSB}}{\alpha_{DSB}}, \tag{2.65}$$

where $D$ is the applied dose, $\alpha_{DSB}$ is the yield of DSB per nucleus and applied unit dose, $\alpha_{SSB}$ is the yield of DSB per nucleus and applied unit dose, $L_{gen}$ is the length of the genome in base pairs (bp) and $t_{SSB}$ is the maximum distance between two SSB on each side of the DNA to form a DSB in bp. The values $\alpha_{DSB} = 30Gy^{-1}$, $\alpha_{SSB} = 1250Gy^{-1}$, $L_{gen} = 5.4Gbp$ and $t_{SSB} = 25$ were found to be appropriate in their studies [65, 203]. The second major change in LEM II was the introduction of an explicit description of radical diffusion. In the more advanced description, the RDD was convoluted with a normal distribution kernel in polar coordinates [65]:

$$f(r, r', \Phi') = \frac{1}{2\pi\sigma^2} e^{-(r^2 - 2rr'cos\Phi' + r'^2)/2\sigma^2}, \tag{2.66}$$

where the standard deviation $\sigma$ characterizes the diffusion length of the radicals and $\Phi'$ describes the angular coordinate. The resulting RDD could then be determined by:

$$\widetilde{D}(r) = \int_0^\infty dr'r' \int_0^{2\pi} d\Phi' D(r') f(r, r', \Phi') = \frac{e^{-r^2/2\sigma^2}}{\sigma^2} \int_0^\infty dr'r'e^{-r'^2/2\sigma^2} I_0\left(\frac{rr'}{\sigma^2}\right) D(r'), \tag{2.67}$$

where $I_0$ is the modified Bessel function of order zero. A standard deviation $\sigma = 4nm$ and a new constant core radius of $r_{min} = 0.3nm$ were found to fit within literature range and describe survival data well [65].

In a smaller extension published in 2008 (LEMIII), the constant core radius was replaced with the energy dependent parametrization described earlier (Equation 2.8) [66]. Probably the largest change up to that point was introduced in 2010 with the fourth version of the LEM (LEM IV) [204]. The sub-volumes were now represented by cubes of the side length $l_{DSB}$ and the number of induced DSB is sampled based on the local dose and $\alpha_{DSB}$. Sub-volumes containing exactly one DSB are called an

*isolated DSB*, while those containing two or more DSB are called a *clustered DSB*. The number of isolated DSB ($N_{iDSB}$) and clustered DSB ($N_{cDSB}$) is then used to determine the *complexity C* [204]:

$$C = \frac{N_{cDSB}^{Ion}}{N_{cDSB}^{Ion} + N_{iDSB}^{Ion}}. \tag{2.68}$$

In the next step, the dose leading to the equivalent complexity assuming homogeneous photon radiation $D_{eq}^{\gamma}$ is determined, as well as the expected amount of lethal lesions at this dose using Equations 2.19 and 2.64:

$$\langle LL \rangle_{eq}^{\gamma} = -\ln \left( S \left( D_{eq}^{\gamma} \right) \right). \tag{2.69}$$

In order to determine the expected number of lethal lesions for the ion irradiation $\langle LL \rangle_{Ion}$, the value found for the homogeneous photon irradiation is scaled based on the number of affected sub-volumes:

$$\langle LL \rangle_{Ion} = \frac{N_{cDSB}^{Ion} + N_{iDSB}^{Ion}}{N_{cDSB}^{\gamma} + N_{iDSB}^{\gamma}} \langle LL \rangle_{eq}^{\gamma}. \tag{2.70}$$

The corresponding survival can then again be determined using Equation 2.19.

In the most recent update of the model, introduced in 2021 by Phuhl in her PhD thesis, the spectrum of the secondary electrons ejected by passing ions is considered, resulting in a modification of the DSB yield [205].

## 2.4.4 Other Models

The MKM and LEM, through their routine clinical use, are probably the most prominent and discussed models of radiation action in the field. In the last decades, a significant number of other advanced models have been proposed and a full account of all relevant models would exceed the scope of this work. However, a small selection of models, which include in some way or form a mechanism inspired approach to modelling the radiation action of charged particles, shall be briefly summarized in this subsection.

The *Repair-Misrepair-Fixation* (RMF) model [206–209] is based on a system of coupled non-linear ordinary differential equations, that describe the induction and processing of DSB. These result in the number of lethal point mutations and chro-

mosomal aberrations, which are used to predict cell survival. Instead of the common utilization of RDD parametrizations, the RMF model makes use of the *Monte Carlo Damage Simulation* (MCDS) [208, 210–216] to describe the induction of DSB and their increased yields for charged particles at higher LET [193].

The *Biophysical Analysis of Cell Death and Chromosomal Aberration* (BIANCA) [217–223] is based on the induction of so called clustered lesions (CL), which lead to the formation of two independent chromosomal fragments. Dependent on their distance, these can *misrejoin* or *unrejoin* and lead to different forms of chromosomal aberrations. Different sub-types of chromosomal aberrations are deemed lethal for the cell. The distribution of induced CL for charged particles is based on the Kiefer-Chatterjee parametrization. The yield of CL and the *unrejoining parameter $f$* are adjustable parameters, where the former is dependent on the radiation quality and the cell-line, while the latter is only cell-line dependent.

McMahon and his colleagues published their model first in 2016 [224] for low-LET radiation and the extension to charged particles in 2017 [225]. In its latest version from 2021 [226] the model was extended to consider classical dose-rate effects and was given the name *Mechanistic DNA Repair and Survival Model* (Medras). Medras bases its predictions on the distribution of induced DSB and simulates their repair kinetics, as well as their distance dependent misrejoining rate. Based on these mechanisms the model is able to predict a number of endpoints, including chromosomal aberrations, mutational burden and survival after irradiation. As it also considers the different repair pathways available at different cell phases, it is also able to make predictions on the effect of deficiencies in given repair processes, such as NHEJ. For charged particles, Medras bases its initial DSB distributions on results from a detailed external Monte Carlo engine called Geant4 [227] and their DNA toolkit [228, 229].

In 2014 Surdutovich and Solov'yov published the *Multiscale approach* [230], including comprehensive consideration of the ionization of the medium, transport of secondary particles, chemical interactions and thermo-mechanical pathways of biological damage [231]. Ultimately, cell survival is determined based on the clustering of damages within a certain geometry and the ability to repair such damages is assumed to be cell line specific.

The model proposed by Wang and his colleagues in 2018 [232] parametrizes the DSB yield induced by charged particles based on results from the MCDS. The model

than assumes that rejoining of induced DSB by NHEJ is the dominant process post-induction and determines the probability of correct repair based on the distance between the damages. Cell survival probability is then determined after correcting for the saturation effect and considering the cell line dependent sensitivity to misrepair.

# Chapter 3

# The UNIVERSE - Thesis Outline

For the biophysical models presented in Section 2.4, only a few of the modifiers of radiation action mentioned in the introduction were in some form either included in the original version or introduced in later extensions (e.g., hypoxia [216, 231, 233–235], DNA repair dependent radiosensitivity [224–226, 236], classical dose-rate effect [187, 226, 237–241]). At the same time, the sparing effects at ultra-high dose-rates have up to this point only been described based on physico-chemical models linked to phenomenological descriptions of radiation effect [147, 148, 150]. Addressing the need for a *theoretical framework versatile enough to describe and predict the effect of the different modifiers under a unified model of radiation action for conventional and ion beam radiation* outlined in the introduction, this thesis describes the development, benchmark, capabilities, challenges and outlook of the so called *UNIfied and VERSatile bio response Engine*, or in short: UNIVERSE. Conceptually, the framework strives to be as explicit and mechanistic yet simple and efficient in its description of radiation action as possible. Such an approach is thought to not only lead to a more comprehensible model in general but also facilitate its modification and extension which plays a crucial role in this project.

A key concept at the core of UNIVERSE was first introduced by Elsässer et al. in 2010 in connection with LEM IV: The chromosomal material is subdivided into domains containing about 2 million base pairs, resembling substructures referred to as *giant loops* [242–246]. Accumulations of DSB within such a giant loop were found to resist swift repair [138, 139] and are thought to be subject to a higher chance of chromatin loss, posing a larger threat to the clonogenic potential of a cell [247]. Based on the local dose deposition and an empirically determined DSB yield per

nucleus and applied unit dose ($\alpha_{DSB}$) that is assumed to be cell line independent and constant within the range of clinically applied doses [216], the amount of DSB induced within individual domains can be computed. Elsässer et al. introduced the terms of *isolated DSB* (iDSB) for all domains containing a single DSB as well as *clustered/complex DSB* (cDSB) for all domains containing two or more DSB.[1]

Around 2012, Mairani et al. [248] and Friedrich et al. [247] simultaneously introduced an analytical model (which the latter group named *Giant LOop Binary LEsion*(GLOBLE)), in which the expected amount of iDSB and cDSB, $\langle N_{iDSB} \rangle$ and $\langle N_{cDSB} \rangle$, induced in a nucleus after irradiation with sparsely ionizing radiation is determined based on the Poisson distribution. Furthermore, each instance of an isolated or complex DSB is assigned a probability $K_{iDSB}$ or $K_{cDSB}$, respectively, of leading to the loss of clonogenic potential in a cell. Later, in the context of UNIVERSE these probabilities are often referred to as *lethality parameters*. In GLOBLE the expected amount of lethal lesions is ultimately defined as

$$\langle LL \rangle = \langle N_{iDSB} \rangle \cdot K_{iDSB} + \langle N_{cDSB} \rangle \cdot K_{cDSB} \tag{3.1}$$

and the resulting survival fraction of the cell population is determined using Equation 2.19 ($S = exp(-\langle LL \rangle)$).[2] Furthermore, Mairani et al. [248] included the effect of hypoxia for sparsely ionizing radiation. Based on the suggestions by Carlson et al. [130] and Stewart et al. [216] the OER (cp. Section 2.3.3) at a given oxygen level is re-interpreted as the ratio between the DSB yield at normoxia ($\alpha_{DSB}$) and the given oxygen level ($\alpha_{DSB}^{O_2}$) and re-named *hypoxia reduction factor* (HRF). Hypoxia is believed to not affect the repair of DSB [130], so that its effect can be accounted for solely by applying a modified DSB yield of $\alpha_{DSB}^{O_2} = \alpha_{DSB}/HRF$. From 2013 to 2015, Tommassino et al. [137, 249] showed that the predicted ratio between isolated and complex DSB matched well with that of the fast and slow component of the biexponential DSB repair kinetics observed after irradiation and by assigning repair half-life times ($T_{iDSB}^{1/2}$ and $T_{cDSB}^{1/2}$) to each damage class, Herr et al. [237, 238] managed to include classical dose-rate effects into GLOBLE and LEM IV.

---

[1] The expression *domains* has established itself in the context of UNIVERSE. However, Elsässer et al. used the term *sub-volumes* in their 2010 publication, which was also chosen in the Fundamentals section on LEM IV to achieve a clearer transition from the description of previous LEM versions. Their motivation based on giant loops was omitted in that section for the sake of clarity.

[2] In GLOBLE and its extensions commonly the notation $\epsilon_i$ and $\epsilon_c$ is used instead of $K_{iDSB}$ and $K_{cDSB}$ as well as $n_i$ and $n_c$ instead of $\langle N_{iDSB} \rangle$ and $\langle N_{cDSB} \rangle$.

While GLOBLE is a purely analytical model and LEM IV determines cell survival over several intermediate steps and conversions based on the effect of a photon beam predicted to induce the same *complexity* of damages (cp. Section 2.4.3), UNIVERSE takes a distinct approach: For any radiation quality, the damage pattern induced inside a nucleus is simulated for a large number of iterations using the Monte Carlo method. For each iteration, based on the number of isolated and clustered DSB ($N_{iDSB}$ and $N_{cDSB}$), the survival probability of cells with the given damage pattern is computed by applying the basic probabilistic equation

$$S = (1 - K_{iDSB})^{N_{iDSB}} \cdot (1 - K_{cDSB})^{N_{cDSB}} . \qquad (3.2)$$

The average of this value over all iterations is used to predict the survival fraction after a given irradiation. In the publication introducing GLOBLE [247], such a probabilistic concept was suggested as a possible alternative approach to the there presented analytical low-LET model which would avoid the need for some assumptions regarding the frequencies of the damage classes. Nevertheless, only the analytical solution was pursued further, as it was shown to be sufficiently accurate within the clinically relevant dose range and enables quicker calculations. However, the explicit simulation and representation of the damage pattern and the application of the identical simple equation (Equation 3.2) to determine cell survival for both low and high LET radiation in UNIVERSE was thought to enable a more straightforward and comprehensible way to unify the description of different radiation qualities under one framework. The chosen approach also implies that the response of a cell to a certain damage pattern is fully independent from the radiation quality that caused it. This leads to the hypothesis that if any mechanism which acts on the damage pattern itself - or modifies its lethality to the cell - is not explicitly dependent on radiation quality, its effect on the survival after irradiation in any radiation field should be accurately predicted solely by providing the damage patterns induced in each case and making no change to the mechanism itself (Figure 3.1).

The strategy set out for the development of UNIVERSE is derived directly from this hypothesis: First, identify the mechanism underlying a certain modifier of radiation action. Second, develop, implement and benchmark the mechanism based on the simulations of low LET damage patterns and the more readily available corresponding data. Ultimately, if applicable, carry out the transition to the high LET
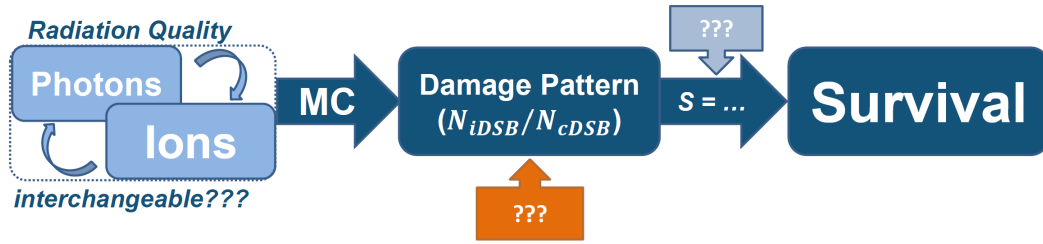
Figure 3.1: The effect chain in UNIVERSE: The damage patterns induced by the irradiation are simulated via Monte Carlo methods. Based solely on the damage patterns, the survival probability of cells is determined using Equation 3.2. Hypothesis: The effect of mechanisms manipulating the damage pattern or its lethality to the cell, which are independent of the radiation quality, (arrows with question marks) should be predictable in any radiation field by providing the corresponding initial damage pattern without any modifications of the mechanism itself.

regime by introducing an appropriate simulation of the damage pattern and benchmark or study the resulting predictions.

In the context of this thesis, several modifiers of radiation action were successfully implemented and benchmarked for low LET radiation applying the Monte Carlo based UNIVERSE approach described earlier. Each of these low LET sub-models have merit on their own, providing platforms to predict and study the effect of clinically relevant variables of radiation efficacy. Most importantly however, a description of high LET radiation action was successfully introduced to UNIVERSE and was shown to be able to transition and describe the effect of some of the modifiers, supporting the hypothesis formulated earlier. More specifically, the following projects (listed in chronological order of the publication date) were realized in the framework of this thesis and were published in internationally acclaimed peer-reviewed journals, resulting in this work to be presented in the form of a cumulative thesis (cp. Chapter 4):

**Publication 1** (Section 4.1)

Introduction of the Monte Carlo based low LET framework of UNIVERSE and the model of radiosensitization caused by deficiency or inhibition of DNA damage repair enzymes under normoxia and hypoxia.

**Publication 2** (Section 4.2)

Implementation of a distinction between direct and indirect damages after low LET radiation and the action of radical scavengers under normoxia and hypoxia.

**Publication 3** (Section 4.3)

Development of the time dependent version of the low LET model in UNI-VERSE, based on DNA repair kinetics as well as oxygen depletion and reoxygenation during irradiation to predict dose-rate effects including cell and tissue sparing at ultra-high dose-rates. Study of possible key variables determining the observation of ultra-high dose-rate sparing.

**Publication 4** (Section 4.4)

Establishment of the high LET framework in UNIVERSE, including a description of the microscopic dose distribution of ion fields and the induced DNA damage along with its implementation on GPU. Transition of the effect of DNA damage repair inhibition to survival in ion beams. Patient planning study exploring potential implications of the model in a clinical setting.

**Publication 5** (Section 4.5)

Refinement of the model of ultra-high dose-rate sparing at low LET by including DNA damage fixation kinetics, a dose-rate dependent oxygen depletion rate, and consideration of the exact pulse structure of the radiation source.

**Publication 6** (Section 4.6)

Implementation of DNA repair kinetics into the high LET model of UNI-VERSE allowing the prediction of classical dose-rate effects in ion beams. Study of the dose and LET dependency of predicted dose-rate effects as well as the possible impact of reference and ion beam dose-rates on RBE modeling and measurement.

While the development and extension of the capabilities of UNIVERSE as well as the study of its predictions and their implications are foundational for this work and the relevance of the created framework, a special emphasis was put on assessing the ability of UNIVERSE to accurately predict measured data on the effects and dependencies of interest. In each of the listed publications, the model was thus benchmarked against data available in the literature or in some cases (Publication 1 and 4) experimentally obtained as part of the study itself.

# Chapter 4

# Peer Reviewed Publications

This works is written in the form of a *cumulative thesis*, comprising 6 peer-reviewed articles published in internationally acclaimed scientific journals, presented individually in chronological order of their publication date below. Besides the list of authors, the publication status, the journal reference and the DOI, a detailed list of the authors' contributions is given for each included publication. The original manuscripts are removed from the online version of this thesis to avoid copyright concerns. During the time these studies were conducted, the author contributed to further publications, which were not directly related to this body of work or ineligible for inclusion. These additional contributions are listed in the chapter *List of Publications*.

## 4.1 Modeling the Effect of Hypoxia and DNA Repair Inhibition on Cell Survival after Photon Irradiation

**Authors**: <u>Hans Liew</u>, Carmen Klein, Frank T. Zenke, Amir Abdollahi, Jürgen Debus, Ivana Dokic, Andrea Mairani

**Publication status**: Published 30 November 2019

**Journal reference**: International Journal of Molecular Sciences, Volume 20, Number 23, Pages 6054

**DOI**: 10.3390/ijms20236054

**Authors' contributions**: <u>HL</u> is the first author of this publication. <u>HL</u>, ID and

AM conceptualized the study. <u>HL</u> and AM developed the Monte Carlo based low LET framework of UNIVERSE and the included model of radiosensitization. <u>HL</u>, with the assistance of AM, conducted all UNIVERSE based analyses. CK and ID conducted and analyzed the biological experiments. <u>HL</u> constructed all visualizations. <u>HL</u>, with the assistance of ID, wrote the original draft of the manuscript. <u>HL</u>, CK, FTZ, AA, JD and AM contributed to the review and editing of the final manuscript. FTZ, AA and JD provided resources. AA and JD provided funding and clinical direction.

## 4.2 Modeling Direct and Indirect Action on Cell Survival After Photon Irradiation under Normoxia and Hypoxia

**Authors' contributions**: <u>HL</u> is the first author of this publication. AM conceptualized the study. <u>HL</u> and AM implemented the distinction between direct and indirect damages after low LET radiation and the action of radical scavengers under normoxia and hypoxia. <u>HL</u>, ID and AM conducted all presented analyses. AM constructed the visualizations. <u>HL</u>, with the assistance of ID and AM, wrote the original draft of the manuscript. <u>HL</u>, SM, JD, ID and AM contributed to the review and editing of the final manuscript. JD provided funding and clinical direction.

# 4.3 Deciphering Time-Dependent DNA Damage Complexity, Repair, and Oxygen Tension: A Mechanistic Model for FLASH-Dose-Rate Radiation Therapy

**Authors**: <u>Hans Liew</u>, Stewart Mein, Ivana Dokic, Thomas Haberer, Jürgen Debus, Amir Abdollahi, Andrea Mairani

**Authors' contributions**: <u>HL</u> is the first author of this publication. <u>HL</u> and AM conceptualized the study. <u>HL</u> and AM developed the time dependent version of the low LET model in UNIVERSE, based on DNA repair kinetics as well as oxygen depletion and reoxygenation during irradiation. <u>HL</u>, with the assistance of AM, conducted all presented analyses and constructed all visualizations. <u>HL</u> wrote the original draft of the manuscript. <u>HL</u>, SM, ID, TH, JD, AA and AM contributed to the review and editing of the final manuscript. TH, AA and JD provided resources, funding and clinical direction.

## 4.4 Combined DNA Damage Repair Interference and Ion Beam Therapy: Development, Benchmark, and Clinical Implications of a Mechanistic Biological Model

**Authors**: <u>Hans Liew</u>, Sarah Meister, Stewart Mein, Thomas Tessonnier, Benedikt Kopp, Thomas Held, Thomas Haberer, Amir Abdollahi, Jürgen Debus, Ivana Dokic, Andrea Mairani

**Authors' contributions**: <u>HL</u> is the first author of this publication. <u>HL</u> and AM conceptualized the study. <u>HL</u> and AM developed the high LET framework in UNIVERSE, including a description of the microscopic dose distribution of ion fields and the induced DNA damage. The GPU implementation of parts of the model was realized by <u>HL</u>, BK and AM. <u>HL</u> established the optimal choice of the model parameters and the radial dose distribution parameterization as well as the approximation of its diffused form necessary for its use on GPU. Figure 1 and 2 were conceptualized by <u>HL</u> and AM, created by <u>HL</u> based on analyses conducted by <u>HL</u>. Figure 3 was conceptualized, created and based on analyses by <u>HL</u> and AM. Figure 4 was conceptualized by <u>HL</u>, StM and AM, created by <u>HL</u> and StM and based on analyses by <u>HL</u>, StM and AM. The biological experiment providing the data for Figure 4 was conceptualized by <u>HL</u>, SaM, ID and AM, conducted by SaM and ID with the dosimetric assistance by TT and analyzed by SaM and ID. Figure 5 was conceptualized by <u>HL</u>, StM and AM, using treatment plans provided by THe, created by StM and based on analyses by <u>HL</u>, StM and AM. <u>HL</u> wrote the original draft of the manuscript. <u>HL</u>, SaM, StM, TT, BK, THe, THa, AA, JD, ID and AM contributed to the review and editing of the final manuscript. TH, AA and JD provided resources, funding and clinical direction.

# 4.5 The Impact of Sub-Millisecond Damage Fixation Kinetics on the In Vitro Sparing Effect at Ultra-High Dose Rate in UNIVERSE

**Authors' contributions**: <u>HL</u> is the first author of this publication. <u>HL</u> and AM conceptualized the study. <u>HL</u> and AM developed the refined model of ultra-high dose-rate sparing at low LET by including DNA damage fixation kinetics, a dose-rate dependent oxygen depletion rate, and consideration of the exact pulse structure of the radiation source. <u>HL</u> and AM conducted all presented analyses and constructed all visualizations. <u>HL</u>, with the assistance of AM, wrote the original draft of the manuscript. <u>HL</u>, SM, TT, AA, JD, ID and AM contributed to the review and editing of the final manuscript. AA and JD provided resources, funding and clinical direction.

# 4.6 Impact of DNA Repair Kinetics and Dose-Rate on RBE Predictions in the UNIVERSE

**Authors**: <u>Hans Liew</u>, Stewart Mein, Thomas Tessonnier, Christian Karger, Amir Abdollahi, Jürgen Debus, Ivana Dokic, Andrea Mairani

**Authors' contributions**: <u>HL</u> is the first author of this publication. <u>HL</u> and AM conceptualized the study. <u>HL</u> developed the time dependent version of the high LET model of UNIVERSE, implementing DNA repair kinetics. AM conducted FLUKA simulations including mMKM and dose-rate analysis of the investigated SOBP. <u>HL</u> and AM conducted all remaining analyses and constructed all visualizations. <u>HL</u>, with the assistance of AM, wrote the original draft of the manuscript. <u>HL</u>, SM, TT, CK, AA, JD, ID and AM contributed to the review and editing of the final manuscript. AA and JD provided resources, funding and clinical direction.

# Chapter 5

# Discussion

This thesis aims to present the initial steps of the development of a framework including a unified model of conventional and ion beam radiation, versatile enough to describe and predict the effect of modifiers of radiation action, the *UNIfied and VERSatile bio response Engine*. It may serve to optimize and personalize patient care, support clinical decision-making as well as deepen our understanding of central radiobiological processes. Here, key contributions of the projects included in this work towards these goals will be discussed. To improve clarity, this chapter is arranged thematically and will not follow the chronological order of the publication date of each manuscript. However, for the sake of comparability, the publications (Pub.) will be referred to with the numbers assigned in Chapter 4. Ultimately, challenges concerning the introduction of the UNIVERSE into clinical practice will be considered and possible future projects involving the UNIVERSE are laid out.

**DNA Damage Repair Interference and the Ion Beam Model**  Assuming the already high lethality of complex DSB to not significantly increase if DNA repair is disrupted and thus projecting the change in radiosensitity onto the lethality of isolated DSB [236], the effect of DNA damage repair interference (DDRi) (cp. Section 2.3.3) was implemented into the low LET model of UNIVERSE in Pub. 1. The *radiosensitization factor* (RSF) was introduced to parametrize the effect of DDRi by a mutation or a drug, acting as a multiplier to the lethality of isolated DSB. It was shown that this simple approach was sufficient to describe the effects of DDRi and that the RSF was oxygen level independent for different drugs and mutations. As mentioned earlier, hypoxia in tumors has been linked to treatment failure in radiotherapy [8, 28, 29] and the application of drugs interfering with DDR

have not only been generally considered to improve treatment outcome but also to overcome hypoxia induced radioresistance [37–39, 250]. UNIVERSE could thus not only adapt its predictions based on possible mutations within the DDR machinery of patients but also assist the assessment and planning of dual treatment approaches. Crucial for the aims of this thesis was the translation of the DDRi mechanism to high LET predictions in Pub. 4. Based on model parameters solely derived from photon data and adapting the microscopic dose distribution, UNIVERSE accurately predicted the effect of different DDRi agents on cell survival after mono-energetic or mixed proton and helium irradiation. The model was successfully benchmarked on an array of experimental data from the literature as well as an experiment conducted specifically for the study. Further, the framework correctly predicted the reduced effect of DDRi with increasing LET found in the data, resulting in lower RBE for ion beams irradiating cells affected by DDRi. The success of this project adds weight to a key hypothesis laid out at the beginning of this thesis [1].

However, developing the ion beam model itself was not as straightforward. From the representation of the nucleus and domain geometry over the description of the microscopic dose distribution to the damage yield, appropriate models had to be chosen and their parameters needed to be defined. Ultimately, 8 parameters emerged: volume and radius of the nucleus represented as a cylinder, genome length, side length of a domain, effective diffusion distance of radicals, maximum interaction distance between two SSB, yield of DSB and yield of SSB. While these parameters were tuned to benchmarking data, they were kept within the ranges reported in literature. Although some of these parameters are known to vary between cell lines, they were set constant to reduce the number of free variables. Thus, also for ion beams, UNIVERSE only requires the two lethality parameters (and optionally an RSF value) as input. Some notable intersections and differences exist between UNIVERSE and the two clinical models, MKM and LEM (cp. Sections 2.4.2 and 2.4.3), laid out in more detail in Pub. 4. An important conceptual parallel is the use of microscopic domains and the calculation of the yield of lesions within them based solely on the local energy deposition. All three models thus imply a parity between low and high LET radiation on a microscopic level to unify the description of their action. However, key differences exist in the derivation of the biological effect: While the MKM

---

[1] "The effect of mechanisms manipulating the damage pattern or its lethality to the cell, which are independent of the radiation quality, should be predictable in any radiation field by providing the corresponding initial damage pattern without any modifications of the mechanism itself."

defines the expected amount of (not further defined) *lethal lesions* using the specific dose deposited in a domain and derives the ultimate lethality from the stochastics of energy depositions, both LEMIV and UNIVERSE, use the number of induced DSB to define isolated and complex DSB as their initial step. However, LEMIV compares the *complexity index* (Equation 2.68) of the overall damage pattern to a photon reference to determine the yield of lethal lesions, while in UNIVERSE the explicit description of the damage pattern is conserved and damages are associated with certain probabilities to inactivate the cell (cp. Chapter 3). The computational costs of explicitly describing the microscopic dose and damage distribution required the use of GPU computation techniques (cp. Section 2.2.2). While the development of GPU codes introduced own challenges (e.g., cp. Appendix), the explicit simulations avoids potential issues with assumptions about the stochastics of energy depositions, which have for example lead to overhauls of the MKM [190]. The explicit description of the damages is furthermore believed to have facilitated the implementation of the mechanisms covered in this thesis. While the *Medras* model (cp. Section 2.4.4) considers certain DDRi effects over the LET, it has yet to be benchmarked in fields of mixed radiation quality, making UNIVERSE the first mechanistic model of combined DDRi and particle radiation comprehensively benchmarked in mixed fields to the best knowledge of the author. Presently, mixed field predictions for UNIVERSE are based on the TDRA (cp. Section 2.4.1). However, the full particle and energy spectrum is currently being implemented on GPU which might improve the accuracy of predictions and allow to investigate possible differences to the widespread TDRA based approach. The capability to make predictions for mixed fields is crucial, as most clinically relevant fields in ion beam therapy contain primary particles and fragments of multiple energies. Using real patient plans, the potential effects of DDRi in a clinical scenario were investigated for photon, proton and helium beams in Pub. 4. The study allowed novel insights into possible differences in the combination of DDRi and the distinct radiation modalities in practice, including the fact that despite the loss in RBE, ion beams might offer a safer treatment than photon beams which were found to exhibit a reduced therapeutic window when assuming DDRi to be systemic. In the future, UNIVERSE could thus help to assess the clinical benefit of combined use of DDRi drugs and different radiation qualities or to adapt the latter for individual patients based on known mutations in the DDR machinery or parameters derived from biomarkers.

Up to know, published UNIVERSE predictions only included protons and helium ions. To achieve reasonable predictions for heavier ions (e.g., clinically relevant carbon ions), the increased importance of ion species resulting from their fragmentation needs to be considered. Their implementation is currently underway. Furthermore, ongoing investigations indicate a tendency of overestimating the biological effectivity of carbon ions at certain energies that might be due to an overproduction of DSB. The current implementation predicts a monotonic increase of the DSB yield with LET based on SSB clustering (Equation 2.65), while some MCS indicate a saturation beginning above $\sim$100 kev/µm [251]. While an empirical reduction of the interaction distance between SSB can act as a solution to this issue, alternative parametrizations of the DSB yield might be considered in coming developments.

**Effects of Dose Rate and Hypoxia in Ion Beams**  Key concepts already being established by the work of others [237, 238] facilitated the implementation of DNA repair kinetics (cp. Section 2.3.3) for low LET (Pub. 3) and high LET beams (Pub. 6). Consistent with the literature [187, 239–241, 252–254], the extended UNIVERSE predicts no significant dose-rate effects for both low and high LET, at doses and dose-rates of conventional radiotherapy approaches. However, substantial effects were observed at larger doses, commonly applied in pre-clinical experiments. In a benchmark based on proton and helium RBE values obtained in high dose *in vivo* experiments [255, 256], the extended UNIVERSE outperformed current clinical approaches and its previous version, which do not consider dose-rate effects. The study implied that models should consider the dose rates applied by the reference as well as ion beams to make accurate predictions and ensure the appropriate assessment of benchmarks. Ultimately, the successful implementation of the classical dose-rate effects not only extended the capabilities of the UNIVERSE but again demonstrated the ability of the framework to include such mechanisms for both low and high LET radiation in a simple and transparent manner.

In contrast, the translation of sparing effects at ultra-high dose-rates (uHDR) (cp. Section 2.3.3) from low to high LET radiation was found to be challenging. In 2014, Favaudon et al. [58] reported the concurrent sparing of normal tissue and iso-effective treatment of tumors in mice when uHDR were applied instead of standard dose-rates (SDR), coining the term *FLASH* irradiation. While sparing of cells and tissue at uHDR is a long-known phenomenon [56, 57, 129, 140–144], the potential increase

of the therapeutic window based on the iso-effective treatment of the tumor kicked off a downright *FLASH hype*. [2] With this, interest also returned to the explanation and modelling of the uHDR sparing effect itself, leading to several physico-chemical models coupled to phenomenological descriptions of radiation effect [147, 148, 150, 151]. Petersson et al. [147], proposed a simple parametrization of a radiochemical oxygen depletion and re-oxygenation process leading to transient hypoxia, one of the first and most prominent proposals for the underlying mechanism of uHDR sparing [56, 59, 60, 142, 147, 148]. Combining this model with the low LET segment of UNIVERSE in Pub. 3 allowed to account for the vastly different experimental conditions (e.g., energy of the applied low LET radiation, oxygen level or type of biological readout) found in published studies, enabling the benchmark of the resulting framework over a large panel of *in vitro* and *in vivo* data from the literature, which lacked for the other models mentioned earlier. The study not only demonstrated the abilities of the extended UNIVERSE to support investigations into this highly topical subject but also highlighted, that within its model the emergence of sparing effects is dependent on numerous variables and thus the common attempt to determine a general dose/dose-rate for sparing effects would be unreasonable.

Although at the core of the interest in FLASH radiotherapy, the explanation for the differential sparing between tumors and normal tissue remains highly debated [60, 147, 152, 153] and a reasonable discussion of existing hypothesis would exceed the scope of this work. Concentrating on the establishment of a cohesive model of uHDR sparing effects, no explicit attempt was made to predict the differential sparing within UNIVERSE up to this point. However, besides trivial solutions such as differential depletion rate constants [257], the consideration of oxygen distributions [153] within the target and the normal tissue could offer an attractive approach. Several key changes to the uHDR model within UNIVERSE were introduced in Pub. 5: First, the temporal pulse structure of the beam was considered, enabling the study of different combinations of pulse-structure parameters (e.g, dose per pulse and pulse frequency), which might offer a more complete indicator for the induction of sparing effects [258] and aid the development of suitable accelerators. Second, motivated by accumulating evidence of reduced oxygen depletion per unit dose for higher dose-rates [257, 259, 260] a dose-rate dependent oxygen depletion rate constant was intro-

---

[2]A search for *FLASH radiotherapy* yields more than 14,000 hits published since 2014 on Google Scholar at the time of writing (September 2022)

duced. Lastly, the DNA damage fixation kinetics of oxygen (cp. Section 2.3.3) was implemented. Despite the increased depletion rate for SDR, these changes enabled a reduction of the assumed oxygen depletion rate, while retaining or even improving the model performance in benchmarks against *in vitro* data. Although the reduced oxygen depletion rate approaches values measured by Cao et al. [257], strengthening the case for the oxygen depletion hypothesis to at least explain some of the uHDR sparing, it remains slightly above the experimental results. While Cao et al. added Bovine serum albumin (BSA) to the irradiated flasks to mimic the presence of bio molecules, it is debatable whether the mixture reasonably represents the chemical milieu within a cell nucleus. The chemical composition of the target can strongly impact the measured amount of oxygen depletion [148, 257, 261, 262], lending a possible explanation for the discrepancy between the measured and assumed depletion rate. Additionally, other mechanisms, such as radical-radical interactions, might also need to be considered for a complete description of the sparing effects. Despite ongoing efforts, it remains challenging to theoretically and experimentally characterize the relevant composition and processes within the cell nucleus.

A key challenge for the transition of the implemented uHDR sparing model to high LET is the absence of a consistent mechanistic description of the oxygen effect for ions in UNIVERSE. There are only few mechanistically motivated models of the overall DSB yield for ion beams as a function of the oxygen concentration [216, 263] and extensions of LEM and MKM are either based on the empirical adaptation of model parameters [234, 235] or of their final predictions [264, 265]. A mechanistic approach for UNIVERSE could be the differentiation between direct and indirect damage, where the latter mediates the majority of the oxygen effect [51] (cp. Section 2.3.1). Anticipating future use cases, a split between the two damage types was introduced to the low LET model of UNIVERSE in Pub. 2: Assuming the oxygen dependent reduction of the DSB yield (cp. Chapter 3) to only affect the indirect fraction, cell survival data for different cell lines, doses, oxygen levels and radical scavenger concentrations were accurately predicted in a coherent extension of the UNIVERSE. For high LET radiation, it is assumed that the fraction of direct damage is increased, explaining their reduced susceptibility to the oxygen effect [15, 16, 103]. Some MCS even suggest that the excess yield of DSB at high LET is caused nearly entirely by direct damages [251]. Thus, calculating the increased DSB yield as before and applying the oxygen dependent reduction only on an unchanged

indirect damage yield could be an approach to model the decreasing oxygen effect towards higher LET. However, as mentioned earlier, the increased yield of DSB for higher LET in UNIVERSE is based on clustering of SSBs. As both the number of DSB and SSB are reduced under hypoxia [130, 216, 266], it appears more consistent to lower their yields before the DSB yield increase based on SSB clustering is applied. A subsequent differentiation between direct and indirect damages would then appear obsolete. On the other hand, as shown in Pub. 5, the oxygen effect does not act instantaneously but follows a kinetic in the order of milliseconds. One could postulate, that the clustering of induced SSB would allow for their *ab initio* processing as DSB concerning their fixation by oxygen. This could justify applying an oxygen dependent yield reduction after calculating the DSB yield increase using the normoxic damage yields. An alternative approach might be the *oxygen-in-the-track* hypothesis: Molecular oxygen is produced within the tracks of charged particles, which could locally revert hypoxia [267–270]. However, several studies suggest that the produced amount of oxygen would have no biological impact [271–273] and its exact amount and distribution remains open. The ultimate choice of the appropriate mechanistic model of the oxygen effect for ions in the UNIVERSE remains difficult as the presented options are not necessarily mutually exclusive and knowledge on the underlying mechanisms as well as suitable benchmarking data is sparse.

Irrespective of the final oxygen effect model, transition of the current uHDR model to ion beams would remain challenging: First, it is to be determined whether the oxygen depletion should be processed analogously to low LET radiation at the microscopic level or if the radiation quality needs to be considered explicitly. Second, it remains open how the (time dependent) microscopic oxygen distribution is to be implemented, considering the heterogeneous energy depositions of an ion field. Besides the fact that oxygen might also be produced (*oxygen-in-the-track*), it can react with - and most importantly - diffuse throughout its environment [262]: For meaningful sparing effects to emerge, ion tracks passing through the target would have to change the oxygen concentration at the locations at which subsequent particle pass. However, this is virtually impossible if oxygen depletion is confined to the extent of the ion track structure, as even for extremely high fluences overlaps of the biologically relevant track cores are rare [274]. Yet, if the initial reduction of oxygen is propagated via diffusion, interactions between subsequently impinging ions are conceivable, especially considering the time scale of damage fixation. With

the remaining ambiguities concerning key variables and processes, as well as the computational burden of a simulation of the oxygen distribution over time, developing effective theories of the described concepts appears to be a reasonable initial step. These could be refined continuously towards a more mechanistic description.

**UNIVERSE in the Clinics and Personalized Treatment Planning** A key vision for this project was to develop a biophysical model that would introduce treatment planning adaptation based on personalized radiobiological information to the clinics. Is such an application feasible with the currently available technology? What can UNIVERSE already offer for clinical practice?

Current treatment planning systems for ion beam therapy do not consider any inter-patient differences in radiosensitivity and included biophysical models are rarely given distinct radiosensitivity parameters for tumors and normal tissues [176]. The irradiation of dissociated biopsy samples and their analysis via clonogenic assays might appear to be a straightforward approach to derive personalized model parameters. However, it has been deemed too slow and labor intensive for clinical practice [275]. Regardless, UNIVERSE would rather show its full potential if high-throughput biomarkers could for example indicate DDRi and the model might only need to introduce an RSF to adapt its predictions. While the loss of key DDR enzymes has been correlated to treatment outcomes [30–35], biomarkers of DDRi have not been implemented clinically yet due to sparsity of evidence and difficulties in quantifying readouts [275, 276]. Furthermore, the target of biomarkers could be distributed heterogeneously. The ultimate goal would thus be to adapt the treatment plan to the spatial distribution of biomarkers. However, planning heterogenous dose (*dose painting*) or LET (*LET painting*) distributions based on functional or molecular imaging has already been long discussed [277–279] and numerous technical issues, including the need for reliable biomarkers detectable by imaging systems, as well as the resolution and quantifiability of their images, have been identified early on [280]. In this regard, while still far from a matured technology, the treatment plan adaptation based on hypoxia maps might have made the most progress. Several magnetic resonance imaging (MRI) and positron emission tomography (PET) based markers have been explored [281]. Maps based on the PET marker [18F]-fluoromisonidazole (FMISO) have been used in early studies demonstrating dose painting for conventional radiotherapy sources [278, 282]. In the context of ion

beam therapy, utilizing phenomenological OER models, FMISO maps where used in recent recalculations studies [283] and treatment planning systems were modified to include hypoxia maps [264, 265, 284]. Unfortunately, imaging of DDRi biomarkers has not made comparable progress. While molecular imaging was seen as a promising technology early on, even providing spatial resolution of p53 expression [285], it continues to face significant challenges [286]. Thus, the full optimization of treatment plans using UNIVERSE based on spatial distributions of DDRi taken from individual patients will still necessitate considerable technological advancements. While this part of UNIVERSE might yet be unable to realize its full potential in the clinics, it is an important first step in establishing a crucial element of the infrastructure necessary for fully personalized radiooncology. Furthermore, its general ion beam model may soon be implemented in treatment planning systems and planning studies such as those conducted in Pub. 4 could already offer general clinical guidelines. In addition, conclusions drawn from UNIVERSE predictions might motivate novel paradigms in radiotherapy. For example, findings in Pub. 4 could imply a different approach to manage heterogeneous distributions of radiosensitivity within a tumor, without the knowledge of the distribution itself: Assuming the heterogeneity of the radiosensitivity to be based on differences of DDR proficiency, its effect should be reduced when applying high LET radiation. Indeed Glowa et al. demonstrated, that in a carbon ion SOBP (mean LET $\sim$75 kev/µm) the impact of tumor heterogeneity was decreased substantially in experimental prostate tumors in comparison to conventional irradiation [287–289]. One might therefore consider actively increasing the applied LET throughout the target by incorporating LET coverage into the treatment plan optimization [4] and/or by adapting advanced treatment techniques for example based on particle arc therapy [290] or combination of multiple ion species [291]. Thus, even before its direct implementation into the clinical pipeline, UNIVERSE could offer impulses to the practice in radiotherapy.

**Ongoing and Future Projects**  Several ongoing projects have already been mentioned: The implementation of the full particle and energy spectrum on GPU, the inclusion of heavier ions, and the development of an oxygen effect model for ion beams. The establishment of the latter is a key prerequisite for the planned transition of the uHDR sparing model to higher LET. While the mechanisms underlying the potentially differential effect of uHDR in tumors and normal tissues might be

implemented once the corresponding evidence has accumulated, UNIVERSE predictions are currently extended and compared to tumor volume kinetics data that has been used to prove the absence of uHDR sparing effects in tumors. If the model is able to predict the observed trends, it could investigate the effect of uHDR on more clinically relevant metrics such as the tumor control probability (TCP). In general, UNIVERSE could be tested in a more clinical context by recalculating retrospective patient data and comparing against the actual treatment outcome.

The ability to predict alternative biological endpoints beyond those based on the survival fraction could aid the establishment of innovative approaches to treatment and its optimization. One could try to derive the spectrum of induced DNA fragments based on the simulated distribution of DSB. These could act as a basis for models of immunogenicity via the cGAS-STING pathway [292] or possible bystander effects [293, 294]. Extending predictions to the frequency of chromosomal aberration could even enable the assessment of the secondary tumor induction probability [295]. In a more profound step in the evolution of the framework as a biophysical model, damage classes could be generalized and concurrently rooted deeper into radiobiological observations: Statistics of ionization events on the nanometer scale have been found to be well correlated to ion beam RBE [296]. On a similar scale, Super-Resolution-Microscopy enables the analysis of the topology - and thus to some extent the complexity – of radiation induced fluorescent foci (RIF) which act as markers of DNA damage [297]. If a connection between the nano-dosimetric description of the radiation field and the statistics of damage topologies/complexities could be established, one might be able to extend the damage description of UNIVERSE to these damage classes and predict their frequencies with a nano-dosimetric simulation. Such a description might improve the accuracy of model predictions. However, each UNIVERSE extension would have to be reestablished based on the new fundamental model of the radiation action.

Ultimately, the accomplished work discussed in this chapter and the many ongoing and planned extensions of UNIVERSE underline the great versatility of this framework. Through that, UNIVERSE is a practical tool to investigate radiobiological mechanisms and is well prepared to follow future trends in radiooncology, where increasing focus will be put on personalized care, innovative multimodal treatment approaches as well as their prescription and planning, which will need to consider an increasing number of inputs from multiple disciplines.

# Chapter 6

# Summary

The application of ion beams in radiotherapy enables superior precision of dose deposition as well as potentially increased biological effectiveness in comparison to conventional radiation and has driven lasting research interest. However, the effect of several factors, such as the target oxygenation, the applied dose-rate, as well as the presence of radical scavengers or radiosensitizing drugs and mutations, which are known to modify the effectiveness of radiation are yet to be fully characterized and understood, especially in ion beam fields. A theoretical framework based on a unified model of radiation action for conventional and ion beam radiation, versatile enough to describe and predict the effect of these modifiers, could be a crucial contributor to the optimization and personalization of treatment plans, the clinical decision-making process as well as the investigation of key radiobiological mechanisms. In an effort to address this need, this thesis presents the initial developments of the *UNIfied and VERSatile bio response Engine* (UNIVERSE). Its underlying model of radiation action in biological systems is based on the clustering of radiation induced DNA double strand breaks (DSB) in microscopic domains within the cell nucleus. One central hypothesis of the UNIVERSE is that the effect of mechanisms manipulating the radiation induced damage pattern or its lethality to the cell, which are independent of the radiation quality, should be predictable in any radiation field by providing the corresponding initial damage pattern without any modifications of the mechanism itself. Thus, the main strategy for this thesis was to establish the mechanism connecting a given damage pattern in the nucleus to the biological effect based on readily available photon data and apply it to the damage patterns simulated within ion beam fields.

This work is put forward in the form of a cumulative thesis containing 6 peer-reviewed publications (Pub.) in total.

In Pub. 1 the effect of DNA damage repair interference (DDRi) was introduced to the low LET model of UNIVERSE. The study showed the effect could be modeled by modifying the lethality of isolated DSB only and that this change was independent of the oxygen level for several mutations and pharmaceutical inhibitors of the DDR. In an important step for the overall framework, the DDRi model was successfully transitioned to higher LET in Pub. 4, where the ion beam model of UNIVERSE was first presented. Model predictions were benchmarked on data obtained after application of monoenergetic or mixed fields of proton and helium beams from the literature and own experiments. The framework correctly predicted several trends reflected in the data, such as the reduced effect of DDRi with increasing LET, resulting in a lower RBE for ion beams irradiating cells with DDRi. With this, to the best knowledge of the author, UNIVERSE contains the first mechanistic model of DDRi in combination with ion beams which has also been benchmarked with data from clinically relevant mixed fields. Patient planning studies based on UNIVERSE predictions allowed novel insights into possible advantages and disadvantages of combining DDRi with different radiation modalities.

The effect of DNA repair kinetics in conjunction with the applied dose-rate (classical dose-rate effects), where first established and benchmarked for low LET radiation in Pub. 3 and transferred to high LET radiation in Pub. 6. There, the study showed that the dose-rates of the reference and ion beam radiation should be considered to ensure accurate predictions and the appropriate assessment of benchmarks, especially in high dose pre-clinical setups. In such a setup, the extended UNIVERSE outperformed its old version and current clinical approaches, which do not consider dose-rate effects.

The topical subject of sparing effects emerging at ultra-high dose-rates (uHDR) applied in FLASH radiotherapy has been addressed in Pub 3., where an oxygen depletion mechanism was implemented into the low LET model of UNIVERSE and was benchmarked on a panel of *in vitro* and *in vivo* data. To the best knowledge of the author, this makes UNIVERSE the first mechanistic and (to this date) the most comprehensively benchmarked model of radiation action including an uHDR sparing effect. The observation of sparing effects was found to be dependent on numerous factors, implying that a general dose or dose-rate threshold would be un-

reasonable. The model was refined in Pub. 5., where the beam pulse structure is explicitly taken into account and the oxygen dependent damage fixation kinetic was implemented. Despite also considering an increasing trend of the oxygen depletion rate towards conventional dose-rates, these changes allowed for an overall reduction of the assumed oxygen depletion rate, approaching measured values, while retaining the predictive capabilities of the model.

The transition of uHDR sparing effects to the high LET model remains challenging, especially due to the current absence of a mechanistic oxygen effect model for ion beams in UNIVERSE. To this end, several possible approaches could be considered, including the differentiation between direct and indirect damages. Such a differentiation was introduced in Pub. 2 for low LET radiation and successfully predicted the effect of a radical scavenger in different concentrations at varying levels of oxygenation.

Unfortunately, even with an established oxygen model for high LET, a mechanistic implementation of uHDR sparing effects for ion beams would face considerable challenges. Furthermore, substantial technical limitations remain to be resolved before a biomarker-based personalized treatment plan adaptation using the UNIVERSE would be possible in the clinics. Nevertheless, the inclusion of diverse modifiers of radiation action into the established framework should be seen as a crucial first step towards the creation of a pipeline which could consider them as variables during treatment plan optimization in the future. Furthermore, UNIVERSE predictions and treatment planning studies can already contribute valuable insights into the effects of the different modifies in clinical settings, which may already support radiooncologists in their decision-making. The ability of UNIVERSE to include mechanisms from distinct areas of radiation sciences, demonstrated in this thesis, emphasizes the versatility of this framework. This makes it a constructive tool to investigate radiobiological phenomena which carries great potential to accompany future trends in radiotherapy, where multimodal approaches will most likely gain growing attention and treatment optimization based on variables from multiple disciplines will become increasingly necessary. Numerous projects extending the capabilities of UNIVERSE are already underway and several future extensions are planned.

# List of Publications

## Articles included in Thesis

- **Liew, H.**, Klein, C., Zenke, F. T., Abdollahi, A., Debus, J., Dokic, I., & Mairani, A. (2019). Modeling the Effect of Hypoxia and DNA Repair Inhibition on Cell Survival After Photon Irradiation. *International journal of molecular sciences, 20*(23), 6054. https://doi.org/10.3390/ijms20236054

- **Liew, H.**, Mein, S., Debus, J., Dokic, I., & Mairani, A. (2020). Modeling Direct and Indirect Action on Cell Survival After Photon Irradiation under Normoxia and Hypoxia. *International journal of molecular sciences, 21*(10), 3471. https://doi.org/10.3390/ijms21103471

- **Liew, H.**, Mein, S., Dokic, I., Haberer, T., Debus, J., Abdollahi, A., & Mairani, A. (2021). Deciphering Time-Dependent DNA Damage Complexity, Repair, and Oxygen Tension: A Mechanistic Model for FLASH-Dose-Rate Radiation Therapy. *International journal of radiation oncology, biology, physics, 110*(2), 574–586. https://doi.org/10.1016/j.ijrobp.2020.12.048

- **Liew, H.**, Meister, S., Mein, S., Tessonnier, T., Kopp, B., Held, T., Haberer, T., Abdollahi, A., Debus, J., Dokic, I., & Mairani, A. (2022). Combined DNA Damage Repair Interference and Ion Beam Therapy: Development, Benchmark, and Clinical Implications of a Mechanistic Biological Model. *International journal of radiation oncology, biology, physics, 112*(3), 802–817. https://doi.org/10.1016/j.ijrobp.2021.09.048

- **Liew, H.**, Mein, S., Tessonnier, T., Abdollahi, A., Debus, J., Dokic, I., & Mairani, A. (2022). The Impact of Sub-Millisecond Damage Fixation Kinetics on the In Vitro Sparing Effect at Ultra-High Dose Rate in UNIVERSE. *International journal of molecular sciences, 23*(6), 2954. https://doi.org/10.3390/ijms23062954

- **Liew, H.**, Mein, S., Tessonnier, T., Karger, C. P., Abdollahi, A., Debus, J., Dokic, I., & Mairani, A. (2022). Impact of DNA Repair Kinetics and Dose Rate on RBE Predictions in the UNIVERSE. *International journal of molecular sciences, 23*(11), 6268. https://doi.org/10.3390/ijms23116268

## Articles not included in Thesis

- Walsh, D., **Liew, H.**, Schlegel, J., Mairani, A., Abdollahi, A., & Niklas, M. (2020). Carbon ion dosimetry on a fluorescent nuclear track detector using widefield microscopy. *Physics in medicine and biology, 65*(21), 21NT02. https://doi.org/10.1088/1361-6560/abb7c5

- Tessonnier, T., Mein, S., Walsh, D., Schuhmacher, N., **Liew, H.**, Cee, R., Galonska, M., Scheloske, S., Schömers, C., Weber, U., Brons, S., Debus, J., Haberer, T., Abdollahi, A., Mairani, A., & Dokic, I. (2021). FLASH Dose Rate Helium Ion Beams: First In Vitro Investigations. *International journal of radiation oncology, biology, physics, 111*(4), 1011–1022. https://doi.org/10.1016/j.ijrobp.2021.07.1703

- Niklas, M., Schlegel, J., **Liew, H.**, Zimmermann, F., Rein, K., Walsh, D., Dzyubachyk, O., Holland-Letz, T., Rahmanian, S., Greilich, S., Runz, A., Jäkel, O., Debus, J., & Abdollahi, A. (2022). Biosensor for deconvolution of individual cell fate in response to ion beam irradiation. *Cell reports methods, 2*(2), 100169. https://doi.org/10.1016/j.crmeth.2022.100169

## Selected Conference Contributions

- **Liew, H.**, Kopp, B., Dokic, I., Abdollahi, A., Debus, J., & Mairani, A. (2020) UNIVERSE: Unifying the modelling of radiosensitization for photons and protons, Oral Presentation and E-Poster, *Particle Therapy Co-Operative Group (PTCOG) Online 2020 Meeting*

- Mairani, A., Tessonnier, T., Mein, S., Walsh, D., **Liew, H.**, Weber, U., Brons, S., Debus, J., Haberer, T., Abdollahi, A., & Dokic, I. (2021) FLASH Dose-Rate Helium Ion Beams: First In Vitro Investigations, Oral Presentation, *American Society for Radiation Oncology (ASTRO) 63rd Annual Meeting*, Chicago, IL, USA. https://doi.org/10.1016/j.ijrobp.2021.07.076

- **Liew, H.**, Meister, S., Mein, S., Tessonnier, T., Kopp, B., Held, T., Haberer, T., Abdollahi, A., Debus, J., Dokic, I., & Mairani, A. (2021) Combined DNA Damage Repair Inhibition and Ion Beam Therapy: Development, Benchmark and Clinical Implications of a Mechanistic Biological Model, E-Poster, *American Society for Radiation Oncology (ASTRO) 63rd Annual Meeting*, Chicago, IL, USA.

# Bibliography

1. Mukherjee, S. *The emperor of all maladies : a biography of cancer* ISBN: 978-1-4391-0795-9 (Scribner, New York, 2010).

2. Ritchie, H. *Cancer death rates are falling; five year survival rates are rising* (last access: December 29th, 2021). Feb. 2019. `https://ourworldindata.org/cancer-death-rates-are-falling-five-year-survival-rates-are-rising`.

3. World Health Organization. *WHO report on cancer: setting priorities, investing wisely and providing care for all.* 2020. `https://apps.who.int/iris/handle/10665/330745`.

4. Cao, B. *et al.* Benchmarking life expectancy and cancer mortality: global comparison with cardiovascular disease 1981-2010. *BMJ* **357.** eprint: `https://www.bmj.com/content/357/bmj.j2765.full.pdf`. `https://www.bmj.com/content/357/bmj.j2765` (2017).

5. Bray, F., Jemal, A., Grey, N., Ferlay, J. & Forman, D. Global cancer transitions according to the Human Development Index (2008–2030): a population-based study. *The Lancet Oncology* **13,** 790–801. `https://doi.org/10.1016/s1470-2045(12)70211-5` (Aug. 2012).

6. Torre, L. A. *et al.* Global cancer statistics, 2012. *CA: A Cancer Journal for Clinicians* **65,** 87–108. `https://doi.org/10.3322/caac.21262` (Feb. 2015).

7. Townsend, N. *et al.* Cardiovascular disease in Europe: epidemiological update 2016. *European Heart Journal* **37,** 3232–3245. `https://doi.org/10.1093/eurheartj/ehw334` (Aug. 2016).

8. *Basic clinical radiobiology* Fifth edition (eds Joiner, M. & Kogel, A. v. d.) ISBN: 978-1-4441-7963-7 (CRC Press/Taylor & Francis Group, Boca Raton, FL, 2018).

9. Delaney, G., Jacob, S., Featherstone, C. & Barton, M. The role of radiotherapy in cancer treatment. *Cancer* **104,** 1129–1137. eprint: `https://acsjournals.onlinelibrary.wiley.com/doi/pdf/10.1002/cncr.21324`. `https://acsjournals.onlinelibrary.wiley.com/doi/abs/10.1002/cncr.21324` (2005).

10. Tobias, J. The role of radiotherapy in the management of cancer–an overview. *Ann Acad Med Singap* **25,** 371–379 (1996).

11. *Medizinische Physik* (eds Schlegel, W., Karger, C. P. & Jäkel, O.) `https://doi.org/10.1007/978-3-662-54801-1` (Springer Berlin Heidelberg, 2018).

12. Röntgen, W. Über eine neue Art von Strahlen: vorläufige Mitteilung. *Sitzungsber. Phys. Med. Gesell.* (1895).

13. Lederman, M. The early history of radiotherapy: 1895–1939. *International Journal of Radiation Oncology\*Biology\*Physics* **7,** 639–648 (May 1981).

14. Bernier, J., Hall, E. & Giaccia, A. Radiation oncology: a century of achievements. *Nature Reviews Cancer* **4,** 737–747 (Sept. 2004).

15. Schardt, D., Elsässer, T. & Schulz-Ertner, D. Heavy-ion tumor therapy: Physical and radiobiological benefits. *Reviews of Modern Physics* **82,** 383–425 (Feb. 2010).

16. Held, K. D. *et al.* Effects of Charged Particles on Human Tumor Cells. *Frontiers in Oncology* **6,** 23. ISSN: 2234-943X. `https://www.frontiersin.org/article/10.3389/fonc.2016.00023` (2016).

17. Wilson, R. Radiological Use of Fast Protons. *Radiology* **47,** 487–491 (Nov. 1946).

18. Chu, W. *Overview of Light-Ion Beam Therapy (LBNL–59883)* in. Conference: ICRU-IAEA working party on Dose and volumespecification for prescribing, recording and reporting ion-beam therapy.,Columbus, Ohio, March 18-21, 2006 (Lawrence Berkeley National Lab. (LBNL), Berkeley, CA (United States), Mar. 2006).

19. Pedroni, E. *et al.* The 200-MeV proton therapy project at the Paul Scherrer Institute: Conceptual design and practical realization. *Medical Physics* **22,** 37–53 (Jan. 1995).

20. Haberer, T., Becher, W., Schardt, D. & Kraft, G. Magnetic scanning system for heavy ion therapy. *Nuclear Instruments and Methods in Physics Research Section A: Accelerators, Spectrometers, Detectors and Associated Equipment* **330,** 296–305 (June 1993).

21. Combs, S. E., Jäkel, O., Haberer, T. & Debus, J. Particle therapy at the Heidelberg Ion Therapy Center (HIT)- Integrated reasearch-driven university-hospital-based radiation oncology service in Heidelberg,Germany. *Radiother. Oncol.* **95,** 41–44 (2010).

22. Particle-Therapy-Co-Operative-Group. *Particle therapy facilities in clinical operation (last update: (December 2021)* (last access 11.12.2021). Dec. 2021. `https://www.ptcog.ch/index.php/facilities-in-operation`.

23. Particle-Therapy-Co-Operative-Group. *Particle therapy facilities under construction (update Dec 2021)* (last access 11.12.2021). Dec. 2021. `https://www.ptcog.ch/index.php/facilities-under-construction`.

24. Particle-Therapy-Co-Operative-Group. *Particle therapy facilities in a planning stage* (last access 1.12.2021). Dec. 2021. `https://www.ptcog.ch/index.php/facilities-in-planning-stage`.

25. Durante, M., Debus, J. & Loeffler, J. Physics and biomedical challenges of cancer therapy with accelerated heavy ions. *Nat Rev Phys* **3,** 777–790 (2021).

26. Particle-Therapy-Co-Operative-Group. *Particle Therapy Patient Statistics (per end of 2018)* (last access 11.12.2021). Dec. 2018.

27. Particle-Therapy-Co-Operative-Group. *Particle Therapy Patient Statistics (per end of 2019)* (last access 11.12.2021). Dec. 2019.

28. Tawk, B. *et al.* Comparative analysis of transcriptomics based hypoxia signatures in head- and neck squamous cell carcinoma. eng. *Radiotherapy and Oncology: Journal of the European Society for Therapeutic Radiology and Oncology* **118,** 350–358. ISSN: 1879-0887 (Feb. 2016).

29. Rofstad, E. K., Sundfør, K., Lyng, H. & Tropé, C. G. Hypoxia-induced treatment failure in advanced squamous cell carcinoma of the uterine cervix is primarily due to hypoxia-induced radiation resistance rather than hypoxia-induced metastasis. eng. *British Journal of Cancer* **83,** 354–359. ISSN: 0007-0920 (Aug. 2000).

30. Pitter, K. L. *et al.* Pathogenic ATM Mutations in Cancer and a Genetic Basis for Radiotherapeutic Efficacy. eng. *Journal of the National Cancer Institute* **113,** 266–273. ISSN: 1460-2105 (Mar. 2021).

31. Hasegawa, T. *et al.* Expression of Ku70 predicts results of radiotherapy in prostate cancer. Ku70-Expression prognostiziert Ergebnisse der Strahlentherapie beim Prostatakarzinom. *Strahlenther Onkol* **193,** 29–37 (July 2017).

32. Someya, M. *et al.* Local tumor control and DNA-PK activity of peripheral blood lymphocytes in prostate cancer patients receiving radiotherapy. *Journal of Radiation Research* **58,** 225–231 (Mar. 2017).

33. Weaver, A. *et al.* DNA double strand break repair defect and sensitivity to poly ADP-ribose polymerase (PARP) inhibition in human papillomavirus 16-positive head and neck squamous cell carcinoma. *Oncotarget* **6,** 26995–27007 (Aug. 25, 2015).

34. Rieckmann, T. *et al.* HNSCC cell lines positive for HPV and p16 possess higher cellular radiosensitivity due to an impaired DSB repair capacity. *Radiotherapy and Oncology* **107,** 242–246 (May 2013).

35. Nickson, C., Moori, P., Carter, R., Rubbi, C. & Parsons, J. Misregulation of DNA damage repair pathways in HPV-positive head and neck squamous cell carcinoma contributes to cellular radiosensitivity. *Oncotarget* **8,** 29963–29975 (Mar. 16, 2017).

36. Begg, A. C., Stewart, F. A. & Vens, C. Strategies to improve radiotherapy with targeted drugs. en. *Nature Reviews Cancer* **11.** Number: 4 Publisher: Nature Publishing Group, 239–253. ISSN: 1474-1768. https://www.nature.com/articles/nrc3007 (2021) (Apr. 2011).

37. Klein, C. *et al.* Overcoming hypoxia-induced tumor radioresistance in non-small cell lung cancer by targeting DNA-dependent protein kinase in combination with carbon ion irradiation. eng. *Radiation Oncology (London, England)* **12,** 208. ISSN: 1748-717X (Dec. 2017).

38. Dohmen, A. J. *et al.* Identification of a novel ATM inhibitor with cancer cell specific radiosensitization activity. *Oncotarget* **8,** 73925–73937. ISSN: 1949-2553 (May 2017).

39. Durant, S. T. *et al.* The brain-penetrant clinical ATM inhibitor AZD1390 radiosensitizes and improves survival of preclinical brain tumor models. eng. *Science Advances* **4,** eaat1719. ISSN: 2375-2548 (2018).

40. Veuger, S. J., Curtin, N. J., Richardson, C. J., Smith, G. C. M. & Durkacz, B. W. Radiosensitization and DNA repair inhibition by the combined use of novel inhibitors of DNA-dependent protein kinase and poly(ADP-ribose) polymerase-1. eng. *Cancer Research* **63,** 6008–6015. ISSN: 0008-5472 (Sept. 2003).

41. King, H. O. *et al.* RAD51 Is a Selective DNA Repair Target to Radiosensitize Glioma Stem Cells. eng. *Stem Cell Reports* **8,** 125–139. ISSN: 2213-6711 (Jan. 2017).

42. Huang, R. & Zhou, P. DNA damage response signaling pathways and targets for radiotherapy sensitization in cancer. *Sig Transduct Target Ther* **5,** 60 (2020).

43. Zenke, F. T. *et al.* Pharmacologic Inhibitor of DNA-PK, M3814, Potentiates Radiotherapy and Regresses Human Tumors in Mouse Models. *Molecular Cancer Therapeutics* **19.** Publisher: American Association for Cancer Research Section: Small Molecule Therapeutics, 1091–1101. ISSN: 1535-7163, 1538-8514 (May 2020).

44. Willoughby, C. E. *et al.* Selective DNA-PKcs inhibition extends the therapeutic index of localized radiotherapy and chemotherapy. *The Journal of Clinical Investigation* **130.** Publisher: American Society for Clinical Investigation, 258–271. ISSN: 0021-9738 (Jan. 2020).

45. Biau, J., Chautard, E., Verrelle, P. & Dutreix, M. Altering DNA Repair to Improve Radiation Therapy: Specific and Multiple Pathway Targeting. *Frontiers in Oncology* **9.** Publisher: Frontiers. ISSN: 2234-943X (2019).

46. Hosoya, N. & Miyagawa, K. Targeting DNA damage response in cancer therapy. eng. *Cancer Science* **105,** 370–388. ISSN: 1349-7006 (Apr. 2014).

47. National Cancer Institute (NCI). *Phase I Trial With Expansion Cohort of DNA-PK Inhibition and IMRT in Cisplatin-Ineligible Patients With Stage 3-4 Local-Regionally Advanced Head and Neck Squamous Cell Carcinoma (HN-SCC)* Clinical trial registration NCT04533750. submitted: August 29, 2020

(clinicaltrials.gov, Apr. 2021). https://clinicaltrials.gov/ct2/show/
NCT04533750 (2021).

48. Krieger, H. *Grundlagen der Strahlungsphysik und des Strahlenschutzes* ISBN:
3834818151 (Vieweg+Teubner Verlag, Apr. 2012).

49. Schlegel, W. & Bille, J. *Medizinische Physik 2* 572 pp. ISBN: 3642629814
(Springer, Sept. 2012).

50. Azzam, E. I., Jay-Gerin, J.-P. & Pain, D. Ionizing radiation-induced metabolic
oxidative stress and prolonged cell injury. eng. *Cancer Letters* **327,** 48–60.
ISSN: 1872-7980 (Dec. 2012).

51. Hirayama, R. *et al.* OH radicals from the indirect actions of X-rays induce
cell lethality and mediate the majority of the oxygen enhancement effect. eng.
*Radiation Research* **180,** 514–523. ISSN: 1938-5404 (Nov. 2013).

52. Jones, J. B., Cramer, H. M., Inch, W. R. & Lampe, H. B. Radioprotective
effect of free radical scavenging enzymes. eng. *The Journal of Otolaryngology*
**19,** 299–306. ISSN: 0381-6605 (Oct. 1990).

53. Johnke, R. M., Sattler, J. A. & Allison, R. R. Radioprotective agents for
radiation therapy: future trends. eng. *Future Oncology (London, England)*
**10,** 2345–2357. ISSN: 1744-8301 (Dec. 2014).

54. Smith, T. A. *et al.* Radioprotective agents to prevent cellular damage due
to ionizing radiation. *Journal of Translational Medicine* **15.** ISSN: 1479-5876
(Nov. 2017).

55. Steel, G. G., Down, J. D., Peacock, J. H. & Stephens, T. C. Dose-rate effects
and the repair of radiation damage. English. *Radiotherapy and Oncology* **5.**
Publisher: Elsevier, 321–331. ISSN: 0167-8140, 1879-0887 (Jan. 1986).

56. Town, C. D. Effect of High Dose Rates on Survival of Mammalian Cells.
*Nature* **215.** Number: 5103 Publisher: Nature Publishing Group, 847–848.
ISSN: 1476-4687 (Aug. 1967).

57. Berry, R. J., Hall, E. J., Forster, D. W., Storr, T. H. & Goodman, M. J.
Survival of mammalian cells exposed to X rays at ultra-high dose-rates. *The
British Journal of Radiology* **42.** Publisher: The British Institute of Radiology,
102–107. ISSN: 0007-1285 (Feb. 1969).

58. Favaudon, V. *et al.* Ultrahigh dose-rate FLASH irradiation increases the differential response between normal and tumor tissue in mice. *Science Translational Medicine* **6.** Publisher: American Association for the Advancement of Science Section: Research Article, 245ra93–245ra93. ISSN: 1946-6234, 1946-6242 (July 2014).

59. Vozenin, M.-C., Hendry, J. H. & Limoli, C. L. Biological Benefits of Ultrahigh Dose Rate FLASH Radiotherapy: Sleeping Beauty Awoken. eng. *Clinical Oncology (Royal College of Radiologists (Great Britain))* **31,** 407–415. ISSN: 1433-2981 (2019).

60. Wilson, J. D., Hammond, E. M., Higgins, G. S. & Petersson, K. Ultra-High Dose Rate (FLASH) Radiotherapy: Silver Bullet or Fool's Gold? eng. *Frontiers in Oncology* **9,** 1563. ISSN: 2234-943X (2020).

61. Seltzer, S. M. *et al.* Fundamental Quantities and Units for Ionizing Radiation (Revised) Report 85. *Journal of the ICRU* **11,** NP.2–NP. `http://dx.doi.org/10.1093/jicru/ndr012` (Apr. 2011).

62. Geiß, O., Krämer, M. & Kraft, G. Efficiency of thermoluminescent detectors to heavy charged particles. *Nuclear Instruments and Methods in Physics Research Section B: Beam Interactions with Materials and Atoms* **142,** 592–598. `https://doi.org/10.1016/s0168-583x(98)00325-5` (Aug. 1998).

63. Sakama, M. *et al.* Responses of a diamond detector to high-LET charged particles. *Physics in Medicine and Biology* **50,** 2275–2289 (Apr. 27, 2005).

64. Kase, Y. *et al.* Biophysical calculation of cell survival probabilities using amorphous track structure models for heavy-ion irradiation. eng. *Physics in Medicine and Biology* **53,** 37–59. ISSN: 0031-9155 (Jan. 2008).

65. Elsässer, T. & Scholz, M. Cluster effects within the local effect model. eng. *Radiation Research* **167,** 319–329. ISSN: 0033-7587 (Mar. 2007).

66. Elsässer, T., Cunrath, R., Krämer, M. & Scholz, M. Impact of track structure calculations on biological treatment planning in ion radiotherapy. *New Journal of Physics* **10.** Publisher: IOP Publishing, 075005. ISSN: 1367-2630 (July 2008).

67. Kiefer, J. & Straaten, H. A model of ion track structure based on classical collision dynamics. eng. *Physics in Medicine and Biology* **31,** 1201–1209. ISSN: 0031-9155 (Nov. 1986).

68. Chatterjee, A. & Schaefer, H. J. Microdosimetric structure of heavy ion tracks in tissue. eng. *Radiation and Environmental Biophysics* **13,** 215–227. ISSN: 0301-634X (Oct. 1976).

69. Krämer, M. & Kraft, G. Calculations of heavy-ion track structure. *Radiation and Environmental Biophysics* **33,** 91–109 (June 1994).

70. Varma, M., Baum, J. & Kuehner, A. Radial Dose, LET, and W for 16 O Ions in N 2 and Tissue-Equivalent Gases. *Radiation Research* **70,** 511 (June 1977).

71. Varma, M. & Baum, J. Energy Deposition in Nanometer Regions by 377 MeV/Nucleon 20 Ne Ions. *Radiation Research* **81,** 355 (Mar. 1980).

72. Fano, U. Penetration of Protons, Alpha Particles, and Mesons. *Annual Review of Nuclear Science* **13,** 1–66. eprint: `https://doi.org/10.1146/annurev.ns.13.120163.000245`. `https://doi.org/10.1146/annurev.ns.13.120163.000245` (1963).

73. Bethe, H. Zur Theorie des Durchgangs schneller Korpuskularstrahlen durch Materie. *Ann. Phys.* **397,** 325–400 (1930).

74. Bloch, F. Zur Bremsung rasch bewegter Teilchen beim Durchgang durch die Materie. *Ann. Phys.* **16,** 285–320 (1933).

75. Leo, W. *Techniques for Nuclear and Particle Physics Experiments, A How-to Approach* (Springer, 1994).

76. Barkas, W. H. *Nuclear Research Emulsions: techniques and theory* en. Google-Books-ID: CJJGnQEACAAJ (Academic Press, 1963).

77. Elsässer, T., Gemmel, A., Scholz, M., Schardt, D. & Krämer, M. The relevance of very low energy ions for heavy-ion therapy. *Physics in Medicine and Biology* **54,** N101–N106. `http://dx.doi.org/10.1088/0031-9155/54/7/N03` (Mar. 2009).

78. Golokov, M., Aleksandrov, D., Chulkov, L., Kraus, G. & Schardt, D. Fragmentation of 270 A MeV carbon ions in water. *Advances in Hadrontherapy (International Congress Series No.1144),* 316–324 (1997).

79. Matsufuji, N. *et al.* Spatial fragment distribution from a therapeutic pencil-like carbon beam in wate. *Phys* **50,** 3393–3403 (2005).

80. Shiver, L., Schardt, D. & Kanai, T. Depth-dose distribution of high-energy carbon,oxsgen and neon beams in water. *Jpn. J. Med. Physics* **18,** 1–21 (1998).

81. Serber, R. Nuclear reactions at high energies. *Phys. Rev.* **72,** 1114–1115 (1947).

82. Gunzert-Marx, K., Iwase, H., Schardt, D. & Simon, R. S. Secondary beam fragments produced by 200 MeV u-112C ions in water and their dose contributions in carbon ion radiotherapy. *New Journal of Physics* **10,** 075003. https://doi.org/10.1088/1367-2630/10/7/075003 (July 2008).

83. Toutaoui, A., Aichouche, A., Adjidir, K. & Chami, A. In-air fluence profiles and water depth dose for uncollimated electron beams. *Journal of Medical Physics* **33,** 141 (2008).

84. Vavilov, P. V. Ionizational losses of high energy heavy particles. *Zh. Eksp. Teor. Fiz* **32,** 749–751 (1957).

85. Bothe, W. Das allgemeine fehlergesetz, die schwankungen der feldstärke in einem dielektrikum und die zerstreuung der a-strahlen. *Zeitschrift für Physik* **5,** 63–69 (Jan. 1921).

86. Molière, G. Theorie der streuung schneller geladener teilchen. *Zeitschrift für Naturforschung A* **10,** 78–97 (1948).

87. Highland, V. L. Some practical remarks on multiple scattering. *Nuclear Instruments and Methods* **129,** 497–499. ISSN: 0029-554X. https://www.sciencedirect.com/science/article/pii/0029554X75907430 (1975).

88. Highland, V. L. Erratum. *Nucl. Instrum. Methods Phys. Res* **161,** 171 (1979).

89. Levin, W., Kooy, H., Loeffler, J. & Delaney, T. Proton beam therapy. *British Journal of Cancer* **93,** 849–854 (Sept. 27, 2005).

90. Jäkel, O. State of the Art in Hadron Therapy. *Aip. Conf. Proc.* **958,** 70–77 (2007).

91. Kroese, D. P., Brereton, T., Taimre, T. & Botev, Z. I. Why the Monte Carlo method is so important today. *Wiley Interdisciplinary Reviews Computational Statistics* **6,** 386–392. `https://app.dimensions.ai/details/publication/pub.1048756283` (2014).

92. Rubinstein, R. Y. & Kroese, D. P. *Simulation and the Monte Carlo Method* `https://doi.org/10.1002/9781118631980` (John Wiley & Sons, Inc., Nov. 2016).

93. Thomopoulos, N. T. *Essentials of Monte Carlo Simulation* `https://doi.org/10.1007/978-1-4614-6022-0` (Springer New York, 2013).

94. Newman, M. E. J. *Computational Physics* ISBN: 9781480145511. `https://books.google.de/books?id=SS6uNAEACAAJ` (Createspace Independent Pub, 2013).

95. Ferrari, A., Sala, P. R., Fassò, A. & Ranft, J. *FLUKA: A multi-particle transport code (program version 2005)* eng. ISBN: 978-92-9083-260-7 (CERN, Geneva, 2005).

96. Böhlen, T. T. *et al.* The FLUKA Code: Developments and Challenges for High Energy and Medical Applications. en. *Nuclear Data Sheets* **120,** 211–214. ISSN: 0090-3752. `https://www.sciencedirect.com/science/article/pii/S0090375214005018` (2021) (June 2014).

97. Van Rossum, G. & Drake, F. L. *Python 3 Reference Manual* ISBN: 1441412697 (CreateSpace, Scotts Valley, CA, 2009).

98. Klöckner, A. *et al.* PyCUDA and PyOpenCL: A scripting-based approach to GPU run-time code generation. English (US). *Parallel Computing* **38,** 157–174. ISSN: 0167-8191 (Mar. 2012).

99. NVIDIA Coporation and affiliates. *CUDA C++ Programming Guide* July 2022. `https://docs.nvidia.com/cuda/cuda-c-programming-guide/index.html`.

100. Karp, G. *Molekulare Zellbiologie* ISBN: 3540238573 (Springer, Berlin Heidelberg New York, 2005).

101. Mediran. (last visited: 03.01.2022). Aug. 2012. `commons.wikimedia.org/wiki/File:Eukaryotic_Cell_(animal).jpg.`.

102. Cadet, J., Davies, K. J. A., Medeiros, M. H., Di Mascio, P. & Wagner, J. R. Formation and repair of oxidatively generated damage in cellular DNA. *Free radical biology & medicine* **107,** 13–34. ISSN: 0891-5849 (June 2017).

103. Hirayama, R. *et al.* Contributions of Direct and Indirect Actions in Cell Killing by High-LET Radiations. *Radiation Research* **171,** 212–218 (Feb. 2009).

104. Ito, A. *et al.* Contribution of Indirect Action to Radiation-Induced Mammalian Cell Inactivation: Dependence on Photon Energy and Heavy-Ion LET. *Radiation Research* **165,** 703–712 (June 2006).

105. Reisz, J., Bansal, N., Qian, J., Zhao, W. & Furdui, C. Effects of Ionizing Radiation on Biological Molecules—Mechanisms of Damage and Emerging Methods of Detection. *Antioxidants & Redox Signaling* **21,** 260–292 (July 10, 2014).

106. Alpen, E. *Radiation Biophysics* ISBN: 9780120530854 (Academic Press, San Diego, Calif, 1998).

107. *Structure and Function of DNA* (last visited: 03.01.2022). `https://courses.lumenlearning.com/microbiology/chapter/structure-and-function-of-dna/`.

108. Felsenfeld, G. & Groudine, M. Controlling the double helix. *Nature* **421,** 448–453 (Jan. 2003).

109. Weinberg, R. A. *The Biology of Cancer: Second Edition* (Garland Publishing Inc, 2013).

110. Schipler, A. & Iliakis, G. DNA double-strand-break complexity levels and their possible contributions to the probability for error-prone processing and repair pathway choice. *Nucleic Acids Research* **41,** 7589–7605 (June 26, 2013).

111. Lukas, J., Lukas, C. & Bartek, J. More than just a focus: The chromatin response to DNA damage and its role in genome integrity maintenance. *Nature Cell Biology* **13,** 1161–1169 (Oct. 2011).

112. Panier, S. & Boulton, S. J. Double-strand break repair: 53BP1 comes into focus. *Nature Reviews Molecular Cell Biology* **15,** 7–18. `https://doi.org/10.1038/nrm3719` (Dec. 2013).

113. Lans, H., Marteijn, J. & Vermeulen, W. ATP-dependent chromatin remodeling in the DNA-damage response. *Epigenetics & Chromatin* **5,** 4 (2012).

114. Hanahan, D. & Weinberg, R. The Hallmarks of Cancer. *Cell* **100,** 57–70 (Jan. 2000).

115. Castedo, M. *et al.* Cell death by mitotic catastrophe: a molecular definition. *Oncogene* **23,** 2825–2837 (Apr. 2004).

116. Galluzzi, L. *et al.* Cell death modalities: classification and pathophysiological implications. *Cell Death & Differentiation* **14,** 1237–1243 (Apr. 13, 2007).

117. Maier, P., Hartmann, L., Wenz, F. & Herskind, C. Cellular Pathways in Response to Ionizing Radiation and Their Targetability for Tumor Radiosensitization. *International Journal of Molecular Sciences* **17,** 102 (Jan. 14, 2016).

118. McMahon, S. J. The linear quadratic model: usage, interpretation and challenges. *Physics in Medicine and Biology* **64,** 01TR01. `https://doi.org/10.1088/1361-6560/aaf26a` (Dec. 2018).

119. O'rourke, S., Mcaneney, H. & Hillen, T. Linear quadratic and tumour control probability modelling in external beam radiotherapy. *Journal of Mathematical Biology* **58,** 799–817 (Sept. 30, 2008).

120. Franken, N. *et al.* Cell survival and radiosensitisation: Modulation of the linear and quadratic parameters of the LQ model. *International Journal of Oncology* **42,** 1501–1515 (Mar. 13, 2013).

121. Bodgi, L. & Foray, N. The nucleo-shuttling of the ATM protein as a basis for a novel theory of radiation response: resolution of the linear-quadratic model*. *International Journal of Radiation Biology* **92,** 117–131 (Feb. 24, 2016).

122. Weber, U. & Kraft, G. Comparison of Carbon Ions Versus Protons. *The Cancer Journal* **15,** 325–332 (July 2009).

123. Goodhead, D. Initial Events in the Cellular Effects of Ionizing Radiations: Clustered Damage in DNA. *International Journal of Radiation Biology* **65,** 7–17 (Jan. 1994).

124. Scholz, M. in *Radiation Effects on Polymers for Biological Use* (ed et al., K. H.) 95–155 (Springer Berlin Heidelberg, Berlin, Heidelberg, 2003).

125. Furusawa, Y. *et al.* Inactivation of aerobic and hypoxic cells from three different cell lines by accelerated (3)He-, (12)C- and (20)Ne-ion beams. eng. *Radiation Research* **154,** 485–496. ISSN: 0033-7587 (Nov. 2000).

126. Belli, M. *et al.* RBE-LET relationships for cell inactivation and mutation induced by low energy protons in V79 cells: further results at the LNL facility. eng. *International Journal of Radiation Biology* **74,** 501–509. ISSN: 0955-3002 (Oct. 1998).

127. Heron, J. *Biological effect of radiotherapy: the oxygen effect* (last visited: 30.01.2018). June 2009. `oncoprof.net/Generale2000/g08_Radiotherapie/Index/g08-gb_idx08.html`.

128. Watts, M. E., Maughan, R. L. & Michael, B. D. Fast kinetics of the oxygen effect in irradiated mammalian cells. eng. *International Journal of Radiation Biology and Related Studies in Physics, Chemistry, and Medicine* **33,** 195–199. ISSN: 0020-7616 (Feb. 1978).

129. Ling, C. C., Michaels, H. B., Epp, E. R. & Peterson, E. C. Oxygen Diffusion into Mammalian Cells Following Ultrahigh Dose Rate Irradiation and Lifetime Estimates of Oxygen-Sensitive Species. *Radiation Research* **76.** Publisher: Radiation Research Society, 522–532. ISSN: 0033-7587. `https://www.jstor.org/stable/3574801` (2021) (1978).

130. Carlson, D. J., Stewart, R. D. & Semenenko, V. A. Effects of oxygen on intrinsic radiation sensitivity: A test of the relationship between aerobic and hypoxic linear-quadratic (LQ) model parameters. eng. *Medical Physics* **33,** 3105–3115. ISSN: 0094-2405 (Sept. 2006).

131. Alper, T. & Howard-Flanders, P. Role of Oxygen in Modifying the Radiosensitivity of E. Coli B. en. *Nature* **178.** Number: 4540 Publisher: Nature Publishing Group, 978–979. ISSN: 1476-4687. `https://www.nature.com/articles/178978a0` (2020) (Nov. 1956).

132. Spiro, I., Ling, C., Stickler, R. & Gaskill, J. Oxygen Radiosensitisation at Low Dose Rate. *The British Journal of Radiology* **58,** 357–363 (Apr. 1985).

133. Sundfør, K., Lyng, H., Tropé, C. G. & Rofstad, E. K. Treatment outcome in advanced squamous cell carcinoma of the uterine cervix: relationships to pretreatment tumor oxygenation and vascularization. *Radiotherapy and Oncology* **54,** 101–107 (Feb. 2000).

134. Barendsen, G. W. Responses of cultured cells,tumours and normal tissues to radiations ofdifferent linear energy transfer. *Current Topics in Radiation Research* **4,** 293–356. https://www.osti.gov/biblio/4500126 (Oct. 1968).

135. Dahm-Daphi, J. & Dikomey, E. Rejoining of DNA double-strand breaks in X-irradiated CHO cells studied by constant- and graded-field gel electrophoresis. *International Journal of Radiation Biology* **69,** 615–621 (Jan. 1996).

136. Núñez, M. *et al.* Radiation-induced DNA double-strand break rejoining in human tumour cells. *British Journal of Cancer* **71,** 311–316 (Feb. 1995).

137. Tommasino, F. *et al.* A DNA Double-Strand Break Kinetic Rejoining Model Based on the Local Effect Model. *Radiation Research* **180.** Publisher: Radiation Research Society, 524–538. ISSN: 0033-7587, 1938-5404 (Oct. 2013).

138. Johnston, P. J. & Bryant, P. E. A Component of DNA Double-strand Break Repair Is Dependent on the Spatial Orientation of the Lesions within the Higher-order Structures of Chromatin. *International Journal of Radiation Biology* **66,** 531–536. ISSN: 0955-3002 (Jan. 1994).

139. Gauter, B., Zlobinskaya, O. & Weber, K.-J. Rejoining of Radiation-Induced DNA Double-Strand Breaks: Pulsed-Field Electrophoresis Analysis of Fragment Size Distributions after Incubation for Repair. *Radiation Research* **157.** Publisher: Radiation Research Society, 721–733. ISSN: 0033-7587, 1938-5404 (June 2002).

140. Epp, E. R., Weiss, H., Djordjevic, B. & Santomasso, A. The Radiosensitivity of Cultured Mammalian Cells Exposed to Single High Intensity Pulses of Electrons in Various Concentrations of Oxygen. *Radiation Research* **52.** Publisher: Radiation Research Society, 324–332. ISSN: 0033-7587 (1972).

141. Michaels, H. B., Epp, E. R., Ling, C. C. & Peterson, E. C. Oxygen sensitization of CHO cells at ultrahigh dose rates: prelude to oxygen diffusion studies. eng. *Radiation Research* **76,** 510–521. ISSN: 0033-7587 (Dec. 1978).

142. Ling, C. Time Scale of Radiation-Induced Oxygen Depletion and Decay Kinetics of Oxygen-Dependent Damage in Cells Irradiated at Ultrahigh Dose Rates. *Radiation Research* **63,** 455 (Sept. 1975).

143. Hornsey, S. & Bewley, D. K. Hypoxia in Mouse Intestine Induced by Electron Irradiation at High Dose-rates. *International Journal of Radiation Biology and Related Studies in Physics, Chemistry and Medicine* **19.** Publisher: Taylor & Francis _eprint: https://doi.org/10.1080/09553007114550611, 479–483. ISSN: 0020-7616 (Jan. 1971).

144. Hendry, J. H., Moore, J. V., Hodgson, B. W. & Keene, J. P. The Constant Low Oxygen Concentration in All the Target Cells for Mouse Tail Radionecrosis. *Radiation Research* **92.** Publisher: Radiation Research Society, 172–181. ISSN: 0033-7587 (1982).

145. Adrian, G. *et al.* The FLASH effect depends on oxygen concentration. *The British Journal of Radiology* **93.** Publisher: The British Institute of Radiology, 20190702. ISSN: 0007-1285. `https://www.birpublications.org/doi/abs/10.1259/bjr.20190702` (2020) (Dec. 2019).

146. Cooper, C. R., Jones, D., Jones, G. D. & Petersson, K. FLASH irradiation induces lower levels of DNA damage ex vivo, an effect modulated by oxygen tension, dose, and dose rate. *The British Journal of Radiology* **95.** `https://doi.org/10.1259/bjr.20211150` (May 2022).

147. Petersson, K., Adrian, G., Butterworth, K. & McMahon, S. J. A Quantitative Analysis of the Role of Oxygen Tension in FLASH Radiation Therapy. English. *International Journal of Radiation Oncology, Biology, Physics* **107.** Publisher: Elsevier, 539–547. ISSN: 0360-3016. `https://www.redjournal.org/article/S0360-3016(20)30884-1/abstract` (2020) (July 2020).

148. Pratx, G. & Kapp, D. S. A computational model of radiolytic oxygen depletion during FLASH irradiation and its effect on the oxygen enhancement ratio. eng. *Physics in Medicine and Biology* **64,** 185005. ISSN: 1361-6560 (Sept. 2019).

149. Weber, U. A., Scifoni, E. & Durante, M. FLASH radiotherapy with carbon ion beams. eng. *Medical Physics.* ISSN: 2473-4209 (July 2021).

150. Labarbe, R., Hotoiu, L., Barbier, J. & Favaudon, V. A physicochemical model of reaction kinetics supports peroxyl radical recombination as the main determinant of the FLASH effect. English. *Radiotherapy and Oncology* **0.** Publisher: Elsevier. ISSN: 0167-8140, 1879-0887. `https://www.thegreenjournal.com/article/S0167-8140(20)30308-X/abstract` (2020) (June 2020).

151. Abolfath, R., Grosshans, D. & Mohan, R. Oxygen depletion in FLASH ultra-high-dose-rate radiotherapy: A molecular dynamics simulation. *Med. Phys* **47,** 6551–6561 (2020).

152. Zhou, G. Mechanisms underlying FLASH radiotherapy, a novel way to enlarge the differential responses to ionizing radiation between normal and tumor tissues. en. *Radiation Medicine and Protection* **1,** 35–40. ISSN: 2666-5557. `http://www.sciencedirect.com/science/article/pii/S2666555720300083` (2020) (Mar. 2020).

153. Taylor, E., Hill, R. P. & Létourneau, D. Modeling the impact of spatial oxygen heterogeneity on radiolytic oxygen depletion during FLASH radiotherapy. *Physics in Medicine and Biology* **67,** 115017. `https://doi.org/10.1088/1361-6560/ac702c` (June 2022).

154. Tessonnier, T. *et al.* FLASH Dose Rate Helium Ion Beams: First In Vitro Investigations. *Int J Radiat Oncol Biol Phys* **111,** 1011–1022 (Nov. 2021).

155. Jolly, S., Owen, H., Schippers, M. & Welsch, C. Technical challenges for FLASH proton therapy. *Physica Medica* **78,** 71–82. ISSN: 1120-1797. `https://www.sciencedirect.com/science/article/pii/S1120179720301964` (2020).

156. Buonanno, M., Grilj, V. & Brenner, D. J. Biological effects in normal cells exposed to FLASH dose rate protons. *Radiotherapy and Oncology* **139.** FLASH radiotherapy International Workshop, 51–55. ISSN: 0167-8140. `https://www.sciencedirect.com/science/article/pii/S0167814019300763` (2019).

157. Diffenderfer, E. S. *et al.* Design, Implementation, and in Vivo Validation of a Novel Proton FLASH Radiation Therapy System. *Int J Radiat Oncol Biol Phys* **106,** 440–448 (Feb. 2020).

158. Tinganelli, W. *et al.* Ultra-High Dose Rate (FLASH) Carbon Ion Irradiation: Dosimetry and First Cell Experiments. *International Journal of Radiation Oncology\*Biology\*Physics* **112,** 1012–1022 (Mar. 2022).

159. Tinganelli, W. *et al.* FLASH with carbon ions: Tumor control, normal tissue sparing, and distal metastasis in a mouse osteosarcoma model. *Radiotherapy and oncology : journal of the European Society for Therapeutic Radiology and Oncology* **22,** 238–239 (May 2022).

160. Rainey, M., Charlton, M., Stanton, R. & Kastan, M. Transient Inhibition of ATM Kinase Is Sufficient to Enhance Cellular Sensitivity to Ionizing Radiation. *Cancer Research* **68,** 7466–7474 (Sept. 15, 2008).

161. Weyrather, W., Ritter, S., Scholz, M. & Kraft, G. RBE for carbon track-segment irradiation in cell lines of differing repair capacity. *Int J Radiat Biol* **75,** 1357–1364 (1999).

162. Osu, N. *et al.* Relative Biological Effectiveness of Carbon Ions for Head-and-Neck Squamous Cell Carcinomas According to Human Papillomavirus Status. *J Pers Med* **10,** 71 (July 25, 2020).

163. Lerch, S. *et al.* HPV-positive HNSCC cell lines show strongly enhanced radiosensitivity after photon but not after carbon ion irradiation. *Radiother Oncol* **151,** 134–140 (Oct. 2020).

164. Bright, S. *et al.* DNA Damage Response Inhibitors of DNA-PKcs, PARP, RAD51, ATR and ATM All Sensitize Cancer Cells to X-Rays and Protons. *International Journal of Radiation Oncology\*Biology\*Physics* **111.** 2021 Proceedings of the ASTRO 63rd Annual Meeting, e230. ISSN: 0360-3016. https://www.sciencedirect.com/science/article/pii/S0360301621016588 (2021).

165. Liew, H. *et al.* Combined DNA Damage Repair Interference and Ion Beam Therapy: Development, Benchmark, and Clinical Implications of a Mechanistic Biological Model. *International Journal of Radiation Oncology \* Biology \* Physics* **112,** 802–817. ISSN: 0360-3016 (Oct. 2021).

166. Liu, Q. *et al.* Lung Cancer Cell Line Screen Links Fanconi Anemia/BRCA Pathway Defects to Increased Relative Biological Effectiveness of Proton Radiation. en. *International Journal of Radiation Oncology\*Biology\*Physics* **91,** 1081–1089. ISSN: 0360-3016. https://www.sciencedirect.com/science/article/pii/S036030161404560X (2021) (Apr. 2015).

167. Zhou, Q. *et al.* Inhibition of ATM induces hypersensitivity to proton irradiation by upregulating toxic end joining. en. *Cancer Research.* Publisher: American Association for Cancer Research Section: Research Article. ISSN: 0008-5472, 1538-7445. https://cancerres.aacrjournals.org/content/early/2021/02/12/0008-5472.CAN-20-2960 (2021) (Jan. 2021).

168. Bright, S. J. *et al.* Nonhomologous End Joining Is More Important Than Proton Linear Energy Transfer in Dictating Cell Death. eng. *International Journal of Radiation Oncology, Biology, Physics* **105,** 1119–1125. ISSN: 1879-355X (Dec. 2019).

169. Niki. Role of vitamin E as a lipid-soluble peroxyl radical scavenger: in vitro and in vivo evidence. *Free Radic Biol Med* **66,** 3–12 (2014).

170. Hirayama, R. *et al.* Radioprotection by DMSO in nitrogen-saturated mammalian cells exposed to helium ion beams. *Radiation Physics and Chemistry* **78,** 1175–1178 (2009).

171. Chapman, J. D. *et al.* Radioprotection by DMSO of mammalian cells exposed to X-rays and to heavy charged-particle beams. en. *Radiation and Environmental Biophysics* **16,** 29–41. ISSN: 1432-2099. `https://doi.org/10.1007/BF01326894` (2020) (Mar. 1979).

172. Bishayee, A., Rao, D. V., Bouchet, L. G., Bolch, W. E. & Howell, R. W. Protection by DMSO against Cell Death Caused by Intracellularly Localized Iodine-125, Iodine-131 and Polonium-210. *Radiation research* **153,** 416–427. ISSN: 0033-7587. `https://www.ncbi.nlm.nih.gov/pmc/articles/PMC3541040/` (2020) (Apr. 2000).

173. Kim, S. E. & Moos, W. S. Radiation protection by topical DMSO application. eng. *Health Physics* **13,** 601–606. ISSN: 0017-9078 (June 1967).

174. Kellerer, A. & Rossi, H. The Theory of Dual radiation Action. *Curr. Top. Radiat. Res. Q* **8,** 85–158 (1972).

175. Kanai, T. *et al.* Irradiation of Mixed Beam and Design of Spread-Out Bragg Peak for Heavy-Ion Radiotherapy. *Radiation Research* **147,** 78 (Jan. 1997).

176. Karger, C. P. & Peschke, P. RBE and related modeling in carbon-ion therapy. eng. *Physics in Medicine and Biology* **63,** 01TR02. ISSN: 1361-6560 (2017).

177. Zaider, M. & Rossi, H. H. The Synergistic Effects of Different Radiations. *Radiation Research* **83.** Publisher: Radiation Research Society, 732–739. ISSN: 0033-7587. `https://www.jstor.org/stable/3575352` (2021) (1980).

178. Kellerer, A. & Rossi, H. A Generalized Formulation of Dual Radiation Action. *Radiation Research* **75,** 471 (Sept. 1978).

179. Hawkins, R. A Statistical Theory of Cell Killing by Radiation of Varying Linear Energy Transfer. *Radiation Research* **140,** 366 (Dec. 1994).

180. Dahle, T. J. *et al.* Sensitivity study of the microdosimetric kinetic model parameters for carbon ion radiotherapy. eng. *Physics in Medicine and Biology* **63,** 225016. ISSN: 1361-6560 (Nov. 2018).

181. Parisi, A., Beltran, C. J. & Furutani, K. M. The Mayo Clinic Florida microdosimetric kinetic model of clonogenic survival: formalism and first benchmark against in vitro and in silico data. *Phys. Med. Biol.* **67,** 185013 (Sept. 2022).

182. Bellinzona, V. E. *et al.* Linking microdosimetric measurements to biological effectiveness in ion beam therapy: A review of theoretical aspects of MKM and other models. *Front. Phys.* **8** (Feb. 2021).

183. Hawkins, R. A Microdosimetric-Kinetic Model for the Effect of Non-Poisson Distribution of Lethal Lesions on the Variation of RBE with LET. *Radiation Research* **160,** 61–69 (July 2003).

184. Hawkins, R. A microdosimetric-kinetic model of cell death from exposure to ionizing radiation of any LET, with experimental and clinical applications. *International Journal of Radiation Biology* **69,** 739–755 (Jan. 1996).

185. Kase, Y. *et al.* Microdosimetric Measurements and Estimation of Human Cell Survival for Heavy-Ion Beams. *Radiation Research* **166,** 629–638 (Oct. 2006).

186. Inaniwa, T. *et al.* Treatment planning for a scanned carbon beam with a modified microdosimetric kinetic model. *Physics in Medicine and Biology* **55,** 6721–6737 (Oct. 28, 2010).

187. Manganaro, L. *et al.* A Monte Carlo approach to the microdosimetric kinetic model to account for dose rate time structure effects in ion beam therapy with application in treatment planning simulations. *Medical Physics* **44,** 1577–1589 (Apr. 2017).

188. Inaniwa, T. & Kanematsu, N. Adaptation of stochastic microdosimetric kinetic model for charged-particle therapy treatment planning. *Physics in Medicine and Biology* **63,** 095011 (May 4, 2018).

189. Chen, Y., Li, J., Li, C., Qiu, R. & Wu, Z. A modified microdosimetric kinetic model for relative biological effectiveness calculation. eng. *Physics in Medicine and Biology* **63,** 015008. ISSN: 1361-6560 (Dec. 2017).

190. Sato, T. & Furusawa, Y. Cell Survival Fraction Estimation Based on the Probability Densities of Domain and Cell Nucleus Specific Energies Using Improved Microdosimetric Kinetic Models. *Radiation Research* **178,** 341–356 (Dec. 2012).

191. Scholz, M. & Kraft, G. Calculation of Heavy Ion Inactivation Probabilities Based on Track Structure, X Ray Sensitivity and Target Size. *Radiation Protection Dosimetry* **52,** 29–33. ISSN: 0144-8420. `https://doi.org/10.1093/oxfordjournals.rpd.a082156` (2021) (Apr. 1994).

192. Scholz, M., Kellerer, A., Kraft-Weyrather, W. & Kraft, G. Computation of cell survival in heavy ion beams for therapy. *Radiation and Environmental Biophysics* **36,** 59–66 (Mar. 26, 1997).

193. Stewart, R. D. *et al.* A comparison of mechanism-inspired models for particle relative biological effectiveness (RBE). en. *Medical Physics* **45.** _eprint: https://aapm.onlinelibrary.wiley.com/doi/pdf/10.1002/mp.13207, e925–e952. ISSN: 2473-4209. `https://aapm.onlinelibrary.wiley.com/doi/abs/10.1002/mp.13207` (2021) (2018).

194. Hagen, U. Bestimmung von Einzel- und Doppelbrüchen in bestrahlter desoxyribonukleinsäure durch die Molekulargewichtsverteilung. de. *Biochimica et Biophysica Acta (BBA) - Nucleic Acids and Protein Synthesis* **134,** 45–58. ISSN: 0005-2787. `https://www.sciencedirect.com/science/article/pii/0005278767900883` (2021) (Jan. 1967).

195. Freifelder, D. & Trumbo, B. Matching of single-strand breaks to form double-strand breaks in DNA. *Biopolymers* **7,** 681–693. ISSN: 1097-0282 (1969).

196. Schans, G. P. v. d., Bleichrodt, J. F. & Blok, J. Contribution of Various Types of Damage to Inactivation of a Biologically-active Double-stranded Circular DNA by Gamma-radiation. *International Journal of Radiation Biology and Related Studies in Physics, Chemistry and Medicine* **23.** Publisher: Taylor & Francis _eprint: https://doi.org/10.1080/09553007314550151, 133–150. ISSN: 0020-7616. `https://doi.org/10.1080/09553007314550151` (2021) (Jan. 1973).

197. Lindenau, D., Hagen, U. & Schnabel, W. On the dynamics of DNA in aqueous solution. Pulse radiolysis studies using the light scattering detection method.

en. *Radiation and Environmental Biophysics* **13,** 287–294. ISSN: 1432-2099. `https://doi.org/10.1007/BF01331173` (2021) (Dec. 1976).

198. Touw, J. H. V., Verberne, J. B., Retèl, J. & Loman, H. Radiation-induced Strand Breaks in Φ X174 Replicative Form DNA: An Improved Experimental and Theoretical Approach. *International Journal of Radiation Biology and Related Studies in Physics, Chemistry and Medicine* **48.** Publisher: Taylor & Francis _eprint: https://doi.org/10.1080/09553008514551621, 567–578. ISSN: 0020-7616. `https://doi.org/10.1080/09553008514551621` (2021) (Jan. 1985).

199. Hempel, K. & Mildenberger, E. Determination of G-values for single and double strand break induction in plasmid DNA using agarose gel electrophoresis and a curve-fitting procedure. eng. *International Journal of Radiation Biology and Related Studies in Physics, Chemistry, and Medicine* **52,** 125–138. ISSN: 0020-7616 (July 1987).

200. Siddiqi, M. A. & Bothe, E. Single- and Double-Strand Break Formation in DNA Irradiated in Aqueous Solution: Dependence on Dose and OH Radical Scavenger Concentration. *Radiation Research* **112.** Publisher: Radiation Research Society, 449–463. ISSN: 0033-7587. `https://www.jstor.org/stable/3577098` (2021) (1987).

201. Klimczak, U., Ludwig, D. C., Mark, F., Rettberg, P. & Schulte-Frohlinde, D. Irradiation of plasmid and phage DNA in water-alcohol mixtures: strand breaks and lethal damage as a function of scavenger concentration. eng. *International Journal of Radiation Biology* **64,** 497–510. ISSN: 0955-3002 (Nov. 1993).

202. Shao, C., Saito, M. & Yu, Z. Formation of single- and double-strand breaks of pBR322 plasmid irradiated in the presence of scavengers. en. *Radiation and Environmental Biophysics* **38,** 105–109. ISSN: 1432-2099. `https://doi.org/10.1007/s004110050145` (2021) (July 1999).

203. Friedrich, T., Durante, M. & Scholz, M. Simulation of DSB yield for high LET radiation. eng. *Radiation Protection Dosimetry* **166,** 61–65. ISSN: 1742-3406 (Sept. 2015).

204. Elsässer, T. *et al.* Quantification of the relative biological effectiveness for ion beam radiotherapy: direct experimental comparison of proton and carbon ion beams and a novel approach for treatment planning. eng. *International Journal of Radiation Oncology, Biology, Physics* **78,** 1177–1183. ISSN: 1879-355X (Nov. 2010).

205. Pfuhl, T. *Influence of secondary electron spectra on the enhanced effectiveness of ion beams* en. PhD thesis (Technische Universität, Darmstadt, 2021), 128, xli Seiten. `http://tuprints.ulb.tu-darmstadt.de/19157/`.

206. Kamp, F. *et al.* Fast Biological Modeling for Voxel-based Heavy Ion Treatment Planning Using the Mechanistic Repair-Misrepair-Fixation Model and Nuclear Fragment Spectra. *International Journal of Radiation Oncology * Biology * Physics* **93,** 557–568 (Nov. 2015).

207. Kamp, F., Carlson, D. & Wilkens, J. Rapid implementation of the repair-misrepair-fixation (RMF) model facilitating online adaption of radiosensitivity parameters in ion therapy. *Physics in Medicine and Biology* **62,** N285–N296 (May 31, 2017).

208. Carlson, D. J., Stewart, R. D., Semenenko, V. A. & Sandison, G. A. Combined use of Monte Carlo DNA damage simulations and deterministic repair models to examine putative mechanisms of cell killing. eng. *Radiation Research* **169,** 447–459. ISSN: 0033-7587 (Apr. 2008).

209. Frese, M., Yu, V., Stewart, R. & Carlson, D. A Mechanism-Based Approach to Predict the Relative Biological Effectiveness of Protons and Carbon Ions in Radiation Therapy. *International Journal of Radiation Oncology * Biology * Physics* **83,** 442–450 (May 2012).

210. Stewart, R. *et al.* Rapid MCNP simulation of DNA double strand break (DSB) relative biological effectiveness (RBE) for photons, neutrons, and light ions. *Physics in Medicine and Biology* **60,** 8249–8274 (Oct. 9, 2015).

211. Stewart, R. Induction of DNA Damage by Light Ions Relative to 60Co $\gamma$-rays. *International Journal of Particle Therapy* **5,** 25–39 (Aug. 2018).

212. Kirkby, C., Ghasroddashti, E., Poirier, Y., Tambasco, M. & Stewart, R. RBE of kV CBCT radiation determined by Monte Carlo DNA damage simulations. *Physics in Medicine and Biology* **58,** 5693–5704 (July 31, 2013).

213. Hsiao, Y. & Stewart, R. D. Monte Carlo simulation of DNA damage induction by x-rays and selected radioisotopes. eng. *Physics in Medicine and Biology* **53,** 233–244. ISSN: 0031-9155 (Jan. 2008).

214. Semenenko, V. & Stewart, R. Fast Monte Carlo simulation of DNA damage formed by electrons and light ions. *Physics in Medicine and Biology* **51,** 1693–1706 (Mar. 7, 2006).

215. Semenenko, V. & Stewart, R. A Fast Monte Carlo Algorithm to Simulate the Spectrum of DNA Damages Formed by Ionizing Radiation. *Radiation Research* **161,** 451–457 (Apr. 2004).

216. Stewart, R. D. *et al.* Effects of radiation quality and oxygen on clustered DNA lesions and cell death. eng. *Radiation Research* **176,** 587–602. ISSN: 1938-5404 (Nov. 2011).

217. Ballarini, F. From DNA Radiation Damage to Cell Death: Theoretical Approaches. *Journal of Nucleic Acids* **2010,** 1–8 (Oct. 5, 2010).

218. Ballarini, F., Altieri, S., Bortolussi, S., Giroletti, E. & Protti, N. A Model of Radiation-Induced Cell Killing: Insights into Mechanisms and Applications for Hadron Therapy. *Radiation Research* **180,** 307–315 (Sept. 2013).

219. Ballarini, F. *et al.* The BIANCA model/code of radiation-induced cell death: application to human cells exposed to different radiation types. *Radiation and Environmental Biophysics* **53,** 525–533 (Mar. 23, 2014).

220. Carante, M. *et al.* Modeling radiation-induced cell death: role of different levels of DNA damage clustering. *Radiation and Environmental Biophysics* **54,** 305–316 (Aug. 2015).

221. Carante, M. & Ballarini, F. Calculating Variations in Biological Effectiveness for a 62 MeV Proton Beam. *Frontiers in Oncology* **6,** 76 (Apr. 6, 2016).

222. Ballarini, F. & Carante, M. P. Chromosome aberrations and cell death by ionizing radiation: Evolution of a biophysical model. English. *Radiation Physics and Chemistry* **128,** 18–25 (2016).

223. Carante, M., Aimè, C., Cajiao, J. & Ballarini, F. BIANCA, a biophysical model of cell survival and chromosome damage by protons, C-ions and He-ions at energies and doses used in hadrontherapy. *Physics in Medicine and Biology* **63,** 075007 (Mar. 26, 2018).

224. McMahon, S., Schuemann, J., Paganetti, H. & Prise, K. Mechanistic Modelling of DNA Repair and Cellular Survival Following Radiation-Induced DNA Damage. *Scientific Reports* **6,** 33290 (Sept. 14, 2016).

225. McMahon, S. J., McNamara, A. L., Schuemann, J., Paganetti, H. & Prise, K. M. A general mechanistic model enables predictions of the biological effectiveness of different qualities of radiation. en. *Scientific Reports* **7.** Number: 1 Publisher: Nature Publishing Group, 10790. ISSN: 2045-2322. https://www.nature.com/articles/s41598-017-10820-1 (2021) (Sept. 2017).

226. McMahon, S. & Prise, K. A Mechanistic DNA Repair and Survival Model (Medras): Applications to Intrinsic Radiosensitivity, Relative Biological Effectiveness and Dose-Rate. *Front Oncol* **11,** 689112 (June 29, 2021).

227. Agostinelli, S. *et al.* GEANT4 - a Simulation Toolkit. *Nucl Instruments Methods Phys Res Sect A Accel Spectrometers Detect Assoc Equip* **506,** 250–303 (2003).

228. Incerti, S. *et al.* THE GEANT4-DNA PROJECT. *International Journal of Modeling, Simulation, and Scientific Computing* **01,** 157–178 (June 2010).

229. Bernal, M. *et al.* Track structure modeling in liquid water: A review of the Geant4-DNA very low energy extension of the Geant4 Monte Carlo simulation toolkit. *Physica Medica* **31,** 861–874 (Dec. 2015).

230. Surdutovich, E. & Solov'yov, A. Multiscale approach to the physics of radiation damage with ions. *The European Physical Journal D* **68,** 353 (Nov. 2014).

231. Verkhovtsev, A., Surdutovich, E. & Solov'yov, A. Multiscale approach predictions for biological outcomes in ion-beam cancer therapy. *Scientific Reports* **6,** 27654 (June 14, 2016).

232. Wang, W. *et al.* Modelling of Cellular Survival Following Radiation-Induced DNA Double-Strand Breaks. *Scientific Reports* **8,** 16202 (Nov. 1, 2018).

233. Zhu, H. *et al.* Development of a DNA damage model that accommodates different cellular oxygen concentrations and radiation qualities. *Medical Physics* **48,** 5511–5521 (Aug. 12, 2021).

234. Bopp, C. *et al.* Adaptation of the microsimetric kinetic model to hypoxia. *Physics in Medicine and Biology* **61,** 7586–7599 (Oct. 7, 2016).

235. Strigari, L. *et al.* Tumour control in ion beam radiotherapy with different ions in the presence of hypoxia: an oxygen enhancement ratio model based on the microdosimetric kinetic model. *Physics in Medicine and Biology* **63,** 065012 (Mar. 16, 2018).

236. Hufnagl, A. *et al.* The link between cell-cycle dependent radiosensitivity and repair pathways: a model based on the local, sister-chromatid conformation dependent switch between NHEJ and HR. eng. *DNA repair* **27,** 28–39. ISSN: 1568-7856 (Mar. 2015).

237. Herr, L., Friedrich, T., Durante, M. & Scholz, M. A Model of Photon Cell Killing Based on the Spatio-Temporal Clustering of DNA Damage in Higher Order Chromatin Structures. en. *PLOS ONE* **9.** Publisher: Public Library of Science, e83923. ISSN: 1932-6203. `https://journals.plos.org/plosone/article?id=10.1371/journal.pone.0083923` (2020) (Jan. 2014).

238. Herr, L. *Modeling of time-dose-LET effects in the cellular response to radiation* ger. Dissertation (Technische Universität, Darmstadt, July 2015). `https://tuprints.ulb.tu-darmstadt.de/4924/` (2020).

239. Inaniwa, T. *et al.* Effects of Dose-Delivery Time Structure on Biological Effectiveness for Therapeutic Carbon-Ion Beams Evaluated with Microdosimetric Kinetic Model. *Radiation Research* **180,** 44–59 (July 2013).

240. Inaniwa, T., Kanematsu, N., Suzuki, M. & Hawkins, R. Effects of beam interruption time on tumor control probability in single-fractionated carbon-ion radiotherapy for non-small cell lung cancer. *Physics in Medicine and Biology* **60,** 4105–4121 (May 1, 2015).

241. Takei, H. & Inaniwa, T. Effect of Irradiation Time on Biological Effectiveness and Tumor Control Probability in Proton Therapy. *International Journal of Radiation Oncology\*Biology\*Physics* **105,** 222–229 (Sept. 2019).

242. Sachs, R. K., van den Engh, G., Trask, B., Yokota, H. & Hearst, J. E. A random-walk/giant-loop model for interphase chromosomes. eng. *Proceedings of the National Academy of Sciences of the United States of America* **92,** 2710–2714. ISSN: 0027-8424 (Mar. 1995).

243. Yokota, H., van den Engh, G., Hearst, J. E., Sachs, R. K. & Trask, B. J. Evidence for the organization of chromatin in megabase pair-sized loops arranged along a random walk path in the human G0/G1 interphase nucleus. eng. *The Journal of Cell Biology* **130,** 1239–1249. ISSN: 0021-9525 (Sept. 1995).

244. Ostashevsky, J. A Polymer Model for the Structural Organization of Chromatin Loops and Minibands in Interphase Chromosomes. *Molecular Biology of the Cell* **9.** Publisher: American Society for Cell Biology (mboc), 3031–3040. ISSN: 1059-1524. `https://www.molbiolcell.org/doi/full/10.1091/mbc.9.11.3031` (2021) (Nov. 1998).

245. Johnston, P. J., Olive, P. L. & Bryant, P. E. Higher-Order Chromatin Structure-Dependent Repair of DNA Double-Strand Breaks: Modeling the Elution of DNA from Nucleoids. *Radiation Research* **148.** Publisher: Radiation Research Society, 561–567. ISSN: 0033-7587. `https://www.jstor.org/stable/3579731` (2020) (1997).

246. Johnston, P. J., MacPhail, S. H., Banáth, J. P. & Olive, P. L. Higher-Order Chromatin Structure-Dependent Repair of DNA Double-Strand Breaks: Factors Affecting Elution of DNA from Nucleoids. *Radiation Research* **149.** Publisher: Radiation Research Society, 533–542. ISSN: 0033-7587. `https://www.jstor.org/stable/3579899` (2020) (1998).

247. Friedrich, T., Durante, M. & Scholz, M. Modeling cell survival after photon irradiation based on double-strand break clustering in megabase pair chromatin loops. eng. *Radiation Research* **178,** 385–394. ISSN: 1938-5404 (Nov. 2012).

248. Mairani, A. *et al.* Modelling of cell killing due to sparsely ionizing radiation in normoxic and hypoxic conditions and an extension to high LET radiation. eng. *International Journal of Radiation Biology* **89,** 782–793. ISSN: 1362-3095 (Oct. 2013).

249. Tommasino, F. *et al.* Induction and Processing of the Radiation-Induced Gamma-H2AX Signal and Its Link to the Underlying Pattern of DSB: A Combined Experimental and Modelling Study. en. *PLOS ONE* **10.** Publisher: Public Library of Science, e0129416. ISSN: 1932-6203. `https://journals.plos.org/plosone/article?id=10.1371/journal.pone.0129416` (2020) (June 2015).

250. Batey, M. A. *et al.* Preclinical evaluation of a novel ATM inhibitor, KU59403, in vitro and in vivo in p53 functional and dysfunctional models of human cancer. eng. *Molecular Cancer Therapeutics* **12,** 959–967. ISSN: 1538-8514 (June 2013).

251. Kundrát, P. *et al.* Analytical formulas representing track-structure simulations on DNA damage induced by protons and light ions at radiotherapy-relevant energies. en. *Sci. Rep.* **10,** 15775 (Sept. 2020).

252. Matsuura, T. *et al.* Apparent absence of a proton beam dose rate effect and possible differences in RBE between Bragg peak and plateau. *Medical Physics* **37,** 5376–5381 (Sept. 24, 2010).

253. Kasamatsu, K. *et al.* Impact of a spatially dependent dose delivery time structure on the biological effectiveness of scanning proton therapy. en. *Med. Phys.* **49,** 702–713 (Jan. 2022).

254. Schmid, T. E. *et al.* No evidence for a different RBE between pulsed and continuous 20 MeV protons. en. *Radiat. Res.* **172,** 567–574 (Nov. 2009).

255. Saager, M., Peschke, P., Brons, S., Debus, J. & Karger, C. P. Determination of the proton RBE in the rat spinal cord: Is there an increase towards the end of the spread-out Bragg peak? en. *Radiother. Oncol.* **128,** 115–120 (July 2018).

256. Hintz, L. *et al.* Relative biological effectiveness of single and split helium ion doses in the rat spinal cord increases strongly with linear energy transfer. en. *Radiother. Oncol.* **170,** 224–230 (May 2022).

257. Cao, X. *et al.* Quantification of Oxygen Depletion During FLASH Irradiation In Vitro and In Vivo. eng. *International Journal of Radiation Oncology, Biology, Physics* **111,** 240–248. ISSN: 1879-355X (Sept. 2021).

258. Bourhis, J. *et al.* Clinical translation of FLASH radiotherapy: Why and how? en. *Radiotherapy and Oncology. FLASH radiotherapy International Workshop* **139,** 11–17. ISSN: 0167-8140. http://www.sciencedirect.com/science/article/pii/S0167814019303603 (2020) (Oct. 2019).

259. Van Slyke, A. L. *et al.* Oxygen monitoring in model solutions and in vivo in mice during proton irradiation at conventional and FLASH dose rates. en. *Radiat. Res.* **198,** 181–189 (Aug. 2022).

260. Jansen, J. *et al.* Does FLASH deplete oxygen? Experimental evaluation for photons, protons, and carbon ions. en. *Med. Phys.* **48,** 3982–3990 (July 2021).

261. Spitz, D. R. *et al.* An integrated physico-chemical approach for explaining the differential impact of FLASH versus conventional dose rate irradiation on cancer and normal tissue responses. eng. *Radiotherapy and Oncology: Journal of the European Society for Therapeutic Radiology and Oncology* **139,** 23–27. ISSN: 1879-0887 (Oct. 2019).

262. Wardman, P. Radiotherapy Using High-Intensity Pulsed Radiation Beams (FLASH): A Radiation-Chemical Perspective. *Radiation Research* **194,** 607–617. ISSN: 0033-7587. `https://doi.org/10.1667/RADE-19-00016` (2021) (May 2020).

263. Lai, Y., Chi, Y. & Jia, X. Mechanistic modelling of oxygen enhancement ratio of radiation via Monte Carlo simulation-based DNA damage calculation. en. *Phys. Med. Biol.* **67,** 175009 (Aug. 2022).

264. Scifoni, E. *et al.* Including oxygen enhancement ratio in ion beam treatment planning: model implementation and experimental verification. en. *Phys. Med. Biol.* **58,** 3871–3895 (June 2013).

265. Tinganelli, W. *et al.* Kill-painting of hypoxic tumours in charged particle therapy. en. *Sci. Rep.* **5,** 17016 (Nov. 2015).

266. Skov, K. A. The contribution of hydroxyl radical to radiosensitization: a study of DNA damage. en. *Radiat. Res.* **99,** 502–510 (Sept. 1984).

267. Alper, T. & Bryant, P. E. Reduction in oxygen enhancement ratio with increase in LET: tests of two hypotheses. en. *Int. J. Radiat. Biol. Relat. Stud. Phys. Chem. Med.* **26,** 203–218 (Sept. 1974).

268. Baverstock, K. F. & Burns, W. G. Primary production of oxygen from irradiated water as an explanation for decreased radiobiological oxygen enhancement at high LET. en. *Nature* **260,** 316–318 (Mar. 1976).

269. Meesungnoen, J. & Jay-Gerin, J.-P. High-LET radiolysis of liquid water with 1H+, 4He2+, 12C6+, and 20Ne9+ ions: effects of multiple ionization. en. *J. Phys. Chem. A* **109,** 6406–6419 (July 2005).

270. Meesungnoen, J. & Jay-Gerin, J.-P. High-LET ion radiolysis of water: oxygen production in tracks. en. *Radiat. Res.* **171,** 379–386 (Mar. 2009).

271. Frankenberg-Schwager, M., Frankenberg, D., Harbich, R. & Beckonert, S. Evidence against the ?oxygen-in-the-track? hypothesis as an explanation for the radiobiological low oxygen enhancement ratio at high linear energy transfer radiation. en. *Radiat. Environ. Biophys.* **33,** 1–8 (Mar. 1994).

272. Sauer, M. C., Schmidt, K. H., Jonah, C. D., Naleway, C. A. & Hart, E. J. High-LET pulse radiolysis: O 2 - and oxygen production in tracks. *Radiat. Res.* **75,** 519 (Sept. 1978).

273. Stuglik, Z. On the 'oxygen in heavy-ion tracks' hypothesis. en. *Radiat. Res.* **143,** 343–348 (Sept. 1995).

274. Goodhead, D. T. Energy deposition stochastics and track structure: what about the target? en. *Radiat. Prot. Dosimetry* **122,** 3–15 (2006).

275. Domina, E. A., Philchenkov, A. & Dubrovska, A. Individual response to ionizing radiation and personalized radiotherapy. en. *Crit. Rev. Oncog.* **23,** 69–92 (2018).

276. Bibault, J.-E. *et al.* Personalized radiation therapy and biomarker-driven treatment strategies: a systematic review. en. *Cancer Metastasis Rev.* **32,** 479–492 (Dec. 2013).

277. Ling, C. C. *et al.* Towards multidimensional radiotherapy (MD-CRT): biological imaging and biological conformality. en. *Int. J. Radiat. Oncol. Biol. Phys.* **47,** 551–560 (June 2000).

278. Alber, M., Paulsen, F., Eschmann, S. M. & Machulla, H. J. On biologically conformal boost dose optimization. en. *Phys. Med. Biol.* **48,** N31–5 (Jan. 2003).

279. Bassler, N., Jäkel, O., Søndergaard, C. S. & Petersen, J. B. Dose- and LET-painting with particle therapy. en. *Acta Oncol.* **49,** 1170–1176 (Oct. 2010).

280. Bentzen, S. M. Theragnostic imaging for radiation oncology: dose-painting by numbers. en. *Lancet Oncol.* **6,** 112–117 (Feb. 2005).

281. Gérard, M. *et al.* Hypoxia imaging and adaptive radiotherapy: A state-of-the-art approach in the management of glioma. en. *Front. Med. (Lausanne)* **6,** 117 (June 2019).

282. Thorwarth, D., Eschmann, S.-M., Paulsen, F. & Alber, M. Hypoxia dose painting by numbers: a planning study. en. *Int. J. Radiat. Oncol. Biol. Phys.* **68,** 291–300 (May 2007).

283. Dahle, T. J. *et al.* The FLUKA Monte Carlo code coupled with an OER model for biologically weighted dose calculations in proton therapy of hypoxic tumors. en. *Phys. Med.* **76,** 166–172 (Aug. 2020).

284. Sokol, O., Krämer, M., Hild, S., Durante, M. & Scifoni, E. Kill painting of hypoxic tumors with multiple ion beams. en. *Phys. Med. Biol.* **64,** 045008 (Feb. 2019).

285. Doubrovin, M. *et al.* Imaging transcriptional regulation of p53-dependent genes with positron emission tomography in vivo. en. *Proc. Natl. Acad. Sci. U. S. A.* **98,** 9300–9305 (July 2001).

286. Serganova, I. & Blasberg, R. G. Molecular imaging with reporter genes: Has its promise been delivered? en. *J. Nucl. Med.* **60,** 1665–1681 (Dec. 2019).

287. Glowa, C. *et al.* Carbon ion radiotherapy decreases the impact of tumor heterogeneity on radiation response in experimental prostate tumors. en. *Cancer Lett.* **378,** 97–103 (Aug. 2016).

288. Glowa, C. *et al.* Carbon ion radiotherapy: impact of tumor differentiation on local control in experimental prostate carcinomas. en. *Radiat. Oncol.* **12** (Dec. 2017).

289. Glowa, C., Peschke, P., Brons, S., Debus, J. & Karger, C. P. Intrinsic and extrinsic tumor characteristics are of minor relevance for the efficacy of split-dose carbon ion irradiation in three experimental prostate tumors. en. *Radiother. Oncol.* **133,** 120–124 (Apr. 2019).

290. Mein, S. *et al.* Spot-scanning hadron arc (SHArc) therapy: A study with light and heavy ions. en. *Adv. Radiat. Oncol.* **6,** 100661 (May 2021).

291. Kopp, B. *et al.* Development and validation of single field multi-ion PaRticle thErapy treatments. en. *Int. J. Radiat. Oncol. Biol. Phys.* **106,** 194–205 (Jan. 2020).

292. Hopfner, K.-P. & Hornung, V. Molecular mechanisms and cellular functions of cGAS-STING signalling. en. *Nat. Rev. Mol. Cell Biol.* **21,** 501–521 (Sept. 2020).

293. Mittra, I. *et al.* Cell-free chromatin from dying cancer cells integrate into genomes of bystander healthy cells to induce DNA damage and inflammation. en. *Cell Death Discov.* **3** (Dec. 2017).

294. Kirolikar, S. *et al.* Prevention of radiation-induced bystander effects by agents that inactivate cell-free chromatin released from irradiated dying cells. en. *Cell Death Dis.* **9** (Dec. 2018).

295. Durante, M., Bonassi, S., George, K. & Cucinotta, F. Risk estimation based on chromosomal aberrations induced by radiation. *Radiat. Res.* **156.** Part 2, 662–667 (2001).

296. Conte, V., Selva, A., Colautti, P., Hilgers, G. & Rabus, H. Track structure characterization and its link to radiobiology. *Radiat. Meas.* **106,** 506–511 (Nov. 2017).

297. Hofmann, A., Krufczik, M., Heermann, D. & Hausmann, M. Using persistent homology as a new approach for super-resolution localization microscopy data analysis and classification of $\gamma$H2AX foci/clusters. *Int. J. Mol. Sci.* **19,** 2263 (Aug. 2018).

298. Brons, S., Taucher-Scholz, G., Scholz, M. & Kraft, G. A track structure model for simulation of strand breaks in plasmid DNA after heavy ion irradiation. eng. *Radiation and Environmental Biophysics* **42,** 63–72. ISSN: 0301-634X (Apr. 2003).

# Appendix

## Implementation of the diffused RDD on GPU

For the ion beam model within the UNIVERSE, the Kiefer-Chatterjee parametrization (Equation 2.10) of the radial dose distribution (RDD) was used to describe the microscopic dose distribution surrounding the path or particles. This parametrization is also used in combination with the MKM since the late 2000s [64] (cp. Section 2.4.2). Furthermore, a diffusion kernel (Equations 2.66 and 2.67), first introduced for LEMII [298](cp. Section 2.4.3), was applied to the RDD to simulate the diffusion of radical species. This combination was chosen, it was shown to match MCS of RDD with subsequent diffusion well [66]. However, implementing the resulting expression of the RDD ($\widetilde{D}(r)$) directly onto the GPU was found to be inefficient and an approximative description had to be developed.

The following section has been taken from the supplementary material of Paper 4 which can be found under `doi:10.1016/j.ijrobp.2021.09.048`.

To enable practical and efficient implementation of the diffused radial dose distribution (RDD) on the Graphics Processing Units (GPU), a three-step approximation of the RDD ($\hat{D}(r)$) was developed and applied in this study (Figure S1). The approximate form comprises a constant inner core of the radius $\hat{r}_{min}$ with a core dose $\hat{D}_c$, a steeper inner penumbra up to a transition radius $\hat{r}_{trans}$ inside which the dose reduces by the exponent $\hat{x}$ and an outer penumbra, that equals the penumbra of the Kiefer-Chatterjee parametrization. The maximum electron range is extended to $\hat{r}_{max} = r_{max} + 2\sigma$, to approximate the extended range by diffusion. In summary,

$\hat{D}(r)$ can be written as:

$$\hat{D}(r) = \begin{cases} \hat{D}_c & r \leq \hat{r}_{min} \\ \left(\frac{\hat{r}_{min}}{r}\right)^{\hat{x}} \cdot \hat{D}_c & \hat{r}_{min} < r \leq \hat{r}_{trans} \\ K_p \cdot r^{-2} & \hat{r}_{trans} < r \leq \hat{r}_{max} \end{cases} \quad (6.1)$$

The value of $\hat{D}_c$ was defined as $\hat{D}_c = \widetilde{D}(r_{min}/100)$. In order to determine $\hat{x}$ for the inner penumbra, the turning point of the $\widetilde{D}(r)$ inside it in the log-log representation (as in Figure S1), $\hat{r}_{turn}$, had to be calculated. It was found empirically that this value could be determined numerically as a minimum of the third derivative of $\widetilde{D}(r)$ with respect to $r$. Using one radius value slightly above $(\hat{r}_{turn+})$ and slightly below $(\hat{r}_{turn-})$ the turning point $\hat{r}_{turn}$, one can derive an expression for the exponent $\hat{x}$:

$$\hat{x} = log_{\left(\frac{\hat{r}_{turn+}}{\hat{r}_{turn-}}\right)}\left(\frac{\widetilde{D}(\hat{r}_{turn-})}{\widetilde{D}(\hat{r}_{turn+})}\right). \quad (6.2)$$

Reshaping the expression for the intermediate range from Equation 6.1, one can derive $\hat{r}_{min}$, the radius where the inner penumbra reaches the core dose, using:

$$\hat{r}_{min} = \left(\frac{\widetilde{D}(\hat{r}_{turn+})}{\hat{D}_c}\right)^{\frac{1}{\hat{x}}} \cdot \hat{r}_{turn+}. \quad (6.3)$$

The transition radius $\hat{r}_{trans}$, at which the inner penumbra cuts the Kiefer-Chatterjee penumbra can be derived to be given by:

$$\hat{r}_{trans} = \left(\hat{r}_{min}^{\hat{x}} \cdot \frac{\hat{D}_c}{K_p}\right)^{\frac{1}{\hat{x}-2}}. \quad (6.4)$$

While this approximate form of the diffused RDD significantly simplifies the implementation and calculation on GPU, it inevitably introduces a systematic deviation from the underlying diffused RDD. To ensure that during the simulations the LET applied by the approximate RDD does resemble the input as close as possible and the dose that is to be applied is conserved, the approximate RDD is divided by a scaling factor $\kappa$ in the final step. This factor was determined by:

$$\kappa = \frac{2\pi\rho \int_0^{\hat{r}_{max}} \hat{D}(r)rdr}{LET}, \quad (6.5)$$

where $LET$ is in this case the input value. For low particle energies, the scaling factor was found to be energy-dependent, while for larger Energies it was approximately constant. A three-part function was applied to describe these trends (a gaussian, an exponential and constant region):

$$\kappa(E) = \begin{cases} 0.261^2 \cdot e^{-139.1 \cdot (E-0.23)^2} + 1.49 & E < 0.24 \frac{MeV}{u} \\ 0.485 \cdot e^{-3.46 \cdot E} + 1.37 & 0.24 \frac{MeV}{u} < E \leq 1.5 \frac{MeV}{u} \\ 1.35 & E \geq 1.5 \frac{MeV}{u} \end{cases} \tag{6.6}$$

The simplicity of the parametrization comes with the cost of deviations at the boundaries between the sections and at $\sim 20 \frac{MeV}{u}$. However, applying the scaling factor given by the parametrization and comparing the applied LET of the scaled RDD and the input LET, it appears, that inside the range of energies analyzed in this work the deviation does not exceed 2%. This suggests that the deviations of the parametrization of the scaling factor have no significant impact on the simulation of dose distributions.
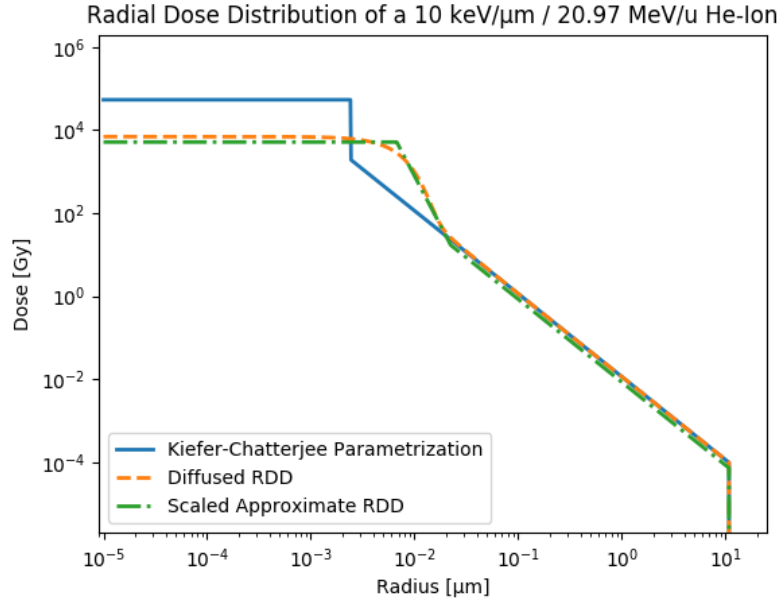


Figure S1: The radial dose distribution (RDD) of a 10 keV/µm / 20.97 MeV/u He-4 ion as described by the Kiefer-Chatterjee parametrization (blue solid line), after convolution with the diffusion kernel (orange dashed line) and the approximate version scaled with the factor $\kappa$ applied in this study (green dash-dotted line).

# Acknowledgements

I want to express my gratitude to my seniors at the BioPT group **Ben**, **Mac** and **Thomas**, whose mentoring and willingness to answer any questions surrounding scientific issues was only outdone by the friendships that grew throughout our time together. Similarly I would like to thank my fellow students of the group, **Celine**, **Filipa**, **Friderike**, **Judith**, **Luisa**, **Nish**, **Peter**, **Selver** for the shared time and close bonds that formed.

Above all I need to thank my supervisor **Prof. Dr. Andrea Mairani**. Andrea, since the first day in your group, you gave me the feeling that you took my opinion as seriously as your own. When we explored new or long forgotten niches of science together, you openly communicated your own boundaries of knowledge, inspiring me to think openly and creatively. Even when I felt overwhelmed in certain situations, I was always able to honestly address my issues and was never met with anything other than understanding and encouragement. Besides the large amount of scientific knowledge, you taught me not only how to fish for hand drawn data from the 1950s or find the best color combination for plots but also how to stay resilient when facing overly negative referees during the peer review process or how to handle difficult exchanges with other members of the scientific community. I am deeply grateful for your mentorship and my growth under your guidance.

Countless **friends and family members** have supported me throughout the last years and unfortunately I cannot list them all. Nevertheless, I want them to know that I am deeply grateful for their encouragement and interest in my success. I would like to point out **my parents** who never showed a shred of doubt that their son could achieve his goals. I hope you are proud of this work.

Finally, to my wife **Eleonore**: Thank you for your endless stream of support, encouragement and love. Only with you at my side was I able to overcome the challenges of this special period of our young life together.

# Erklärung

Ich erkläre hiermit, dass ich die vorgelegte Dissertation selbst verfasst und mich dabei keiner anderen, als der von mir ausdrücklich bezeichneten Quellen und Hilfen bedient habe.

Heidelberg, den ........................,